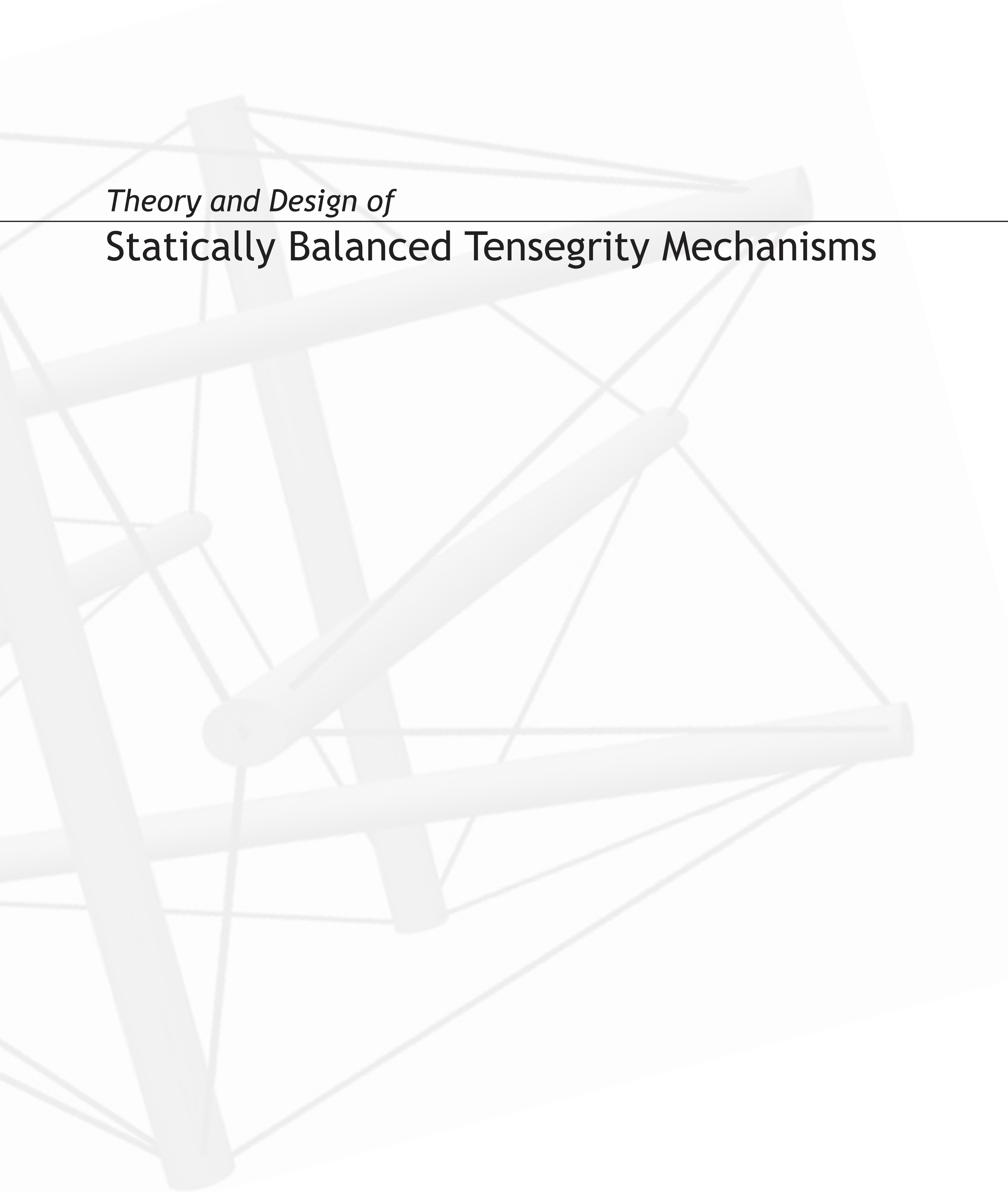

Theory and Design of

Statically Balanced Tensegrity Mechanisms

MSc. Thesis

Mark Schenk
February 2006

Department of BioMechanical Engineering

Faculty of Mechanical, Maritime and Materials Engineering

TU Delft
Delft University of Technology

Report title: Theory and Design of Statically Balanced Tensegrity Mechanisms
Report type: MSc. Thesis
Report number: 993

Author: Mark Schenk
Date: February 2006

Institute: Delft University of Technology
Faculty of Mechanical, Maritime and Materials Engineering
Department of BioMechancial Engineering

Exam committee: prof. dr. ir. P.A. Wieringa
dr. ir. J.L. Herder
dr. S.D. Guest
dr. ir. A.L. Schwab

Preface

This Master's Thesis concludes my research on Statically Balanced Tensegrity Mechanisms, at the Delft University of Technology. The concept of tensegrity structures had caught my imagination from the outset, and the combination with static balancing added another exciting dimension. The research was largely theoretical, but – initially to my own surprise – I thoroughly enjoyed the process of trying to understand the intricacies of the stiffness of prestressed structures. I believe my efforts paid off, and the result lies before you.

During my project I had help from a lot of people, in manners great and small. All who helped me will know they have, and I'm grateful to them. Still, I have a few words of particular thanks.

First of all to my supervisor Just Herder, who is possibly even more enthusiastic about the topic than I am. Thanks for all the time you devoted to, and interest you showed in, my research!

An important part of the theory was developed during my four month internship at the Cambridge University Engineering Department, and I'm very grateful to Simon Guest for hosting me, as well as for all the valuable help and discussions after my stay.

I would further like to thank Professor Connelly for some very fruitful discussions during my brief visit to Cambridge in October.

To the various students also working in the graduation workspace at MMS: thanks for the fun working environment! The seemingly endless supply of Senseo coffee, discussions on the benefits of using LaTeX, exclamations on the downsides of using LaTeX, problems with MATLAB, weekend stories, drinking stories, anything-but-work stories; it all combined to make this a very pleasant setting to finish my last months as a student. Special thanks is due to Daan 'Don V' Venekamp, who always patiently listened to my rambles, proofread my paper, and now knows more about tensegrities than he ever would have liked!

Last but not least: I would not have been able to study and do this research in the first place, if it hadn't been for the continuous support of my parents. Dank jullie wel!

Mark Schenk
February 2006

Summary

The fields of *static balancing* and *tensegrity structures* are combined into *statically balanced tensegrity mechanisms.* This combination results in a new class of prestressed structures that behave like mechanisms: although member lengths and orientations change, they can be deformed into a wide range of positions, while continuously remaining in equilibrium; in other words, the structures have zero stiffness. The key to these structures is the use of zero-free-length springs as tension members.

The tools of structural engineering were used to search for, and understand, zero-stiffness modes in the tangent stiffness matrix of prestressed pin-jointed bar frameworks. To this end the recently uncovered parallels between structural engineering and mathematical rigidity theory were exploited. Mathematical literature described that affine transformations preserve the equilibrium of a tensegrity structure; these findings gained value when translated from a mathematical concept into the engineering terms rigid-body motions, shear and dilation. Not only did these transformations prove to be instrumental for describing zero stiffness, but it also provided new insight in the form-finding methods for tensegrity structures: the minimum nullity requirement for the stress matrix is formed by the affine transformations.

In this research it was shown that affine transformations of the structure that preserve the length of conventional members are zero-stiffness modes valid over finite displacements: these are *statically balanced zero-stiffness modes.* What is more, for prestress stable structures with a positive semi-definite stress matrix of maximal rank – meaning there are only affine transformations in its nullspace – those are the only possible zero-stiffness modes. The length-preserving affine transformations exist if and only if the directions of the conventional members lie on a conic at infinity. If all conventional member directions lie on a conic, the number of independent length-preserving affine transformations can then be found with a simple counting rule.

A systematic analysis of the zero-stiffness modes in the tangent stiffness matrix of a prestressed pin-jointed bar framework yielded several interesting scenarios that warrant further attention, as they cannot be fully described within the currently developed framework.

Finally, a demonstration prototype was designed and constructed to illustrate the properties of statically balanced tensegrity mechanisms; the prototype serves as a proof of concept, not as a practically applicable design. Prior to construction, the range of motion of the tensegrity used for the prototype was extensively analysed using the analytic equilibrium conditions. The results were instrumental in dimensioning the prototype.

Contents

Preface iii

Summary v

1 Introduction 1
1.1 Outline 2

2 Zero Stiffness Tensegrity Structures 3
2.1 Introduction 3
2.2 Equilibrium and stiffness of prestressed structures 5
2.3 Affine transformations and zero-stiffness modes 8
2.4 Length-preserving affine transformations 12
2.5 Example 15
2.6 Summary and Conclusions 18

3 Overview of Zero Stiffness in Prestressed Bar Frameworks 21
3.1 Introduction 21
3.2 Stiffness of prestressed structures 22
3.3 Zero stiffness and matrix nullspace 25
3.4 Contributions of $\hat{\mathbf{K}}$ and $\tilde{\mathbf{\Omega}}$ cancel out 29
3.5 Conclusion 30

4 Conclusions 33

Bibliography 35

Appendices

A Tensegrity Equilibrium 37
A.1 Introduction 37
A.2 Equilibrium configuration 37
A.3 Twist angle 39
A.4 Equilibrium tensions 40
A.5 Literature comparison 42
A.6 Spring stiffness ratios 44
A.7 Conclusion 45

B Tangent Stiffness Matrix **47**
B.1 Introduction 47
B.2 Modified axial stiffness 47
B.3 Geometrically non-linear FEA 50
B.4 Comparison 52
B.5 Conclusion 53

C MATLAB Code Description **55**
C.1 Introduction 55
C.2 Code outline 55
C.3 Custom functions 56
C.4 Various remarks 57
C.5 Conclusion 57

D Prototype Design **59**
D.1 Introduction 59
D.2 Design requirements 59
D.3 Prototype description 60
D.4 Design detailing 62
D.5 Design Evaluation 69

E Zero Stiffness Examples **79**
E.1 Introduction 79
E.2 ‘Babytoy’ equilibrium 79

F Future Work **85**
F.1 Introduction 85
F.2 Future work 85
F.3 Conclusion 88

Bibliography **89**

Chapter 1

Introduction

This thesis concludes the efforts to investigate the theory and design of *statically balanced tensegrity mechanisms*, a hitherto unexplorered combination of two fields of research, *tensegrity structures* and *statically balanced systems*.

Tensegrity structures, or tensegrities, are a special type of prestressed pin-jointed bar frameworks with unique properties: the tension elements are usually replaced by cables, resulting in aesthetic, light-weight structures that seem to defy gravity. The structures are generally both statically and kinematically indeterminate, and they derive their stability from the state of self-stress, which stabilizes any internal mechanisms present.

Statically balanced systems are in equilibrium in every configuration in their workspace, even when no friction is present: they are neutrally stable, and have zero stiffness. As a consequence, these systems can be operated with much less effort as compared to the unbalanced situation. Hence, static balancing is used for energy-efficient design in for instance prosthetics and rehabilitation technology. A classic every day example is the ‘Anglepoise’ desk lamp which can be positioned virtually anywhere without external force.

The combination of the two fields was expected to produce mechanical frameworks with very interesting properties: tensegrities that can be deformed into a wide range of shapes without external work, and thus displaying mechanism-like properties. These structures are in a fascinating state of balance: during deformation, the internal forces remain in harmony, but they change and shift from member to member. Understanding these structures was expected to provide new insights into both fields, and perhaps yield a more fundamental understanding of static balancing.

A note is due about the terminology of these structures, as they are at once both structure and mechanism. In the current research we have used the tools of structural eningeering to analyse their properties, and will therefore refer to them as *zero stiffness tensegrity structures* in the report. However, any practical application would be for their mechanism properties, and hence the term *statically balanced tensegrity mechanisms* would be more appropriate. In describing these structures both terms are equally valid and may be used interchangeably.

1.1 Outline

The results of the MSc. Thesis are presented as two papers, complemented with a range of Appendices for background information. The papers appear as chapters in this report, but are written as free standing entities: each has its own abstract, introduction and conclusions. This accounts for the fact that some sections appear to be duplicated in both papers.

The first paper describes the underlying theory of "*Zero Stiffness Tensegrity Structures*" and contains the main novelties of the research. It recapitulates the stiffness analysis of tensegrity structures, and describes under which circumstances the structure has zero stiffness when zero-free-length springs are added. The results are illustrated by the numerical analysis of a classic tensegrity.

The second paper complements the first and aims to fill up some of the gaps, by providing a systematic "*Overview of Zero Stiffness in Prestressed Bar Frameworks*", and as far as current knowledge allows, describing its nature. Some intriguing border cases are given, to illustrate the interesting work left.

The conclusion wraps up both papers and the current state of research, and suggests viable directions for continuing the research.

Appendices The appendices provide (detailed) background information to the work described in the papers. The equilibrium conditions and configurations of a special class of prismic rotationally symmetric tensegrities are described in Appendix A. These play a special role in the developed theory about zero-stiffness structures, as they form an entire family of statically balanced structures. The derivation and comparison of the formulation of the tangent stiffness matrix used extensively throughout the research is provided in Appendix B. Appendix D describes in detail the design process of the demonstration prototype, and contains useful information about the design problems encountered. Appendix E shows several examples of zero stiffness tensegrity structures, followed by an extensive list of suggestions for future research work in Appendix F.

CDROM Enclosed with the report is a CDROM, which aside from a digital copy of this report includes the MATLAB code described in Appendix C, as well as *pdf* copies of a lot of the references.

WWW This report is also available online, along with presentations and MATLAB code, at: *http://www.markschenk.com/tensegrity/*

Chapter 2

Zero Stiffness Tensegrity Structures

M.Schenk[a], S.D.Guest[b], J.L.Herder[a]

[a] *Mechanical, Maritime and Materials Engineering, Delft University of Technology, Mekelweg 2, 2628 CD Delft, The Netherlands*

[b] *Department of Engineering, University of Cambridge, Trumpington Street, Cambridge CB2 1PZ, United Kingdom*

Abstract

Tension members with a zero rest length allow the construction of tensegrity structures that are in equilibrium over a continuous range of positions and thus exhibit mechanism-like properties: they are neutrally stable, or equivalently have zero stiffness. Those zero-stiffness modes are not internal mechanisms, as they involve first-order changes in member length, but are a direct result of the use of the special tension members. These modes correspond to an affine transformation of the structure that preserves the length of conventional members, and are present if and only if the directional vectors of those members lie on a conic. This geometric interpretation provides an entire family of zero stiffness tensegrity structures.

Keywords: zero stiffness, tensegrity structures, tensegrity mechanisms, static balancing, affine transformations

---

2.1 Introduction

This paper will describe and analyse a new and special class of 'tensegrity' structures that straddle the border between mechanisms and structures: although member lengths and orientations change, the structures can be deformed over large displacements whilst continuously remaining in equilibrium. In other words, they remain neutrally stable, require no external work to deform, and

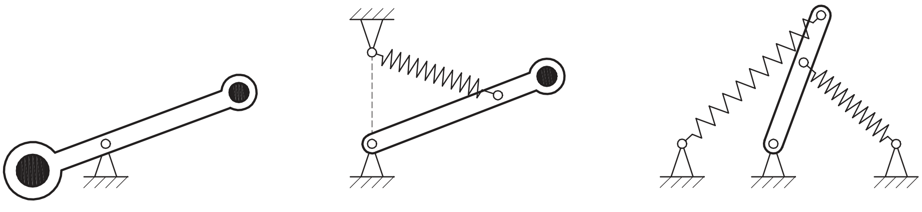

(a) (b) (c)

Figure 2.1: Static balancing: the three structures shown are in equilibrium for any position of the bar, as long as in (a) the masses (black circles) are correctly chosen, and in (b) and (c) the springs are zero-free-length springs with appropriately chosen stiffness.

hence have zero stiffness. Although zero stiffness is uncommon in the theory of stability, several examples exist. Tarnai (2003) describes two systems that display zero stiffness, respectively related to bifurcation of equilibrium paths, and to snap-through type loss of stability of unloaded structures in a state of self-stress. These structures require specific external loads or states of self-stress to exhibit zero stiffness. The key to the structures discussed in this paper, however, is the use of tension members that, in their working range, appear to have a zero rest length – their tension is proportional to their length. Such members are not merely a mathematical abstraction; it is for instance possible to wind a close-coiled spring with initial tension that ensures, when the spring is extended, that the exerted force is proportional to the length.

The utility of zero-free-length springs was initially exploited in the design of the classic 'Anglepoise' lamp (French and Widden, 2000), but is more generally applied in the field of static balancing (Herder, 2001)(see Figure 2.1). Statically balanced systems are in equilibrium in every configuration in their workspace, and as they require little to no effort to operate, they are used for energy-efficient design in for instance robotics and medical settings. Herder (2001) discovered some basic examples of statically balanced tensegrities, which formed the inspiration for the current research. Acquired knowledge in this research is suspected to lead to a more fundamental understanding of, and new synthesis tools for, statically balanced systems.

'Tensegrity' is a term that is not consistently defined in literature, see Motro (1992) for a discussion. Here we take it to mean free-standing prestressed pin-jointed structures, which are in general both statically and kinematically indeterminate. The state of self-stress ensures that each member carries a non-zero, purely tensile or compressive load, under absence of external loads and constraints. Previously, the analysis of tensegrity structures, either by a structural mechanics approach (e.g. Pellegrino and Calladine, 1986) or a mathematical rigidity theory approach (e.g. Connelly and Whiteley, 1996), has only been concerned with whether or not a structure is stable. We shall only consider structures that, were they constructed with conventional tension and compression members, are prestress stable (i.e. have a positive-definite tangent stiffness matrix, modulo rigid-body motions). The novel feature of this paper is that we then replace some or all of the tension members with zero-free-length springs, in search of zero-stiffness modes.

The zero-stiffness tensegrities described in this paper walk a fine line between structures and mechanisms. Here we shall refer to them as *tensegrity structures*, as we will be using the tools of structural engineering and not mechanism theory. For other purposes, the term *tensegrity mechanisms* might be more applicable. Practical applications of this new class of structure will most likely also take place on the borderline of structures and mechanisms, such as, for example, deployable structures which are in equilibrium throughout deployment.

There are clear hints to the direction taken in this paper in the affine transformations considered by Connelly and Terrell (1995) or the 'tensegrity similarity transformation' considered by Masic et al. (2005). Unlike in those papers, here the affine transformations are translated from a mathematical abstraction into a real physical response of structures that can be constructed.

The paper is laid out as follows. Section 2.2 recapitulates the equilibrium and stiffness analysis of prestressed structures. In particular it describes the consequences of using zero-free-length springs by means of a recent formulation of the tangent stiffness matrix. Section 2.3 introduces affine transformations and shows that affine modes which preserve the length of the conventional members are statically balanced zero-stiffness modes. A general existence criterion for length-preserving affine transformations is discussed in section 2.4. An example analysis of a classic tensegrity structure fitted with zero-free-length springs, in section 2.5 illustrates the theory laid down priorly.

2.2 Equilibrium and stiffness of prestressed structures

This section aims to lay the groundwork for the coming sections, by first briefly recapitulating the tensegrity form-finding method from rigidity theory, followed by the description of the tangent stiffness matrix that clearly shows the effects of using zero-free-length springs. The section is concluded by a discussion of zero-stiffness modes in conventional tensegrity structures.

2.2.1 Equilibrium position

This paper is primarily concerned with the stiffness of a tensegrity structure in a known configuration, and not with *form finding*, i.e. finding an initial equilibrium configuration (Tibert and Pellegrino, 2003). Nevertheless, a brief description will be given, as there are interesting and useful parallels between the stiffness of a prestressed structure and the *energy method* of rigidity theory (or, equivalently, the engineering *force density method*) used in form finding.

The energy method in rigidity theory considers a stress state ω to be a state of self-stress if the internal forces at every node sum to zero, i.e. the following equilibrium condition holds at each node i

$$\sum_j \omega_{ij} \left(\mathbf{p}_j - \mathbf{p}_i\right) = \mathbf{0} \tag{2.1}$$

where $\mathbf{p}_i$ are the coordinates for node i, and ω_{ij} is the tension in the member connecting nodes i and j, divided by the length of the member; ω_{ij} is referred to as a *stress* in rigidity theory, but is known in engineering as a *force density* or *tension coefficient.* If all the nodal coordinates are written together as a vector $\mathbf{p}$, $\mathbf{p}^T = [\mathbf{p}_1^T, \mathbf{p}_2^T, \ldots, \mathbf{p}_n^T]$, the equilibrium equations at each node can be combined to obtain the matrix equation

$$\tilde{\mathbf{\Omega}}\mathbf{p} = \mathbf{0} \tag{2.2}$$

where $\tilde{\mathbf{\Omega}}$ is the *stress matrix* for the entire structure. In fact, because equation 2.1 consists of the same coefficients for each of d dimensions, the stress matrix can be written as the Kronecker product of a *reduced stress matrix* $\mathbf{\Omega}$ and a d-dimensional identity matrix $\mathbf{I}^d$

$$\tilde{\mathbf{\Omega}} = \mathbf{\Omega} \otimes \mathbf{I}^d. \tag{2.3}$$

The coefficients of the reduced stress matrix are then given, from equation 2.1, as

$$\Omega_{ij} = \begin{cases} -\omega_{ij} = -\omega_{ji} & \text{if } i \neq j \text{, and \{i,j\} a member,} \\ \sum_{k \neq i} \omega_{ik} & \text{if } i = j, \\ 0 & \text{if there is no connection between } i \text{ and } j. \end{cases} \tag{2.4}$$

Although the stress matrix is here defined entirely by *equilibrium* of the structure, we shall see the same matrix recurring in the *stiffness* equations in section 2.2.2. This dual role of the stress matrix allows the combination and application of insights from rigidity theory – where the stress matrix has been the object of study – to engineering stiffness analysis.

Form-finding methods require the symmetric matrix $\mathbf{\Omega}$ to have a nullity $\mathcal{N} \geq d + 1$, and thus for $\tilde{\mathbf{\Omega}}$ a nullity $\mathcal{N} \geq d(d+1)$[1]. If the nullity requirement is not met, the only possible configurations of the structure will be in a subspace of a lower dimension. For example, form finding in 3 dimensions would only be able to produce planar equilibrium configurations (Tibert and Pellegrino, 2003). The significance of this requirement will be further elucidated in section 2.3, when affine transformations are introduced. If $\tilde{\mathbf{\Omega}}$ has a nullity equal to $d(d+1)$, we shall describe it as being of *maximal rank.*

2.2.2 Tangent stiffness matrix

Stability analysis considers small changes from an equilibrium position. For a prestressed structure account must be taken not only of the deformation of the elements and the consequent changes in internal tension, but also of the effects of the changing geometry on the orientation of already stressed elements. This results in the *tangent stiffness matrix* $\mathbf{K}_t$, that relates infinitesimal displacements $\mathbf{d}$ to force perturbations $\mathbf{f}$

$$\mathbf{K}_t\mathbf{d} = \mathbf{f}. \tag{2.5}$$

---

[1] The nullity of a square matrix is equal to its dimension minus its rank.

The tangent stiffness matrix is well-known in structural analysis, and many different formulations for it exist (e.g. Murakami, 2001; Masic et al., 2005). Different formulations with identical underlying assumptions will produce identical numerical results, but may provide a different *understanding* of the stiffness. The formulation used in this paper is derived by Guest (2006), and incorporates large strains. It is written as

$$\begin{aligned}\mathbf{K}_t &= \hat{\mathbf{K}} + \tilde{\boldsymbol{\Omega}} \\ &= \mathbf{A}\hat{\mathbf{G}}\mathbf{A}^T + \tilde{\boldsymbol{\Omega}}\end{aligned} \tag{2.6}$$

where $\tilde{\boldsymbol{\Omega}}$ is the stress matrix as described earlier, $\hat{\mathbf{K}}$ is the *modified material stiffness matrix*, $\mathbf{A}$ is the *equilibrium matrix* for the structure and $\hat{\mathbf{G}}$ is a diagonal matrix whose entries consist of the *modified axial stiffness* for each of the members. The modified axial stiffness $\hat{g}$ is defined as

$$\hat{g} = g - \omega \tag{2.7}$$

where g is the conventional axial stiffness and ω the tension coefficient. For conventional members, $\hat{g}$ will be little different from g. It will certainly always be positive, and hence the matrix $\hat{\mathbf{G}}$ will always be positive definite. However, for a zero-free-length spring, because the tension t is proportional to the length, $t = gl$, the tension coefficient is equal to the axial stiffness, $\omega = t/l = g$, and the modified axial stiffness $\hat{g} = g - \omega = 0$. Thus structures constructed with zero-free-length springs will have zeros along the diagonal of $\hat{\mathbf{G}}$ corresponding to these members, and $\hat{\mathbf{G}}$ will now only be positive *semi*-definite.

Normally, a zero axial stiffness would be equivalent to the removal of that member (Deng and Kwan, 2005). This is not the case for the zero modified axial stiffness of zero-free-length springs, because the contribution of the member is still present in the stress matrix $\tilde{\boldsymbol{\Omega}}$. This leads to the observation that for zero-free-length springs the geometry (i.e. the equilibrium matrix $\mathbf{A}$) is irrelevant and only the tension coefficient and member connectivity (i.e. the stress matrix $\tilde{\boldsymbol{\Omega}}$) define their reaction to displacements.

2.2.3 Zero-stiffness modes and internal mechanisms

The main interest of this paper lies in displacements that have a zero stiffness; in other words, displacements that are in the *kernel*, or *nullspace*, of the tangent stiffness matrix. A zero tangent stiffness for some deformation $\mathbf{d}$ requires, from equation 2.6, either that $\hat{\mathbf{K}}\mathbf{d} = -\tilde{\boldsymbol{\Omega}}\mathbf{d}$, or that both $\hat{\mathbf{K}}\mathbf{d}$ and $\tilde{\boldsymbol{\Omega}}\mathbf{d}$ are zero. We will briefly discuss in section 2.3.3 why the first possibility is not of interest, and will concentrate on the second case, i.e. $\mathbf{d}$ lies in the nullspace of both $\hat{\mathbf{K}}$ and $\tilde{\boldsymbol{\Omega}}$.

For a conventional structure, as $\hat{\mathbf{G}}$ is positive definite, the nullspace of $\hat{\mathbf{K}} = \mathbf{A}\hat{\mathbf{G}}\mathbf{A}^T$ is equal to the nullspace of $\mathbf{A}^T$, and hence $\mathbf{A}^T\mathbf{d} = \mathbf{0}$. The matrix $\mathbf{C} = \mathbf{A}^T$ is the *compatibility matrix* (closely related to the *rigidity matrix* in rigidity theory) of the structure, and the extension of members $\mathbf{e}$ is given by $\mathbf{C}\mathbf{d} = \mathbf{e}$; i.e. $\mathbf{e} = \mathbf{0}$ for a zero-stiffness mode. Thus, for a conventional structure a zero tangent stiffness requires the deformation to be an *internal mechanism*: a deformation that to first order causes no member elongation. In addition $\tilde{\mathbf{\Omega}}\mathbf{d}$ must be zero, which implies that the mechanism is not stabilized by the self-stress in the structure. One obvious mode is that rigid-body displacements of the entire structure will have no stiffness. However, in general there may also be other non-stiffened (higher-order) infinitesimal, or even finite, internal mechanisms present (see e.g., Pellegrino and Calladine, 1986; Kangwai and Guest, 1999). Infinitesimal mechanisms may eventually stiffen due to the higher-order elongations of members, but finite internal mechanisms have no stiffness over a finite path. Thus, the stability of a structure requires that all displacements have a positive stiffness. This means that, modulo rigid-body motions, all eigenvalues of the tangent stiffness matrix are positive and the matrix is thus positive definite.

Some of the above observations change when a structure includes zero-free-length springs, which have modified axial stiffness $\hat{g} = 0$. A key observation is that the nullspace of $\hat{\mathbf{K}} = \mathbf{A}\hat{\mathbf{G}}\mathbf{A}^T$ is no longer the same as the nullspace of $\mathbf{A}^T$, as $\hat{\mathbf{G}}$ is now only positive semi-definite. The increased nullity of the modified material stiffness matrix $\hat{\mathbf{K}}$ is of great importance to this study, as it will prove to be key to finding the desired zero-stiffness modes (see section 2.3). Note that the stress matrix $\tilde{\mathbf{\Omega}}$ is invariant when zero-free-length springs are added to the structure.

We introduce the term '*statically balanced zero-stiffness mode*' to distinguish between zero-stiffness modes found in conventional tensegrity structures, such as internal mechanisms and rigid-body motions, and (finite) zero-stiffness modes introduced by the presence of zero-free-length springs. In contrast with (finite) internal mechanisms, these latter modes involve first-order changes in member length, and thus energy exchange among the members.

2.3 Affine transformations and zero-stiffness modes

This section introduces the concept of affine transformations, leading up to the key conclusion that affine transformations that preserve the length of 'conventional' members are statically balanced zero-stiffness modes that are valid over finite displacements. It shall further be argued that for prestress stable tensegrity structures with a positive semi-definite stress matrix of maximal rank, these are the only possible zero-stiffness modes.

2.3.1 Affine transformations

As described in section 2.2.1, the equilibrium position of a freestanding tensegrity structure for a given state of self-stress is given by $\tilde{\mathbf{\Omega}}\mathbf{p} = \mathbf{0}$. Under an *affine transformation* of the nodal coordinates $\mathbf{p}$ this condition still holds (Connelly and Whiteley, 1996; Masic et al., 2005), and hence the new geometry is also in equilibrium for the same set of tension coefficients. An important consequence which had previously not explicitly been observed, is that affine transformations of $\mathbf{p}$ hence remain in the nullspace of $\tilde{\mathbf{\Omega}}$.

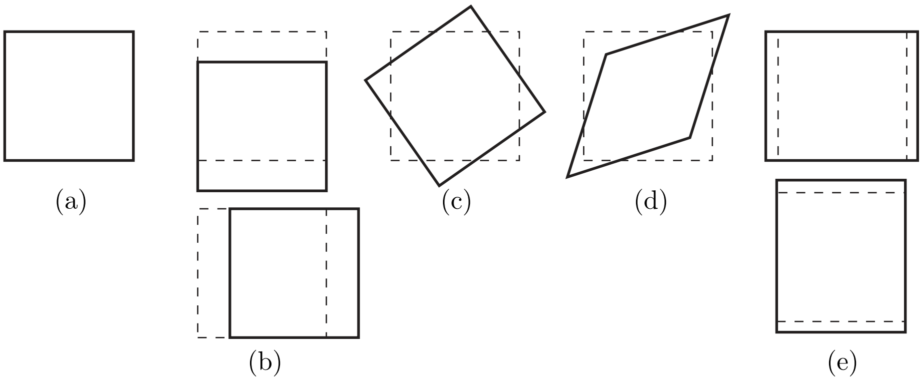

Figure 2.2: The independent affine transformations of an object (a) in 2D space are: (b) two translations, (c) one rotation, (d) one shear, (e) two dilations. The total of 6 transformations complies with the $d(d+1)$ formula for $d = 2$.

Affine transformations are linear transformations of coordinates (of the whole affine plane onto itself) preserving collinearity. Thus, an affine transformation transforms parallel lines into parallel lines and preserves ratios of distances along parallel lines, as well as intermediacy (Coxeter, 1989, pp. 202). We write them as the transformation of the coordinates of node i

$$\mathbf{p}_i \rightarrow \mathbf{U}\mathbf{p}_i + \mathbf{w}$$

where in d-dimensional space $\mathbf{U}$ is a d-by-d matrix, and $\mathbf{w} \in E^d$. This provides a total of $d(d+1)$ independent affine transformations. Affine transformations are well-known to engineers, but under a different guise. Recall that the square matrix $\mathbf{U}$ can be expressed as the sum of a symmetric and a skew-symmetric component. Then the half of the $d(d+1)$ affine transformations constituted by $\mathbf{w}$ and the skew-symmetric part of $\mathbf{U}$, is better known to engineers as rigid-body motions (e.g. 6 rigid-body motions in 3-dimensional space). The interpretation of the other half – the symmetric part of $\mathbf{U}$ – is less obvious, but it turns out to be equivalent to the basic strains found in continuum mechanics: shear and dilation. For instance, for a 3-dimensional strain, infinitesimal affine deformations give the six independent strain quantities (e_{xx}, e_{yy}, e_{zz}, e_{xy}, e_{xz}, e_{yz}) (Love, 1927). For two dimensions, the complete set of affine transformations is shown in Figure 2.2.

It is obvious that the equilibrium of a tensegrity structure holds for rigid-body motions, but it is less clear for the other affine transformations. This knowledge can be used to great advantage in form finding to obtain new equilibrium shapes (Masic et al., 2005), but it also has important consequences for static balancing and the study of zero-stiffness modes. The above also clarifies the $\mathcal{N} \geq d(d+1)$ nullity requirement for $\tilde{\mathbf{\Omega}}$ found in form finding: there must be at least $d(d+1)$ affine transformations in the kernel of $\tilde{\mathbf{\Omega}}$ if a solution for the form finding is to be found in d-space – provided there are sufficient nodes to span d-space.

2.3.2 Statically balanced zero-stiffness modes

A structure has a zero stiffness if for a given displacement vector $\mathbf{d}$ – in the nullspace of the tangent stiffness matrix $\mathbf{K}_t$ – the following equation

$$\begin{aligned} \mathbf{K}_t\mathbf{d} &= \hat{\mathbf{K}}\mathbf{d} + \tilde{\mathbf{\Omega}}\mathbf{d} \\ &= \mathbf{A}\hat{\mathbf{G}}\mathbf{A}^T\mathbf{d} + \tilde{\mathbf{\Omega}}\mathbf{d} = \mathbf{0} \end{aligned} \tag{2.8}$$

returns zero. We focus here on the situation where both $\mathbf{A}\hat{\mathbf{G}}\mathbf{A}^T\mathbf{d}$ and $\tilde{\mathbf{\Omega}}\mathbf{d}$ are zero – other possibilities are discussed in section 2.3.3. We shall exclude internal mechanisms by only considering tensegrity structures that when built with conventional elements would be stable for the given state of self-stress. Conventional elements are here understood to be tensile or compressive members that have a positive modified axial stiffness. Consequently, any zero-stiffness modes would be a result of the use of zero-free-length springs.

As shown in section 2.3.1, affine transformations of the coordinates $\mathbf{p}$ are in the nullspace of $\tilde{\mathbf{\Omega}}$. For a conventional structure, these modes (excluding the rigid-body motions) are stabilized by the modified material stiffness matrix $\hat{\mathbf{K}}$. For structures with zero-free-length springs, however, the positive *semi*-definiteness of $\hat{\mathbf{G}}$ and the resulting increased nullity in $\hat{\mathbf{K}}$ will result in new zero-stiffness modes. The key therefore is in understanding the solutions to $\mathbf{A}\hat{\mathbf{G}}\mathbf{A}^T\mathbf{d} = \mathbf{0}$. If a displacement $\mathbf{d}$ is length-preserving for the conventional members, then

$$\mathbf{A}^T\mathbf{d} = \mathbf{e} \tag{2.9}$$

returns zero-elongations for those conventional members. Now consider that

$$\hat{\mathbf{G}}\mathbf{A}^T\mathbf{d} = \hat{\mathbf{G}}\mathbf{e} \tag{2.10}$$

always returns zeros for the zero-free-length springs and non-zero for conventional members, due to the zero modified axial stiffness on the diagonal of $\hat{\mathbf{G}}$. Thus, a displacement $\mathbf{d}$ that preserves the length of conventional elements will satisfy $\hat{\mathbf{G}}\mathbf{A}^T\mathbf{d} = \mathbf{0}$ and will hence be in the nullspace of $\mathbf{A}\hat{\mathbf{G}}\mathbf{A}^T$. Combining these observations, it is clear that for an affine transformation that preserves the length of conventional members, both $\hat{\mathbf{K}}\mathbf{d}$ and $\tilde{\mathbf{\Omega}}\mathbf{d}$ are zero and there is a statically balanced zero-stiffness mode. This is illustrated by the simple statically balanced structure shown in Figure 2.3.

Note that when a member length remains constant, so does the tension and thus the tension coefficient. This also follows from the fact that the stress matrix $\tilde{\mathbf{\Omega}}$ remains invariant under the affine transformation that results in new equilibrium, and therefore, so do the tension coefficients. For zero-free-length springs the tension coefficient is equal to their spring stiffness and will therefore always be constant, but for conventional members the only way a tension coefficient can remain constant is when both length and tension are invariant.

Any modes in the tangent stiffness matrix are per definition infinitesimal displacements. This leads to the question whether the aforementioned statically balanced zero-stiffness modes merely hold for infinitesimal, or also for finite deformations. The independence of the zero-free-length springs of their actual

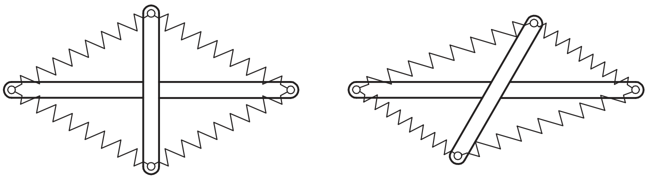

Figure 2.3: Example of a 2D statically balanced structure consisting of two unconnected bars of differing lengths, and four zero-free-length springs of equal stiffness. When the bars are rotated with respect to each other, they remain in equilibrium and their movement thus has zero stiffness. In this example it is clear that the statically balanced mode is a combined shear and scale operation which preserves the bar lengths. Figure adapted from Herder (2001).

geometrical position for their contribution to $\mathbf{K}_t$, suggests an affirmative answer to this question. Formalization of the fact that they are indeed *finite* zero-stiffness modes, takes a different approach, and will be deferred to section 4.3 as it requires additional information.

2.3.3 Additional zero-stiffness modes

Using equation 2.6 for the tangent stiffness matrix, there are two distinct ways the structure may have zero stiffness. Either the contributions of $\hat{\mathbf{K}}$ and $\tilde{\mathbf{\Omega}}$ cancel out, or both are zero.

The situation where $\hat{\mathbf{K}}\mathbf{d} = -\tilde{\mathbf{\Omega}}\mathbf{d}$ is not fully understood, and no example structures are known to the authors. For conventional structures it would also seem a rather unlikely situation as for small strains the contributions of $\hat{\mathbf{K}}$ are generally an order of magnitude greater than those of $\tilde{\mathbf{\Omega}}$. Furthermore it would require the stress matrix $\tilde{\mathbf{\Omega}}$ to have negative eigenvalues, which is undesirable as it may make the structure unstable under certain loading conditions.

Throughout the previous sections we have focused on the case where the zero-stiffness mode is in the nullspace of both components of the tangent stiffness matrix. When zero-free-length springs are added to the structure, the nullspace of the stress matrix is invariant, but the nullspace of $\hat{\mathbf{K}}$ changes significantly. If the newly introduced nullvectors coincide with an affine transformation, the structure has zero stiffness. However, the nullspace of $\tilde{\mathbf{\Omega}}$ is in general not limited to the affine transformations, and theoretically more combinations of the two nullspaces of $\hat{\mathbf{K}}$ and $\tilde{\mathbf{\Omega}}$ are possible. It is beyond the scope of this paper to systematically analyse all possible combinations that produce a zero stiffness.

The situation is considerably simpler when considering structures with a positive semi-definite stress matrix of maximal rank, which are prestress stable when constructed with solely conventional members. Under these conditions the length-preserving affine transformations are the only possible zero-stiffness modes. The maximal rank condition ensures that only affine transformations are in the nullspace of the stress matrix, and by virtue of the prestress stability condition those are not internal mechanisms. The positive semi-definiteness requirement ensures that there are no negative eigenvalues in the stress matrix that can cause zero stiffness by the contributions of $\hat{\mathbf{K}}$ and $\tilde{\mathbf{\Omega}}$ cancelling each other out: $\hat{\mathbf{K}}\mathbf{d} = -\tilde{\mathbf{\Omega}}\mathbf{d}$. These are not considered restrictive requirements as many classic tensegrity structures already seem to comply.

The above conditions provide an additional benefit, as they ensure that any internal mechanisms remain stabilized by the state of self-stress throughout the displacement along the finite affine transformation. The number of internal mechanisms will always remain constant under an affine transformation, as the rank of the equilibrium matrix is constant under a linear transformation (with the exception of a projection on a lower dimension). Disregarding the latter scenario, in all other cases the maximal rank positive semi-definite stress matrix (which is invariant under the affine transformation) will ensure that the state of self-stress will always impart a first-order stiffness to the internal mechanisms.

2.4 Length-preserving affine transformations

In the previous section it has been shown that an affine transformation preserving the length of conventional members is a statically balanced zero-stiffness mode. In this section we will show that such a transformation exists if and only if the directions of the conventional members lie on a conic. The conic form will also prove to be useful in establishing the finiteness of the found zero-stiffness mode.

2.4.1 Length preservation and conic form

In order to understand under which circumstances the length of a member increases, decreases or stays the same under an affine transformation, we shall investigate the squares of the lengths of the members under the affine transformation given by $\mathbf{p}_i \rightarrow \mathbf{U}\mathbf{p}_i + \mathbf{w}$, where $\mathbf{U}$ is a d-by-d matrix, $\mathbf{w} \in E^d$, and $\mathbf{p}_i, \mathbf{p}_j$ are the nodal coordinates:

$$\begin{aligned}
L^2 - L_0^2 &= |(\mathbf{U}\mathbf{p}_i + \mathbf{w}) - (\mathbf{U}\mathbf{p}_j + \mathbf{w})|^2 - |\mathbf{p}_i - \mathbf{p}_j|^2 \\
&= (\mathbf{p}_i - \mathbf{p}_j)^T \mathbf{U}^T \mathbf{U} (\mathbf{p}_i - \mathbf{p}_j) - (\mathbf{p}_i - \mathbf{p}_j)^T \mathbf{I}^d (\mathbf{p}_i - \mathbf{p}_j) \\
&= (\mathbf{p}_i - \mathbf{p}_j)^T [\mathbf{U}^T \mathbf{U} - \mathbf{I}^d] (\mathbf{p}_i - \mathbf{p}_j) \\
&= \mathbf{v}^T \mathbf{Q} \mathbf{v}
\end{aligned}$$

where $\mathbf{I}^d$ denotes the d-dimensional identity matrix, and $\mathbf{v} = (\mathbf{p}_i - \mathbf{p}_j)$ is the member direction. From this calculation it is clear that the symmetric matrix $\mathbf{Q} = \mathbf{U}^T\mathbf{U} - \mathbf{I}^d$ and its associated quadratic form determine when member lengths increase, decrease or stay the same.

We are interested in the situation where $\mathbf{v}^T\mathbf{Q}\mathbf{v} = 0$. For the case of $d = 3$, with directions $\mathbf{v}^T = [v_x\, v_y\, v_z]$ and components of the symmetric $\mathbf{Q}$ given as $q_{kl} = q_{lk}$, this would take the following form

$$v_x^2 q_{11} + 2v_x v_y q_{12} + 2v_x v_z q_{13} + v_y^2 q_{22} + 2v_y v_z q_{23} + v_z^2 q_{33} = 0. \tag{2.11}$$

Equation 2.11 defines a quadratic curve, which (in nondegenerate cases) corresponds to the intersection of a plane with (one or two nappes of) a cone: a conic section (Weisstein, 1999). We can now see that a set of directions defined by

$$C = \{\mathbf{v} \in E^d \,|\, \mathbf{v}^T\mathbf{Q}\mathbf{v} = 0\} \tag{2.12}$$

forms a conic at infinity. This conic is clearly defined since scalar multiples of a vector satisfy the same quadratic equation, including the reversal of direction by a negative scalar. Generally one would expect C to be the set of lines from the origin to the points of, for example, an ellipse in some plane not through the origin (see Figure 2.4).

Supposing D is a set of directions in d-space, then there is an affine transformation $\mathbf{p}_i \to \mathbf{U}\mathbf{p}_i + \mathbf{w}$ that is not a rigid-body motion and that preserves lengths in the directions in D if and only if the directions in D lie on a conic at infinity. Or conversely, when the directions of certain members (in our case conventional elements) lie on a conic given by $\mathbf{Q} = \mathbf{U}^T\mathbf{U} - \mathbf{I}^d$, their length will remain constant under the affine transformation $\mathbf{U}$.

Of interest here are structures where all the conventional member directions lie on a conic, as the corresponding affine transformations will have zero stiffness. This is for instance clear for the structures shown in Table 2.1, where all the bar directions lie on a conic and the other members are zero-free-length springs. This leads to the observation that all the rotationally symmetric tensegrity structures discussed by Hinrichs (1984) and by Connelly and Terrell (1995) can have zero stiffness, when the cables are replaced by appropriate zero-free-length springs.

2.4.2 Number of zero-stiffness modes

Using the conic form, the number of independent length-preserving affine transformations of the structure can easily be determined. It holds that five points in a plane – no three of which collinear – uniquely determine a conic. This follows from the fact that a conic section is a quadratic curve; e.g. dividing equation 2.11 by q_{11} leaves 5 constants. If there are less points, the conic is not uniquely defined and there exists more than one conic that satisfies the quadratic curve.

As shown previously, when all conventional member directions lie on a conic there exists a length-preserving affine transformation which has zero stiffness. However, if there are less than five unique member directions (i.e. unique points on the conic section) there exists more than one conic, and thus more than one length-preserving affine transformation. The number of *additional* conics (and thus zero-stiffness modes) is found by subtracting the number of unique points on the conic section from the five required for uniqueness.

The above can now be summarized in the following counting rule for determining the number of zero-stiffness modes. Provided that all conventional member directions $\mathbf{v}_i$ lie on a conic, and with k unique points on the conic section, the number of zero-stiffness modes is given by

$$\begin{array}{lcrl} k \geq 6 & \rightarrow & 1 & \text{zero-stiffness mode} \\ k < 6 & \rightarrow & (6-k) & \text{zero-stiffness modes} \end{array} \tag{2.13}$$

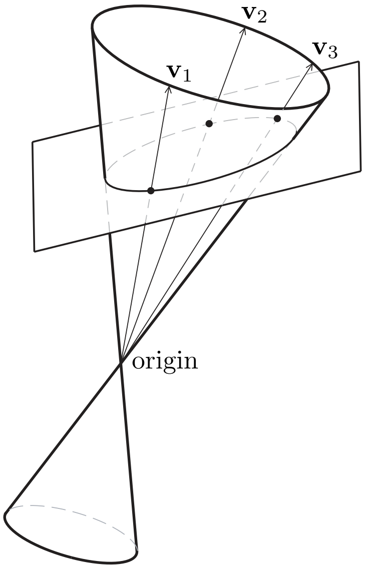

Figure 2.4: A conic intersected by a plane generates a conic section, which is a quadratic curve such as an ellipse, parabola or hyperbola. The directions $\mathbf{v}_i$ on the conic project onto points on the conic section.

Table 2.1: Number of statically balanced zero-stiffness modes for several rotationally symmetric tensegrity structures discussed by Hinrichs (1984). All bar directions lie on a conic, and thus when using appropriate zero-free-length springs the structures will have zero stiffness. The number of bar directions on the conic and the number of zero-stiffness modes fit the counting rule established in section 2.4.2.

	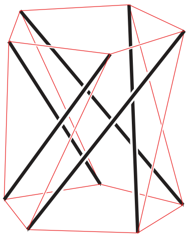	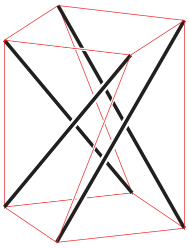	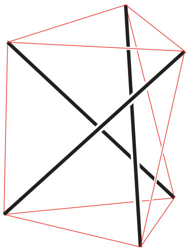
Bar directions on conic	5	4	3
Zero-stiffness modes	1	2	3

Note that only the number of member directions is relevant, not the number of members. In other words, parallel members share a common member direction, and project onto a single point on the conic section. Furthermore, it is as yet unclear how to deal with two-dimensional structures, or structures that are projected onto a lower dimension and are reduced to a planar configuration.

2.4.3 Finiteness of zero-stiffness mode

The conic form is also valuable for showing the finiteness of the statically balanced zero-stiffness modes. If the conventional members lie on a conic, as by previous discussion, there exists an affine transformation that has zero stiffness. If we follow that zero stiffness path for an infinitesimal step, then in the new geometry, because the step is an affine transformation, there will exist a new conic on which the conventional members lie, and hence there will again be a zero-stiffness mode. As a result, the statically balanced zero-stiffness mode will be finite.

2.5 Example

This section describes the numerical analysis of the classic tensegrity structure shown in Figure 2.5. Both the nature and number of the calculated zero-stiffness modes fit the theory laid down in previous sections. This is further illustrated by the construction of a physical model.

2.5.1 Numerical analysis

It is expected that when the cables are replaced by zero-free-length springs, the structure will have three zero-stiffness modes, and that these modes are affine transformations preserving the length of the three bars. This follows from the observation that the structure has three bar directions on a conic, and thus by equation 2.13 there are three independent zero-stiffness modes.

The tangent stiffness of the structure has been found using the formulation of equation 2.6 for two different cases. Firstly, with the structure consisting of conventional elements, and secondly, when made from conventional compressive bars, but using zero-free-length springs as tension members. The equilibrium configuration has been calculated with the analytical solution of Connelly and Terrell (1995), and the level of self-stress – and thus the stress matrix – is identical for both cases. All conventional elements have a 'stiffness' of $EA = 100$N, the horizontal springs 1N/m and the vertical springs $\sqrt{3}$N/m. The internal tension of the structure is uniquely prescribed by these spring stiffnesses. The results are presented as the stiffness of each of the eigenmodes (excluding rigid-body motions) in Tables 2.2(a) and 2.2(b).

For the conventional structure all eigenvalues of the tangent stiffness matrix are positive, and the stress matrix is of maximal rank. The system has an internal mechanism, which is stabilized by the state of self-stress. This can be seen in

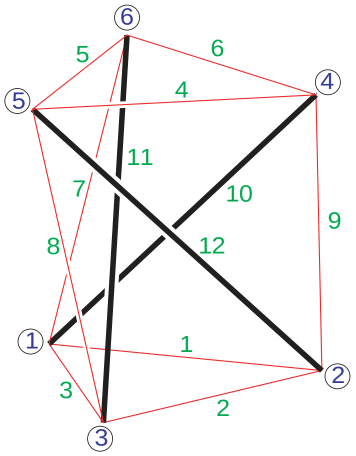

Figure 2.5: Rotationally symmetric tensegrity structure. The structure has a circumscribing radius $R = 1$, height $H = 2$ and the two parallel equilateral triangles (nodes 1–3 and nodes 4–6) are rotated $\pi/6$ with respect to eachother.

Table 2.2: Stiffness of each of the eigenmodes, excluding rigid-body motions, for (a) the conventional structure and (b) the structure with zero-free-length springs as tension members. The total stiffness $\mathbf{K}_t$ is the sum of the contributions of $\hat{\mathbf{K}}$ and $\tilde{\mathbf{\Omega}}$.

(a)

$\mathbf{K}_t$	$\hat{\mathbf{K}}$	$\tilde{\mathbf{\Omega}}$
5.6304	0.0174	5.6130
27.8384	26.1960	1.6424
27.8384	26.1960	1.6424
83.2190	79.1954	4.0236
83.2190	79.1954	4.0236
107.3763	103.0749	4.3014
107.3763	103.0749	4.3014
113.8525	113.5350	0.3175
132.5068	130.4743	2.0325
132.5068	130.4743	2.0325
176.2051	170.2051	6.0000
225.4577	225.3881	0.0696

(b)

$\mathbf{K}_t$	$\hat{\mathbf{K}}$	$\tilde{\mathbf{\Omega}}$
0.0000	0.0000	0.0000
0.0000	0.0000	0.0000
0.0000	0.0000	0.0000
5.6703	0.0267	5.6436
5.6703	0.0267	5.6436
5.7899	0.0174	5.7724
6.0000	0.0000	6.0000
6.0000	0.0000	6.0000
6.0000	0.0000	6.0000
75.5997	75.3721	0.2276
75.7193	75.3629	0.3564
75.7193	75.3629	0.3564

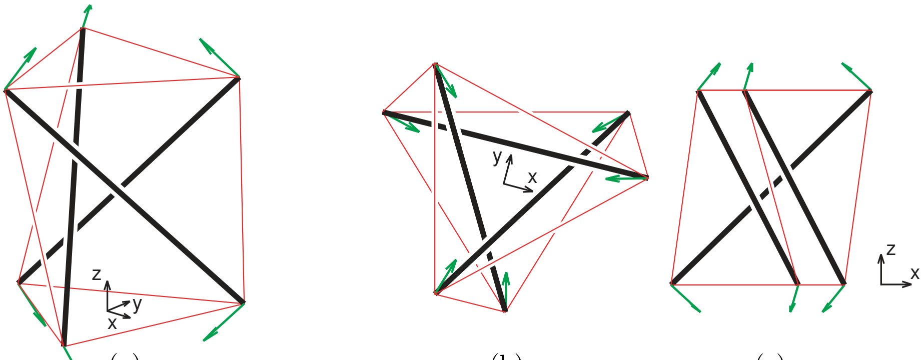

(a) (b) (c)

Figure 2.6: Fully symmetric zero-stiffness mode, with (a) 3D view, (b) top view and (c) side view. All displacement vectors are of equal magnitude, and with equal z-component. In this mode the rotation angle between bottom and top triangle remains constant throughout the displacement.

the first line of Table 2.2(a), where the $\hat{\mathbf{K}}$ component is almost zero (it is not precisely zero because the eigenvectors of $\hat{\mathbf{K}}$ and $\mathbf{K}_t$ are not precisely aligned).

When zero-free-length springs are placed in the structure, three new zero-stiffness modes appear in $\mathbf{K}_t$ – the first three rows of Table 2.2(b) – which are linearly dependent on the affine transformations for shear and dilation. These modes can be considered in a symmetry-adapted form (Kangwai and Guest, 1999) as a totally symmetric mode, and a pair of modes that are symmetric and antisymmetric with respect to a dihedral rotation. The fully symmetric mode is shown in Figure 2.6. It is purely dependent on scaling transformations, and corresponds to a mode where the structure is compressed in the x-y plane and expands in the z-direction.

In conclusion, the numerical results confirm the theoretical predictions: the zero-stiffness modes correspond to affine transformations, the bar lengths remain constant – **Cd** returned zero for the bars – and the number of introduced zero-stiffness modes fits the counting rule established in section 2.4.2.

2.5.2 Physical model

To illustrate that the zero stiffness tensegrity structure is not merely mathematical, a demonstration prototype was constructed. It does not make use of actual zero-free-length springs, but of conventional springs that are attached alongside the bars such that the properties of zero-free-length springs are emulated. As gravity forces were not taken into account in the calculations, if perfectly constructed, the prototype would collapse under its own weight. The friction in the system prevents this from happening, however. As a result the structure requires some external work to deform, but it will nevertheless remain in equilibrium over a wide range of positions (see Figure 2.7).

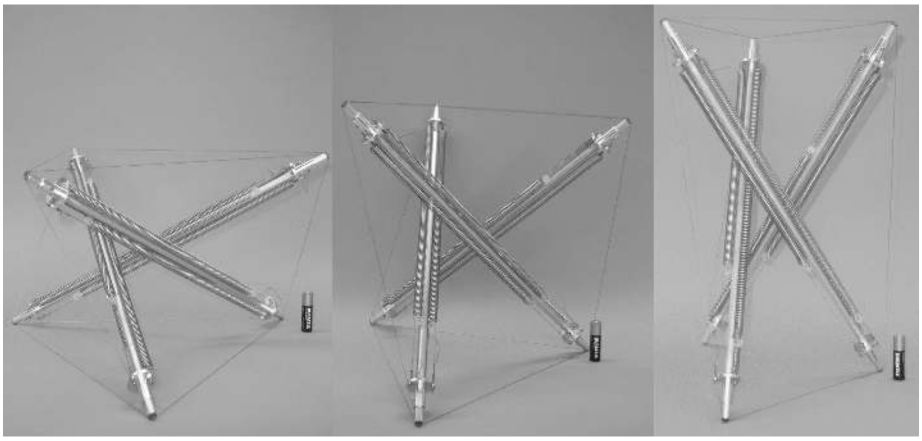

Figure 2.7: The demonstration model deformed in accordance with the symmetrical zero-stiffness mode. The three positions shown do not correspond to the extremes of the working range, as further deformation is still possible.

2.6 Summary and Conclusions

This paper has investigated the zero-stiffness modes introduced to tensegrity structures by the presence of zero-free-length springs. It was shown that under absence of external loads and constraints, affine transformations that preserve the length of conventional members are statically balanced zero-stiffness modes. Those modes involve changing spring lengths, but require no energy to move, even over large displacements. For prestress stable tensegrities with a positive semi-definite stress matrix of maximal rank, we further showed that these are the only possible zero-stiffness modes introduced by the zero-free-length springs.

A general existence criterion was derived, and it was shown that such length-preserving affine transformations are present if and only if the directions of the conventional elements lie on a conic. This geometric interpretation revealed an entire family of tensegrity structures that can exhibit zero stiffness. A simple counting rule was also found, which provides the number of independent length-preserving affine transformations.

By only considering tensegrity structures, the theory in this paper has several inherent restrictions. Future work will attempt to resolve these aspects, starting with the inclusion of external loads and nodal constraints in the analysis of pin-jointed structures. The next phase would be to apply the acquired knowledge to non-pin-jointed structures, in order to describe statically balanced structures such as the ‘Anglepoise’ lamp in a generic way.

Finally, the construction of the physical model has illustrated that this type of structure is not yet suited for practical applications. Once difficulties such as accuracy of spring stiffness ratio, presence of friction and overall complexity of design have been overcome, a totally new class of structures, or mechanisms, will be available to engineers.

Acknowledgements

The authors wish to thank Professor Connelly (Cornell University) for the insight and proof of the link between conic form and length-preserving affine transformations described in section 2.4.

Bibliography

Connelly, R., Terrell, M., 1995. Globally Rigid Symmetric Tensegrities. Structural Topology 21, 59–77.

Connelly, R., Whiteley, W., 1992. The Stability of Tensegrity Frameworks. International Journal of Space Structures 7 (2), 153–163.

Connelly, R., Whiteley, W., 1996. Second-order rigidity and prestress stability for tensegrity frameworks. SIAM Journal of Discrete Mathematics 7 (3), 453–491.

Coxeter, H. S. M., 1989. Introduction to geometry, 2nd Edition. John Wiley & sons, inc.

Deng, H., Kwan, A. S. K., 2005. Unified classification of stability of pin-jointed bar assemblies. International Journal of Solids and Structures 42 (15), 4393–4413.

French, M. J., Widden, M. B., 2000. The spring-and-lever balancing mechanism, George Carwardine and the Anglepoise lamp. Proceedings of the Institution of Mechanical Engineers part C – Journal of Mechanical Engineering Science 214 (3), 501–508.

Guest, S. D., 2006. The stiffness of prestressed frameworks: A unifying approach. International Journal of Solids and Structures 43 (3–4), 842–854.

Herder, J. L., 2001. Energy-Free Systems. Theory, conception and design of statically balanced spring mechanisms. Ph.D. thesis, Delft University of Technology.

Hinrichs, L. A., 1984. Prismic Tensigrids. Structural Topology 9, 3–14.

Kangwai, R. D., Guest, S. D., 1999. Detection of finite mechanisms in symmetric structures. International Journal of Solids and Structures 36 (36), 5507–5527.

Love, A. E. H., 1927. A treatise on the mathematical theory of elasticity, 4th Edition. Dover publications.

Masic, M., Skelton, R. E., Gill, P. E., 2005. Algebraic tensegrity form-finding. International Journal of Solids and Structures 42 (16–17), 4833–4858.

Motro, R., 1992. Tensegrity Systems: The State of the Art. International Journal of Space Structures 7 (2), 75–83.

Murakami, H., 2001. Static and dynamic analyses of tensegrity structures. Part II. Quasi-static analysis. International Journal of Solids and Structures 38, 3615–3629.

Pellegrino, S., Calladine, C. R., 1986. Matrix analysis of statically and kinematically indeterminate frameworks. International Journal of Solids and Structures 22 (4), 409–428.

Tarnai, T., 2003. Zero stiffness elastic structures. International Journal of Mechanical Sciences 45 (3), 425–431.

Tibert, A. G., Pellegrino, S., 2003. Review of Form-Finding Methods for Tensegrity Structures. International Journal of Space Structures 18 (4), 209–223.

Weisstein, E. W., 1999. Conic Section. From Mathworld – a Wolfram Web Resource. http://mathworld.wolfram.com/ConicSection.html.

Chapter 3

Overview of Zero Stiffness in Prestressed Bar Frameworks

M.Schenk[a]

[a] *Mechanical, Maritime and Materials Engineering, Delft University of Technology, Mekelweg 2, 2628 CD Delft, The Netherlands*

Abstract

When a prestressed structure exhibits zero stiffness, this is traditionally considered undesirable as it is associated with internal mechanisms. There exist, however, other types of zero stiffness, which involve first-order changes in bar length, and where the structure remains in equilibrium over a continuous range of motion. This paper catalogues and describes the current state of knowledge considering the zero-stiffness modes in prestressed pin-jointed bar structures by systematically analysing the components of the tangent stiffness matrix.

Keywords: zero stiffness, internal mechanisms, prestressed bar frameworks, affine transformations

3.1 Introduction

Conventional wisdom in the design of prestressed structures dictates that zero stiffness is undesirable; it is associated with internal mechanisms, which result in “floppy” structures. As a result zero stiffness has not been studied systematically in the past, and only occasional examples have appeared in literature (e.g. Tarnai, 2003). This lack of attention is based on the mistaken premise that zero stiffness is always related to internal mechanisms, and therefore always undesirable.

As shown in Herder (2001) there exist structures that are in equilibrium over a continuous range of positions, and are thus neutrally stable and have zero stiffness. A classic example is the 'Anglepoise' lamp, that can be placed into any position without external force. Those statically balanced systems employ a special type of spring that is pretensioned such that it has a zero free length in its working range. The existence of such systems prompted research on how to include the zero-free-length springs in pretensioned structures. Schenk et al. (2006) described the case of zero stiffness tensegrity structures, and found an entire class of structures that exhibit zero stiffness. The zero stiffness described there involves changing member lengths – and thus the energy exchange among members – and is valid over a finite range of motion.

Not only do some types of zero stiffness provide interesting engineering applications (namely those valid over a continuous range of positions), but understanding the various types of zero-stiffness modes can also provide greater insight into the mechanical properties of structures in general.

This paper complements the results in Schenk et al. (2006), and therefore limits itself to tensegrity structures: self-stressed, unloaded and unconstrained pin-jointed bar frameworks. This means that effects such as buckling (and corresponding bifurcations) are not considered. The aim of this paper is then to catalogue and describe the zero stiffness of free-standing prestressed structures by systematically analysing the tangent stiffness matrix described in section 3.2 for possible zero stiffness. Two different types of zero stiffness are distinguished, depending on how the zero stiffness is obtained, and extra attention is paid to structures with zero-free-length springs. The paper finishes with a brief conclusion and a listing of topics warranting further attention.

3.2 Stiffness of prestressed structures

For the stiffness analysis of a prestressed structure, account must be taken not only of the deformation of the elements and the consequent changes in internal tension, but also of the effects of the changing geometry on the orientation of already stressed elements. This results in the *tangent stiffness matrix* $\mathbf{K}_t$ that relates infinitesimal displacements $\mathbf{d}$ to force perturbations $\mathbf{f}$

$$\mathbf{K}_t\mathbf{d} = \mathbf{f}. \tag{3.1}$$

The tangent stiffness matrix is well-known in structural analysis, and many different formulations for it exist. Different formulations with identical underlying assumptions will produce identical numerical results, but may provide a different *understanding* of the stiffness. The formulation used in this paper is derived by Guest (2006) and it incorporates large strains. It is written as

$$\begin{aligned} \mathbf{K}_t &= \hat{\mathbf{K}} + \tilde{\mathbf{\Omega}} \\ &= \mathbf{A}\hat{\mathbf{G}}\mathbf{A}^T + \tilde{\mathbf{\Omega}} \end{aligned} \tag{3.2}$$

where $\tilde{\mathbf{\Omega}}$ is the *stress matrix*, $\hat{\mathbf{K}}$ is the *modified material stiffness matrix*, $\mathbf{A}$ is the *equilibrium matrix* for the structure and $\hat{\mathbf{G}}$ is a diagonal matrix whose entries

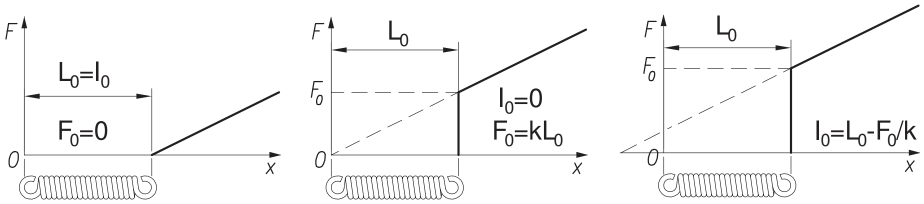

(a) (b) (c)

Figure 3.1: Springs with identical stiffness k and physical length L_0, but with a different rest length l_0 due to the varying level of pretension F_0. The springs respectively have a (a) positive, (b) zero, and (c) negative modified axial stiffness $\hat{g}$.

consist of the *modified axial stiffness* for each of the members. The modified axial stiffness $\hat{g}$ is defined as

$$\hat{g} = g - \omega \tag{3.3}$$

where g is the conventional axial stiffness and ω the *tension coefficient.* The latter is defined as the tension t divided by the length l of the member: $\omega = \frac{t}{l}$. For conventional members, $\hat{g}$ will be little different from g. It will certainly always be positive, and hence the matrix $\hat{\mathbf{G}}$ will be positive definite. However, for a zero-free-length spring, because the tension t is proportional to the length, $t = gl$, the tension coefficient is equal to the axial stiffness, $\omega = t/l = g$, and the modified axial stiffness $\hat{g} = g - \omega = 0$. Thus structures constructed using zero-free-length springs will have zeros along the diagonal of $\hat{\mathbf{G}}$ corresponding to these members, and $\hat{\mathbf{G}}$ will now only be positive *semi*-definite. This will prove to be critical for finding zero-stiffness modes in section 3.3.1. What is more, it is also possible for the modified axial stiffness to take a negative value. This is the case for springs pretensioned such that they have a negative free length in their working range. See Figure 3.1 for an overview.

A very important part is played by the stress matrix $\tilde{\mathbf{\Omega}}$. This matrix serves a dual purpose in the analysis of structures: in form-finding methods for tensegrities it is used to describe the *equilibrium* of the structure (e.g. Connelly and Whiteley, 1996), but here it returns in *stiffness* analysis. This parallel allowed the application of some ideas from form-finding to be applied to zero stiffness analysis of tensegrity structures (Schenk et al., 2006). The stress matrix is composed by summing the internal forces at each of the nodes, and when the nodal coordinates of the structure are written as a vector $\mathbf{p}$, the equilibrium is expressed as

$$\tilde{\mathbf{\Omega}}\mathbf{p} = \mathbf{0}. \tag{3.4}$$

Because the equilibrium is the same for each of the d dimensions, the stress matrix can be written as the Kronecker product of the reduced stress matrix $\mathbf{\Omega}$ and a d-dimensional identity matrix $\mathbf{I}^d$:

$$\tilde{\mathbf{\Omega}} = \mathbf{\Omega} \otimes \mathbf{I}^d. \tag{3.5}$$

Using the tension coefficients ω of each of the members – referred to as *stress* in mathematical Rigidity Theory – the coefficients of the reduced stress matrix are then given as

$$\Omega_{ij} = \begin{cases} -\omega_{ij} = -\omega_{ji} & \text{if } i \neq j, \text{ and \{i,j\} a member,} \\ \sum_{k \neq i} \omega_{ik} & \text{if } i = j, \\ 0 & \text{if there is no connection between } i \text{ and } j. \end{cases} \tag{3.6}$$

Note that the stress matrix merely contains information about element connectivity and tension coefficients, but no information about the geometry of the structure.

This formulation of the tangent stiffness matrix has proven to be especially useful, because it contains two clear links to other fields of research. The equilibrium matrix is used by Pellegrino and Calladine (1986) to analyse prestressed structures, and the stress matrix is of major importance in mathematical Rigidity Theory (e.g. Connelly and Terrell, 1995). These overlaps facilitated the use of ideas from both fields. Furthermore, the introduction of the modified axial stiffness provided crucial insight in the case of zero-free-length springs.

3.2.1 Types of zero stiffness

When a prestressed structure has zero stiffness, this means that there exist displacements $\mathbf{d}$ that require no force $\mathbf{f}$ to move (see equation 3.1). In other words, the displacements are in the nullspace, or kernel, of the tangent stiffness matrix $\mathbf{K}_t$. The objective of the coming sections is therefore to identify and understand (as far as current knowledge allows) which vectors are in its nullspace, using the formulation of equation 3.2.

In the study of zero-stiffness modes in prestressed pin-jointed structures, a first distinction can be made between zero-stiffness modes present in conventional structures (i.e. caused by topology, geometry and prestress levels), and those introduced by special elements (and specifically those with a zero rest length within their working range). There are known examples of structures, that when built with these elements have zero stiffness over a finite range of motion.

A further distinction is provided by the way the total stiffness can become zero. In the present formulation of the tangent stiffness matrix ($\mathbf{K}_t = \hat{\mathbf{K}} + \tilde{\mathbf{\Omega}}$) three possibilities for zero stiffness arise: (i) the contribution of both parts is zero, (ii) the first part is positive and the second negative, and (iii) the first part is negative (e.g. for springs with a negative rest length) and the second positive. We shall first investigate the case where the zero stiffness mode is in the nullspace of both $\hat{\mathbf{K}}$ and $\tilde{\mathbf{\Omega}}$ in section 3.3, followed in section 3.4 by the case where both contributions cancel each other out.

3.3 Zero stiffness and matrix nullspace

3.3.1 Nullspace of modified material stiffness matrix $\hat{\mathbf{K}}$

For conventional structures with a positive definite matrix $\hat{\mathbf{G}}$, the nullspace of the modified material stiffness matrix $\hat{\mathbf{K}} = \mathbf{A}\hat{\mathbf{G}}\mathbf{A}^T$ is identical to that of the *compatibility matrix* $\mathbf{C} = \mathbf{A}^T$ of the structure:

$$\mathbf{A}^T\mathbf{d} = \mathbf{C}\mathbf{d} = \mathbf{e} = \mathbf{0}.$$

The nullspace consists of nodal displacements $\mathbf{d}$ that to a first-order approximation do not result in member elongations $\mathbf{e}$. These are a combination of internal mechanisms and rigid-body motions. The presence of rigid-body motions implies that the structure is not sufficiently constrained and can move in its entirety. The internal mechanisms can subsequently be divided into infinitesimal mechanisms, which may eventually stiffen due to higher-order elongations of the members, and finite mechanisms that involve no member elongations at all. First-order infinitesimal mechanisms may be stabilized by the state of self-stress ($\tilde{\mathbf{\Omega}}$), and the stiffness is then proportional to the level of self-stress. Higher-order and finite mechanisms cannot be stabilized. As the tangent stiffness matrix can also be considered as the Hessian of the energy stored in the system, detailed study of the internal mechanisms would therefore require higher-order variations of the energy, to determine the order of the mechanism.

For structures constructed with zero-free-length springs, things change significantly. As $\hat{\mathbf{G}}$ is no longer positive definite, but positive *semi*-definite, the nullity of $\hat{\mathbf{K}}$ increases. These new zero stiffness modes correspond to deformations of the structure that preserve the lengh of conventional members (i.e. members that have a positive modified axial stiffness). As $\hat{\mathbf{G}}\mathbf{A}^T\mathbf{d} = \hat{\mathbf{G}}\mathbf{e}$ will return zeros for the entries corresponding to the zero-free-length springs, a set of displacements preserving the conventional member lengths will yield $\hat{\mathbf{G}}\mathbf{e} = \mathbf{0}$.

These are the only possible cases of zero stiffness in $\hat{\mathbf{K}}$, as summarized in Table 3.1. Any other cases are not possible due to the orthogonality of the nullspaces of $\mathbf{A}$ and $\mathbf{A}^T$ (Pellegrino and Calladine, 1986): it is not possible for there to be a set of member elongations $\mathbf{A}^T\mathbf{d} = \mathbf{e}$ (or a linear transformation thereof by means of the diagonal matrix $\hat{\mathbf{G}}$) that are in the nullspace of $\mathbf{A}$.

3.3.2 Nullspace of stress matrix $\tilde{\mathbf{\Omega}}$

The stress matrix $\tilde{\mathbf{\Omega}}$ does not change when special elements are added, as it only consists of tension coefficients for the members. It is within the power of this matrix to stabilize the zero-stiffness modes of $\hat{\mathbf{K}}$ by imparting a first-order stiffness proportional to the self-stress, but the nullspaces of both matrices may also coincide and the total structure then has zero stiffness. This calls for the understanding of all the zero-stiffness modes of the stress matrix.

As discussed in the previous section, the stress matrix cannot stabilize all internal mechanisms, and none of the higher-order or finite internal mechanisms; these modes may therefore be in its nullspace. A second source of nullity is

Table 3.1: Nullspace of $\hat{\mathbf{K}} = \mathbf{A}\hat{\mathbf{G}}\mathbf{A}^T$.

Conventional structure	Structure with zero-free-length springs
- $\mathbf{A}^T\mathbf{d} = \mathbf{e} = \mathbf{0}$ internal mechanisms and rigid-body motions	- $\mathbf{A}^T\mathbf{d} = \mathbf{e} = \mathbf{0}$ internal mechanisms and rigid-body motions - $\mathbf{A}^T\mathbf{d} = \mathbf{e}$; $\hat{\mathbf{G}}\mathbf{e} = \mathbf{0}$ length-preserving for conventional elements

introduced by any unstressed nodes in the structure (nodes connected by unstressed members). As can be deduced from equation 3.6, each unstressed node introduces a d (dimension of space) nullity to the stress matrix.

A further source of nullity is reportedly the case of projections of the structure onto a lower dimension (e.g. Connelly and Back, 1998). At present, this is not yet fully understood. When translated into engineering terms, it would for instance describe a planar configuration in 3-space, or a structure where all nodes are collinear. How this translates into three dimensional structures is unclear. It might be related to internal mechanisms, but this is as of yet undetermined, and the topic warrants further investigation.

The most interesting part of the nullspace of the stress matrix, however, is constituted by the *affine transformations*. It was shown that the equilibrium of the structure is maintained under an affine transformation of the coordinates (Masic et al., 2005; Connelly and Terrell, 1995), and by equation 3.4 those displacements are thus in the nullspace of the stress matrix. Affine transformations are linear transformations of coordinates (of the whole affine plane onto itself) preserving collinearity. Thus, an affine transformation transforms parallel lines into parallel lines and preserves ratios of distances along parallel lines, as well as intermediacy (Coxeter, 1989, pp. 202). These transformations are well-known to engineers under a different guise: shear, dilation and rigid-body motions. This means that for an unconstrained structure in d-space, there are $d(d+1)$ affine transformations. The affine transformations determine a lower bound for the nullity of the stress matrix.

It should be noted that the zero stiffness modes discussed in this section are not per definition linearly independent, and may coincide (e.g. internal mechanisms that are affine transformations).

3.3.3 A combination of nullspaces

This section attempts to catalogue and describe the situations where the nullspaces of both parts of the tangent stiffness matrix align. Several examples shown in Figure 3.2 demonstrate that care has to be taken in combining the various nullspaces discussed previously: not all combinations are possible, or may require special circumstances.

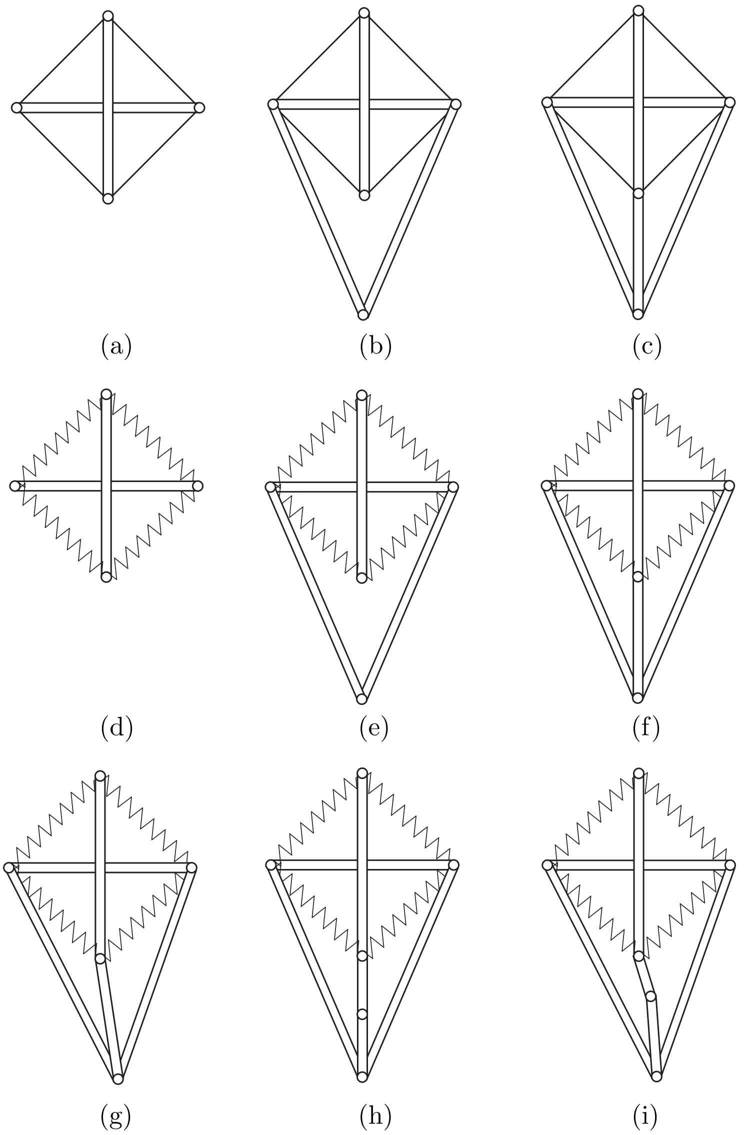

(a) (b) (c) (d) (e) (f) (g) (h) (i)

Figure 3.2: Two dimensional examples of prestressed structures. The basic structure (a) is statically indeterminate and therefore prestressed. It remains stiff when an unstressed node is added in (b) and (c). When the tension elements are replaced by zero-free-length springs in (d), there now exists a length-preserving affine transformation which has zero stiffness. This *finite* zero-stiffness remains in (e) but when another member is added in (f) it reduces to an *infinitesimal* zero-stiffness mode: the structure behaves as if it had an internal mechanism. In both (e) and (f) the zero-stiffness mode no longer corresponds to an affine transformation of the entire structure. If the unstressed node is moved slightly, the structure (g) becomes rigid again. The structure (h) also has an infinitesimal internal mechanism, but (i) suddenly yields a ‘finite’ mechanism; the zero-stiffness mode has a limited working range, but is nevertheless finite.

Table 3.2: Nullspace of $\tilde{\boldsymbol{\Omega}}^*$.

Conventional structure	Structure with zero-free-length springs

- internal mechanisms
- $d(d+1)$ affine transformations (includes rigid-body motions)
- nullity due to unstressed nodes
- projections on a lower dimension

* Note that these are not necessarily linearly independent vectors.

The most obvious case of a zero-stiffness mode is a rigid-body motion, which has no stiffness in either component of the tangent stiffness matrix. A further clear scenario is when the internal mechanisms in $\hat{\mathbf{K}}$ are not stabilized by the state of self-stress. This is the traditional interpretation of zero stiffness in prestressed structures, and results in “floppy” structures. Internal mechanisms in $\hat{\mathbf{K}}$ may also coincide with affine transformations of the structure, or zero-stiffness modes in $\tilde{\boldsymbol{\Omega}}$ due to the unstressed nodes. These zero-stiffness modes in the tangent stiffness matrix are finite if and only if the internal mechanism is finite.

The zero-stiffness modes in $\tilde{\boldsymbol{\Omega}}$ caused by unstressed nodes are per definition linked to displacements of those unstressed nodes, and thus only involve elongations of conventional members (the zero-free-length springs are by definition stressed). Those elongations therefore correspond to positive values on the diagonal of $\hat{\mathbf{G}}$, which remain unchanged by the addition of zero-free-length springs. As a result these modes cannot, *by themselves*, coincide with the length-preserving modes introduced by the zero-free-length springs in $\hat{\mathbf{K}}$.

An interesting combination is where the affine transformations coincide with the length-preserving zero-stiffness modes introduced by zero-free-length springs. This scenario was described in detail by Schenk et al. (2006), and it was shown that those zero-stiffness modes are finite, and that for structures with a maximal rank positive semi-definite stress matrix they are the only possible zero-stiffness modes. The maximal rank condition requires the nullity to be equal to the $d(d+1)$ affine transformations. For three dimensions it was shown that these modes are present in a structure if and only if the conventional member directions lie on a conic. It are these zero-stiffness modes that provide the understanding for the statically balanced structures described in Herder (2001).

However, complications arise when the stress matrix is no longer maximal rank, as is described in Figure 3.2. Then there exist (finite/infinitesimal) zero-stiffness modes introduced by the zero-free-length springs – which preserve the length of conventional members – that are no longer an affine transformation of the *entire* structure. Numerical analysis of the examples suggests that the zero-stiffness modes in the stress matrix correspond to a combination of affine transformations and displacements of the unstressed node. It is conjectured that modes correspond to an affine transformation of the ‘stressed’ part of the structure, and that understanding these phenomena might be a first step towards describing non-pin-jointed structures.

Table 3.3: Combination of nullspaces of $\hat{\mathbf{K}}$ and $\tilde{\mathbf{\Omega}}$.

Conventional structure	Structure with zero-free-length springs
- unstabilized internal mechanisms (may coincide with affine transformations or nullity due to unstressed nodes) - rigid-body motions	- unstabilized internal mechanisms (may coincide with affine transformations or nullity due to unstressed nodes) - rigid-body motions - finite length-preserving affine transformations - length-preserving mode with combination of affine and unstressed modes - more?

As the projections of the structures onto a lower dimension are currently not sufficiently understood, the discussion of combinations with other zero-stiffness modes would be nothing more than conjecture.

3.4 Contributions of $\hat{\mathbf{K}}$ and $\tilde{\mathbf{\Omega}}$ cancel out

The second scenario is where $\hat{\mathbf{K}}\mathbf{d} = -\tilde{\mathbf{\Omega}}\mathbf{d}$ and their sum is thus zero. For conventional structures $\hat{\mathbf{K}}$ is per definition positive semi-definite, and therefore $\tilde{\mathbf{\Omega}}$ would need to have a negative eigenvalue. It should be noted that many practical tensegrity structures have a positive semi-definite stress matrix (i.e. no negative eigenvalues), and in those structures this scenario cannot occur. The cancellation could theoretically occur in conventional structures, but due to small strains the contributions of $\hat{\mathbf{K}}$ are generally an order of magnitude greater than those of $\tilde{\mathbf{\Omega}}$, and this scenario therefore seems mostly of theoretical value.

For structures with zero-free-length springs, the zeros in the $\hat{\mathbf{G}}$ corresponding to those elements will result in a reduced contribution of $\hat{\mathbf{K}}$ to the tangent stiffness. As a result, the likelihood of both contributions cancelling each other out will therefore increase. It is also theoretically possible, in the case of springs with a negative free length and thus with a negative modified axial stiffness, that the first part is negative and the latter positive.

Regarding these zero-stiffness modes, it should be noted that no example structures are known to the authors, and it is unknown whether the zero stiffness is always infinitesimal, or sometimes finite.

3.5 Conclusion

The systematic analysis of zero stiffness in the tangent stiffness matrix of prestressed pin-jointed bar frameworks described in this paper complements the results in Schenk et al. (2006). Several additional types of zero stiffness have been described, both in the case where the mode is in the nullspace of $\hat{\mathbf{K}}$ and $\tilde{\mathbf{\Omega}}$, and in the case where both contributions cancel each other out.

Although the possible zero-stiffness modes have been catalogued, the analysis has possibly raised more questions than it has answered. A large number of zero-stiffness modes introduced by zero-free-length springs are not yet fully understood, and neither is the scenario where the contributions of both components of the tangent stiffness matrix cancel out. Therefore several potential directions for future research have been formulated as follows:

- Investigate the zero stiffness caused by the cancelation of the contributions of the two components of the tangent stiffness matrix. Can these modes be finite, or are they always infinitesimal?
- Investigate the combination of unstressed nodes and affine transformations in the nullspace of the stress matrix. Considering only the stressed parts of the structure for affine transformations might be a first step towards analysing non-pin-jointed structures.
- Investigate the nullity in the stress matrix caused by projections onto a lower dimension; how does this translate into engineering terms?
- Incorporate external forces and constraints in zero stiffness analysis in order to describe more general structures.

Acknowledgements

Several of the example structures in Figure 3.2 result from personal communications with Dr. Simon Guest (University of Cambridge).

Bibliography

Connelly, R., Back, W., 1998. Mathematics and Tensegrity. American Scientist 86, 142–151.

Connelly, R., Terrell, M., 1995. Globally Rigid Symmetric Tensegrities. Structural Topology 21, 59–77.

Connelly, R., Whiteley, W., 1996. Second-order rigidity and prestress stability for tensegrity frameworks. SIAM Journal of Discrete Mathematics 7 (3), 453–491.

Coxeter, H. S. M., 1989. Introduction to geometry, 2nd Edition. John Wiley & sons, inc.

Guest, S. D., 2006. The stiffness of prestressed frameworks: A unifying approach. International Journal of Solids and Structures 43 (3–4), 842–854.

Herder, J. L., 2001. Energy-Free Systems. Theory, conception and design of statically balanced spring mechanisms. Ph.D. thesis, Delft University of Technology.

Masic, M., Skelton, R. E., Gill, P. E., 2005. Algebraic tensegrity form-finding. International Journal of Solids and Structures 42 (16–17), 4833–4858.

Pellegrino, S., Calladine, C. R., 1986. Matrix analysis of statically and kinematically indeterminate frameworks. International Journal of Solids and Structures 22 (4), 409–428.

Schenk, M., Guest, S. D., Herder, J. L., 2006. Zero Stiffness Tensegrity Structures, to be submitted.

Tarnai, T., 2003. Zero stiffness elastic structures. International Journal of Mechanical Sciences 45 (3), 425–431.

Chapter 4

Conclusions

The findings of this Master Thesis can be summarized in the following points:

- the use of structural engineering methods to investigate statically balanced tensegrity mechanisms has proven to be successful, by searching for zero stiffness in the tangent stiffness matrix of prestressed pin-jointed bar frameworks;
- the parallels between mathematical rigidity theory and structural engineering have been exploited and provided several important insights;
- affine transformations are known to engineers as rigid-body motions, shears and dilations;
- the equilibrium of a freestanding tensegrity structure is preserved under an affine transformation, i.e. affine transformations are in the nullspace of the stress matrix;
- the minimum nullity requirement for the stress matrix found in form finding is now better understood, as it is formed by the affine transformations;
- for conventional tensegrity structures, zero-stiffness modes are in general internal mechanisms and rigid-body motions;
- for tensegrity structures with zero-free-length springs as tension members, new zero-stiffness modes are introduced, and they are termed statically balanced zero-stiffness modes;
- affine transformations of the structure that preserve the length of conventional members are statically balanced zero-stiffness modes valid over finite displacements;
- for prestress stable structures with a maximal rank (only affine transformations in the nullspace) positive semi-definite stress matrix, those are the only possible zero-stiffness modes;
- a structure contains length-preserving affine transformations if and only if the conventional member directions lie on a conic at infinity;

- if all conventional member directions lie on a conic, a simple counting rule allows to find the number of independent zero-stiffness modes;
- numerical analysis of several classic tensegrity structures supports the developed theory;
- a systematic enumeration of possible zero-stiffness modes in the tangent stiffness matrix yielded interesting cases which are not yet fully understood within the current knowledge;
- the construction of a prototype has demonstrated the theory, although the model exhibits some shortcomings, notably a high level of friction.

Recommendations

A detailed discussion of recommendations, along with some pointers, for future research is given in Appendix F. Here the main points are recapitulated:

- extend theory to structures with external loads and constraints;
- extend theory to cover structures with unstressed nodes and other sources of nullity in the stress matrix;
- extend theory to non-pin-jointed structures;
- clarify link to static balancing by validating (and extending) the modification rules of Herder (2001);
- investigate range of motion of the tensegrity mechanisms;
- explore links to mechanism theory, such as the number of degrees of freedom of mechanisms;
- investigate constructibility and practical applications of statically balanced tensegrity mechanisms.

Bibliography

Calladine, C. R., 1978. Buckminster Fuller's 'tensegrity' structures and Clerk Maxwell's rules for the construction of stiff frames. International Journal of Solids and Structures 14, 161–172.

Calladine, C. R., Pellegrino, S., 1991. First-order infinitesimal mechanisms. International Journal of Solids and Structures 27 (4), 505–515.

Calladine, C. R., Pellegrino, S., 1992. Further remarks on first-order infinitesimal mechanisms. International Journal of Solids and Structures 29 (17), 2119–2122.

Connelly, R., 1999. Tensegrity structures: Why are they stable? In: Thorpe, M. F., Duxbury, P. M. (Eds.), Rigidity Theory and Applications. Kluwer Academic/Plenum Publishers, pp. 47–54.

Connelly, R., Back, W., 1998. Mathematics and Tensegrity. American Scientist 86, 142–151.

Connelly, R., Terrell, M., 1995. Globally Rigid Symmetric Tensegrities. Structural Topology 21, 59–77.

Connelly, R., Whiteley, W., 1992. The Stability of Tensegrity Frameworks. International Journal of Space Structures 7 (2), 153–163.

Connelly, R., Whiteley, W., 1996. Second-order rigidity and prestress stability for tensegrity frameworks. SIAM Journal of Discrete Mathematics 7 (3), 453–491.

Coxeter, H. S. M., 1989. Introduction to geometry, 2nd Edition. John Wiley & sons, inc.

Crisfield, M. A., 1991. Non-linear Finite Element Analysis of Solids and Structures. Volume 1: Essentials. John Wiley & Sons.

Deng, H., Kwan, A. S. K., 2005. Unified classification of stability of pin-jointed bar assemblies. International Journal of Solids and Structures 42 (15), 4393–4413.

French, M. J., Widden, M. B., 2000. The spring-and-lever balancing mechanism, George Carwardine and the Anglepoise lamp. Proceedings of the Institution of Mechanical Engineers part C – Journal of Mechanical Engineering Science 214 (3), 501–508.

Guest, S. D., 2006. The stiffness of prestressed frameworks: A unifying approach. International Journal of Solids and Structures 43 (3–4), 842–854.

Herder, J. L., 2001. Energy-Free Systems. Theory, conception and design of statically balanced spring mechanisms. Ph.D. thesis, Delft University of Technology.

Hinrichs, L. A., 1984. Prismic Tensigrids. Structural Topology 9, 3–14.

Kangwai, R. D., Guest, S. D., 1999. Detection of finite mechanisms in symmetric structures. International Journal of Solids and Structures 36 (36), 5507–5527.

Love, A. E. H., 1927. A treatise on the mathematical theory of elasticity, 4th Edition. Dover publications.

Masic, M., Skelton, R. E., Gill, P. E., 2005. Algebraic tensegrity form-finding. International Journal of Solids and Structures 42 (16–17), 4833–4858.

Motro, R., 1992. Tensegrity Systems: The State of the Art. International Journal of Space Structures 7 (2), 75–83.

Murakami, H., 2001. Static and dynamic analyses of tensegrity structures. Part II. Quasi-static analysis. International Journal of Solids and Structures 38, 3615–3629.

Pellegrino, S., 1990. Analysis of Prestressed Mechanisms. International Journal of Solids and Structures 26 (12), 1329–1350.

Pellegrino, S., Calladine, C. R., 1986. Matrix analysis of statically and kinematically indeterminate frameworks. International Journal of Solids and Structures 22 (4), 409–428.

Schenk, M., Guest, S. D., Herder, J. L., 2006. Zero Stiffness Tensegrity Structures, to be submitted.

Tarnai, T., 2003. Zero stiffness elastic structures. International Journal of Mechanical Sciences 45 (3), 425–431.

Tibert, A. G., Pellegrino, S., 2003. Review of Form-Finding Methods for Tensegrity Structures. International Journal of Space Structures 18 (4), 209–223.

Weisstein, E. W., 1999. Conic Section. From Mathworld – a Wolfram Web Resource. http://mathworld.wolfram.com/ConicSection.html.

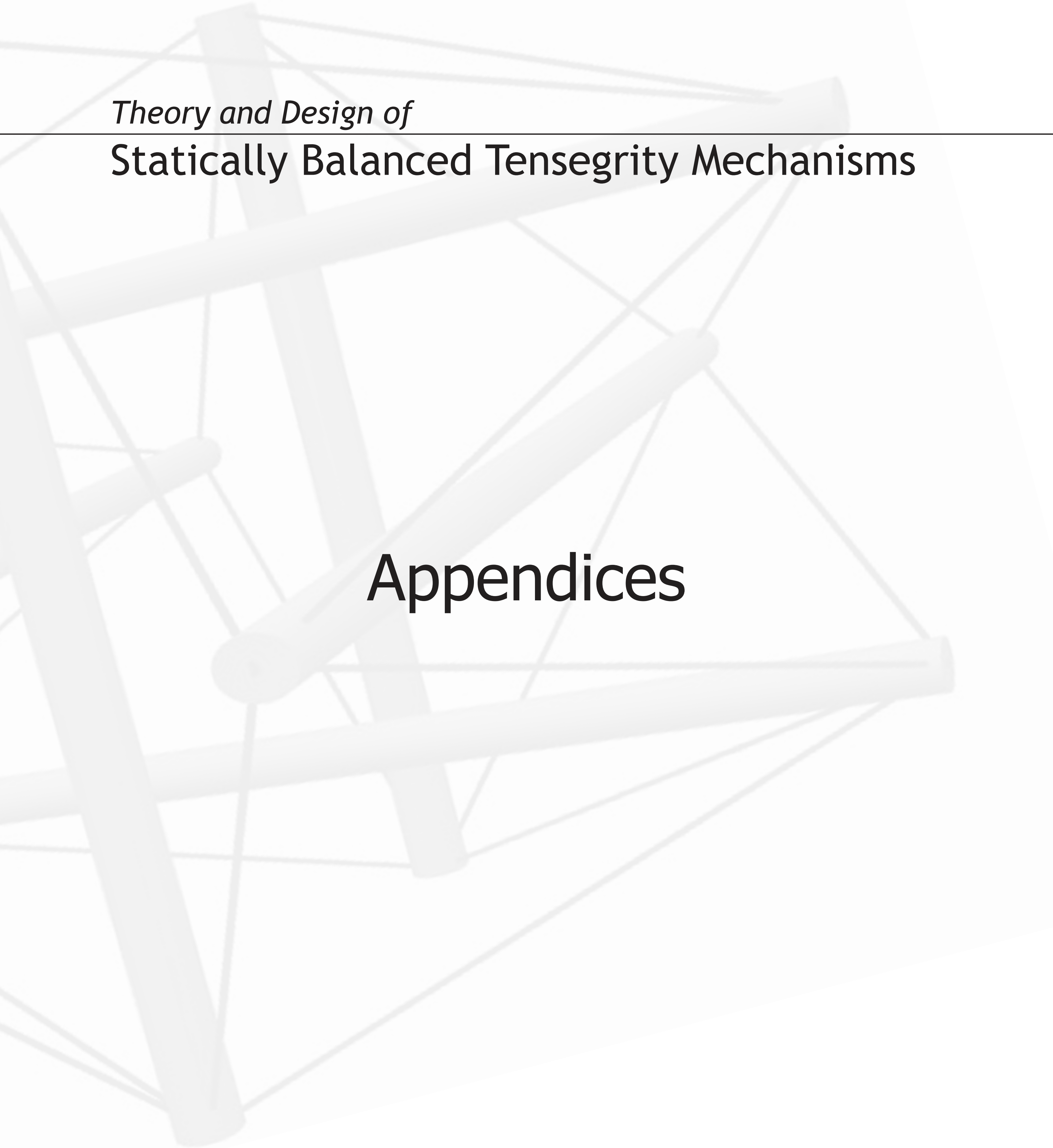

Theory and Design of

Statically Balanced Tensegrity Mechanisms

Appendices

MSc. Thesis - Appendices

Mark Schenk
February 2006

Department of BioMechanical Engineering
Faculty of Mechanical, Maritime and Materials Engineering

TUDelft
Delft University of Technology

Appendix A

Tensegrity Equilibrium

A.1 Introduction

Rotationally symmetric tensegrity structures have been the object of study in the past (e.g. Hinrichs, 1984; Connelly and Terrell, 1995), and seemed – and subsequently proved – to be a good starting point for investigating specific examples of zero-stiffness tensegrities. In this appendix the analytical equilibrium conditions for a class of rotationally symmetric tensegrity structures will be derived.

In their overview article of form-finding methods Tibert and Pellegrino (2003) distinguished two types of methods: the *kinematic* and *static* method; the kinematic methods utilize the fact that in tensegrities bar lengths reach a maximum, and cable lengths a minimum at the equilibrium position; the static method works from the equilibrium of forces at each of the nodes. The analytical solutions to the equilibrium position will be derived via both routes, and the results compared with Murakami (2001) (kinematic) and Connelly and Terrell (1995) (static).

Additionally, for the three bar tensegrity structure used for the demonstration prototype of a statically balanced tensegrity structure, the required spring stiffness ratios were derived.

A.2 Equilibrium configuration

The rotationally symmetric structure under consideration is shown in Figure A.1. It consists of n bars, connecting the vertices of two regular n-polygons on two parallel planes, twisted over an angle α with respect to eachother. The structure has height h, top radius r_h and bottom radius r_0. With these values all aspects of the structure can be calculated.

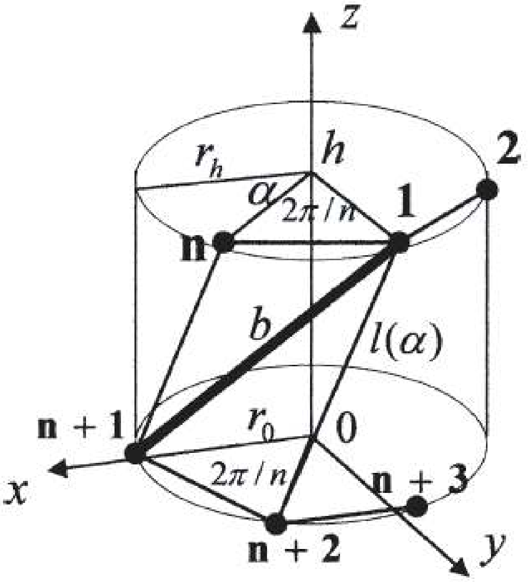

Figure A.1: Rotationally symmetric tensegrity structure with n bars, height h, radii r_0 and r_h, and twist angle α. Figure copied from Murakami (2001).

A.2.1 Element lengths

For the calculation of the element lengths, the cosine rule was used extensively:

$$c^2 = a^2 + b^2 - 2ab\cos(\gamma). \tag{A.1}$$

With equation A.1 the bar length is then written as

$$b^2 = h^2 + r_0^2 + r_h^2 - 2r_0r_h\cos(\frac{2\pi}{n} + \alpha), \tag{A.2}$$

the vertical cable length as

$$l^2 = h^2 + r_0^2 + r_h^2 - 2r_0r_h\cos(\alpha), \tag{A.3}$$

and the horizontal cable lengths as (with either r_0 or r_h):

$$l_0^2 = 2r_0^2 - 2r_0^2\cos(\frac{2\pi}{n}). \tag{A.4}$$

The length of the horizontal cables will now be rewritten in a simpler form:

$$\begin{aligned} l_0 &= r_0\sqrt{2 - 2\cos(\frac{2\pi}{n})} \\ &= r_0\sqrt{\frac{4 - 4\cos(\frac{2\pi}{n})}{2}} \end{aligned}$$

$$
\begin{aligned}
&= 2r_0\sqrt{\frac{1-1\cos\left(\frac{2\pi}{n}\right)}{2}} \\
&= 2r_0\sin\left(\frac{\pi}{n}\right). \qquad \text{(A.5)}
\end{aligned}
$$

For the last step, the following goniometric relationship was used:

$$\sin\left(\frac{\gamma}{2}\right) = \sqrt{\frac{1-\cos\gamma}{2}}. \qquad \text{(A.6)}$$

It is now obvious that the length of the cable could immediately have been written in the simpler form of equation A.5, as that is required to solve the formulas at a later stage.

A.3 Twist angle

There are now two ways to calculate the twist angle α, the *static* and *kinematic* way. Both will be discussed, but the static method will prove to be most useful as it also allows the easy calculation of internal tensions.

A.3.1 Kinematic

The length of the cable as a function of α is:

$$l(\alpha) = \sqrt{b^2 + 2r_h r_0\left(\cos\left(\frac{2\pi}{n}+\alpha\right) - \cos(\alpha)\right)} \qquad \text{(A.7)}$$

where the height h in equation A.3 is replaced by substituting equation A.2. At the equilibrium configuration the cable length reaches its minimum, which can be found by equating the derivative $\frac{dl}{d\alpha}$ to zero. This results in

$$\sin\left(\frac{2\pi}{n}+\alpha\right) = \sin\alpha = \sin(\pi-\alpha), \qquad \text{(A.8)}$$

and we find that

$$
\begin{aligned}
\frac{2\pi}{n}+\alpha &= \pi-\alpha \\
2\alpha &= \pi - \frac{2\pi}{n} \\
\alpha &= \frac{\pi}{2} - \frac{\pi}{n}. \qquad \text{(A.9)}
\end{aligned}
$$

The kinematic method has given us the twist angle for which the structure is in equilibrium, but calculating the internal tensions is problematic. Therefore it is easier to now consider the static method and equate the forces at the nodes.

A.3.2 Static

We are considering the nodal equilibrium at node $n+1$ in figure A.1, with tension s_b in the bar, tension s_v in the vertical cable and s_0, s_h the tension in the bottom and top horizontal cables respectively.

First we consider equilibrium in the z-direction, which merely involves the vertical cable and bar:

$$\frac{s_b}{b}h + \frac{s_v}{l}h = 0 \tag{A.10}$$

which yields that

$$s_v = -\frac{s_b}{b}l. \tag{A.11}$$

Next the equilibrium in the y-direction is derived. Due to symmetry considerations on the horizontal cables we can say that the contributions of the bar and vertical cable should cancel eachother out. This analysis yields:

$$\sin(\alpha) r_h \frac{s_v}{l} + \sin(\frac{2\pi}{n} + \alpha) r_h \frac{s_b}{b} = 0 \tag{A.12}$$

which with equation A.11 becomes

$$r_h \frac{s_b}{b}(\sin(\frac{2\pi}{n} + \alpha) - \sin\alpha) = 0. \tag{A.13}$$

For this to hold for any α we obtain

$$\sin(\frac{2\pi}{n} + \alpha) = \sin\alpha = \sin(\pi - \alpha) \tag{A.14}$$

and once again find that

$$\begin{aligned} \frac{2\pi}{n} + \alpha &= \pi - \alpha \\ 2\alpha &= \pi - \frac{2\pi}{n} \\ \alpha &= \frac{\pi}{2} - \frac{\pi}{n}. \end{aligned} \tag{A.15}$$

So, as expected, both the kinematic and static method produce the same twist angle.

A.4 Equilibrium tensions

With the equilibrium twist angle now known, we wish to find the corresponding internal tensions. It was already shown in equation A.11 that

$$s_v = -\frac{s_b}{b}l.$$

To calculate the tensions in the horizontal cables, the force equilibrium in x-direction at node $n+1$ is considered. The contributions of the vertical cable and bar to that equilibrium, $f_{x,vert}$, can be written as:

$$(r_0 - \cos\alpha r_h)\frac{s_v}{l} + \left(r_0 - \cos\left(\frac{2\pi}{n} + \alpha\right) r_h\right)\frac{s_b}{b} = f_{x,vert} \tag{A.16}$$

which, when using equation A.11 becomes:

$$\left(\cos\alpha - \cos\left(\frac{2\pi}{n} + \alpha\right)\right) r_h \frac{s_b}{b} = f_{x,vert}. \tag{A.17}$$

With $\alpha = \frac{\pi}{2} - \frac{\pi}{n}$ we can write

$$\left(\cos\left(\frac{\pi}{2} - \frac{\pi}{n}\right) - \cos\left(\frac{\pi}{n} + \frac{\pi}{2}\right)\right) r_h \frac{s_b}{b} = f_{x,vert} \tag{A.18}$$

and using the following goniometric relationships

$$\cos(\gamma + \beta) = \cos\gamma\cos\beta - \sin\gamma\sin\beta$$

$$\cos(\gamma - \beta) = \cos\gamma\cos\beta + \sin\gamma\sin\beta$$

we find

$$\begin{aligned} \left(\sin\left(\frac{\pi}{n}\right) + \sin\left(\frac{\pi}{n}\right)\right) r_h \frac{s_b}{b} &= f_{x,vert} \\ f_{x,vert} &= 2\sin\left(\frac{\pi}{n}\right) r_h \frac{s_b}{b}. \end{aligned} \tag{A.19}$$

Next, the effect of the tensions in the horizontal cables in the x-direction can be written as:

$$\begin{aligned} 2\left(r_0 - \cos\left(\frac{2\pi}{n}\right) r_0\right)\frac{s_0}{l_0} &= f_{x,horz} \\ f_{x,horz} &= 2\left(1 - \cos\left(\frac{2\pi}{n}\right)\right)\frac{r_0 s_0}{l_0}. \end{aligned} \tag{A.20}$$

Now the two contributions are summed, and the solution to $f_{x,vert} + f_{x,horz} = 0$ yields:

$$\begin{aligned} 2\left(1 - \cos\left(\frac{2\pi}{n}\right)\right)\frac{r_0 s_0}{l_0} &= -2\sin\left(\frac{\pi}{n}\right) r_h \frac{s_b}{b} \\ \left(1 - \cos\left(\frac{2\pi}{n}\right)\right)\frac{r_0 s_0}{2 r_0 \sin\left(\frac{\pi}{n}\right)} &= -\sin\left(\frac{\pi}{n}\right) r_h \frac{s_b}{b} \\ \left(1 - \cos\left(\frac{2\pi}{n}\right)\right) s_0 &= -2\sin^2\left(\frac{\pi}{n}\right) r_h \frac{s_b}{b} \\ \left(1 - 1 + 2\sin^2\left(\frac{\pi}{n}\right)\right) s_0 &= -2\sin^2\left(\frac{\pi}{n}\right) r_h \frac{s_b}{b} \\ s_0 &= -r_h \frac{s_b}{b} \end{aligned} \tag{A.21}$$

where use is made of

$$\cos(2\gamma) = 1 - 2\sin^2(\gamma). \tag{A.22}$$

Reasoning that in A.21 the r_h has to be replaced by r_0 to obtain the tension s_h all the tensions in the system can be written as follows:

$$[s_v \quad s_h \quad s_0] = -\frac{s_b}{b}[l \quad r_0 \quad r_h] \tag{A.23}$$

which corresponds to the results found by Murakami (2001). We can now calculate all tensions in the tensegrity structure.

A.5 Literature comparison

The above equilibrium configuration and tensions have been derived before in literature, although the full derivation is never given. To check their validity, the above results will be compared with two literature sources.

A.5.1 Murakami (2001)

Murakami used the kinematic approach to derive the twist angle. He did not explicitly derive the internal tensions, but stated them in the form of equation A.23.

A.5.2 Connelly and Terrell (1995)

Connelly and Terrell (1995) derived the equilibrium equations and internal tensions for more generic connectivity cases than Murakami, but with fixed radius for top and bottom polygons. Their classification scheme is based on Hinrichs (1984) and it is advisable to read the latter paper to understand the scheme.

They define two polygons with n vertices on two planes at distance h, and the connectivity is determined with two integers $j, k = 1, 2, \ldots, n-1$. The tensegrities are classified as

$$P_n(j, k),$$

where n determines the number of nodes on each polygon, j determines the connectivity between upper and lower polygon, and k determines connectivity within a polygon. Hinrichs (1984) described k as the number of successive vertices to where the horizontal cables are attached, and j the number of successive vertices counting from the bottom of the strut, to which the top of the strut is connected by the vertical cable. See Figure A.2.

For these tensegities, Connelly and Terrell (1995) derive the formulas for the *stress* ω in the members – which is equivalent to the engineering *force density*

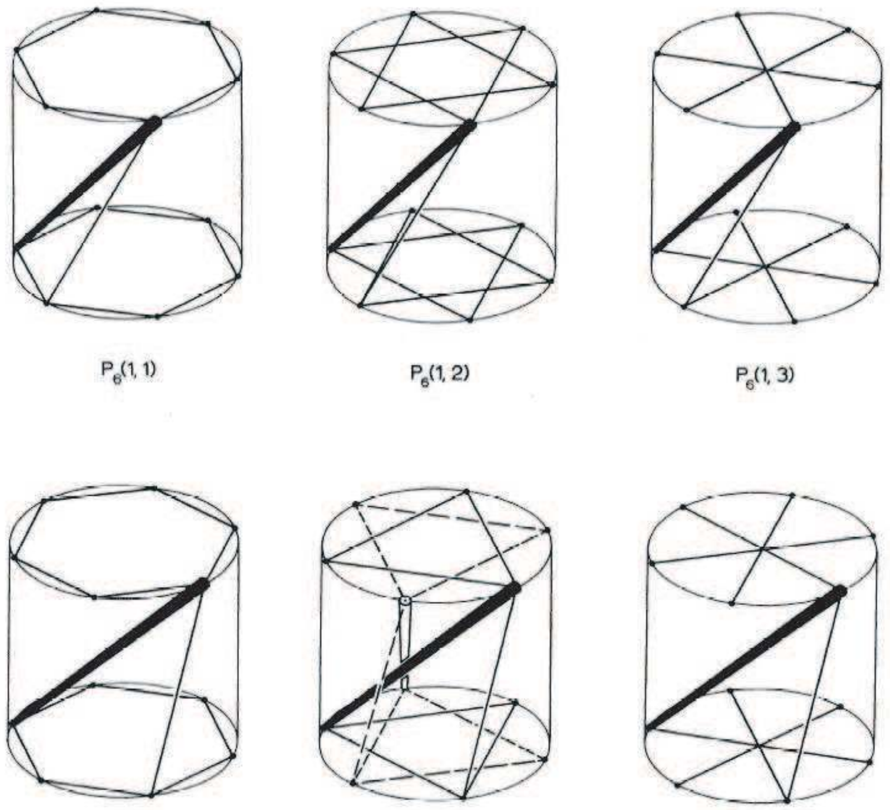

$P_6(1,1)$ $P_6(1,2)$ $P_6(1,3)$

$P_6(2,1)$ $P_6(2,2)$ $P_6(2,3)$

Figure A.2: Hinrichs' method of classifying rotationally symmetric tensegrities. Figure copied from Hinrichs (1984).

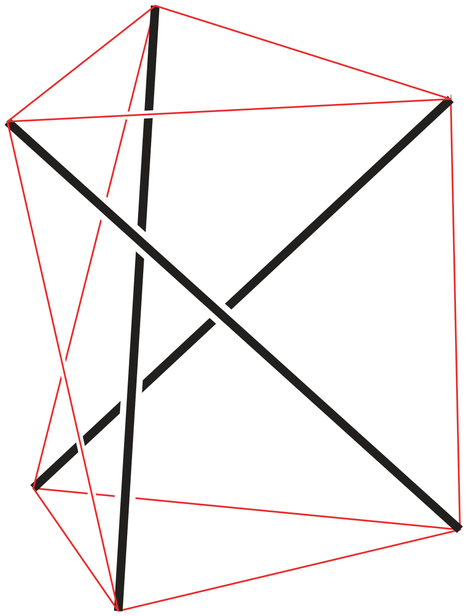

Figure A.3: Three bar rotationally symmetric tensegrity structure.

or *tension coefficient*. They are given as functions of a chosen positive value for the stress in the horizontal cables:

$$\omega_{hor} = \gamma > 0 \tag{A.24}$$

$$\omega_{ver} = 2\gamma \frac{\sin^2\left(\frac{k}{n}\pi\right)}{\sin\left(\frac{j}{n}\pi\right)} \tag{A.25}$$

$$\omega_{bar} = -2\gamma \frac{\sin^2\left(\frac{k}{n}\pi\right)}{\sin\left(\frac{j}{n}\pi\right)} \tag{A.26}$$

The structures considered by Murakami would have $k = 1$ and $j = 1$, and equivalence with equation A.23 can then quite easily be established.

A.6 Spring stiffness ratios

The three bar tensegrity used for the demonstration model of a statically balanced tensegrity, is shown in Figure A.3. In the terminology of Hinrichs (1984) it is a $P_3(1,1)$ tensegrity, or when we adhere more strictly to his convention: a $P_3(-1,1)$, as it is actually a mirror image of a $P_3(1,1)$ tensegrity.

In the analysis of statically balanced tensegrity structures the cables are replaced by zero-free-length springs. This leads to the question what the stiffness (ratios) of those springs must be in order to preserve equilibrium. Our case is somewhat simplified as $r_0 = r_h = r$ and $s_0 = s_h = s_{hor}$. Using equation A.23 we then find that

$$\frac{s_{hor}}{r} = \frac{s_v}{l} = K_{ver}$$

$$\begin{aligned}
\frac{K_{hor} l_{hor}}{r} &= K_{ver} \\
\frac{l_{hor}}{r} &= \frac{K_{ver}}{K_{hor}} \\
\frac{2r \sin\left(\frac{\pi}{n}\right)}{r} &= \frac{K_{ver}}{K_{hor}} \\
2 \sin\left(\frac{\pi}{n}\right) &= \frac{K_{ver}}{K_{hor}} \qquad \text{(A.27)}
\end{aligned}$$

and for our tensegrity prism with $n = 3$ we obtain:

$$2 \sin\left(\frac{\pi}{3}\right) = \frac{K_{ver}}{K_{hor}} = \sqrt{3} \qquad \text{(A.28)}$$

This could also be derived immediately from equation A.25 when we realize that the stiffness of a zero-free-length spring is identical to its tension coefficient; with $j, k = 1$ and $n = 3$, it results in the same value for the spring stiffness ratio.

A.7 Conclusion

The derivation of the equilibrium conditions for the rotationally symmetric tensegrities was of great use to the research, as it provided a whole class of structures for which the solutions are known analytically. This class of structures eventually proved to be especially interesting to zero-stiffness research as it was shown that the entire class can be statically balanced by replacing the cables with zero-free-length springs. What is more, the analytical solutions made detailed analysis possible for the design of the three bar demonstration model, as described in Appendix D.

Appendix B

Tangent Stiffness Matrix

B.1 Introduction

The objective of this appendix is to provide a different route to the geometrically non-linear tangent stiffness matrix found in Guest (2006) and to identify some of the underlying assumptions in its derivation. Guest's work introduces the concept of a 'modified axial stiffness' in the formulation of the tangent stiffness matrix for prestressed pin-jointed structures. This variable provides valuable (and otherwise not immediately intuitive) insight into the special case of introducing zero-free-length springs (Herder, 2001) to structures.

Due to the fundamental importance of this step in the study of zero-stiffness structures with zero-free-length springs it was deemed relevant to verify the resulting tangent stiffness matrix via another route: geometrically non-linear Finite Element Analysis. Literature on non-linear FEA (e.g. Crisfield, 1991) is known to be meticulous in keeping track of deformed and undeformed lengths during the creation of the tangent stiffness matrix. This will lead to a slightly more complex formulation, from which it is possible to establish which assumptions were used in Guest (2006).

B.2 Modified axial stiffness

Figure B.1 shows a free body diagram of a bar in three-dimensional space. The external forces $\mathbf{f}_1$ and $\mathbf{f}_2$ are in equilibrium with the internal bar tension t, and the nodes have position vectors, $\mathbf{x}_1$ and $\mathbf{x}_2$.

The equilibrium at the two nodes 1 and 2 can be expressed in terms of the bar tension t and the unit vector $\mathbf{n} = (\mathbf{x}_1 - \mathbf{x}_2)/l$,

$$\mathbf{f}_1 = \mathbf{n}t \tag{B.1}$$

$$\mathbf{f}_2 = -\mathbf{n}t. \tag{B.2}$$

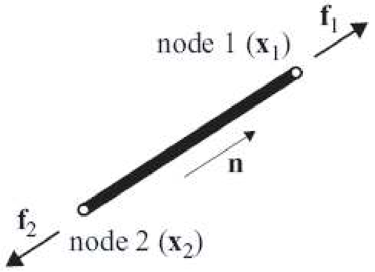

Figure B.1: A single bar floating in space, connecting two nodes $\mathbf{x}_1$ and $\mathbf{x}_2$. Figure copied from Guest (2006).

Alternatively, with a *tension coefficient* or *force density* defined as $\hat{t} = t/l$, the equilibrium can be rewritten as

$$\mathbf{f}_1 = (\mathbf{x}_1 - \mathbf{x}_2)\hat{t} \tag{B.3}$$

$$\mathbf{f}_2 = (-\mathbf{x}_1 + \mathbf{x}_2)\hat{t}. \tag{B.4}$$

These equilibrium equations are now differentiated with respect to the nodal coordinates (effectively a Jacobian matrix) which will develop into the tangent stiffness matrix,

$$\frac{\partial \mathbf{f}}{\partial \mathbf{x}} = \begin{bmatrix} \frac{\partial f_{1i}}{\partial x_{1i}} & \cdots & \frac{\partial f_{1i}}{\partial x_{2k}} \\ \vdots & \ddots & \vdots \\ \frac{\partial f_{2k}}{\partial x_{1i}} & \cdots & \frac{\partial f_{2k}}{\partial x_{2k}} \end{bmatrix} \tag{B.5}$$

with

$$\mathbf{f} = \begin{bmatrix} \mathbf{f}_1 \\ \mathbf{f}_2 \end{bmatrix} \quad \text{and} \quad \mathbf{x} = \begin{bmatrix} \mathbf{x}_1 \\ \mathbf{x}_2 \end{bmatrix}$$

where the vectors $\mathbf{f}_a$ and $\mathbf{x}_a$ are 3-dimensional, with corresponding sub-indices i, j, k. For the sake of brevity, the calculation will only be continued for the top left quarter of the Jacobian; a full derivation is provided in Guest (2006). Now, using equation B.3 we obtain

$$\frac{\partial \mathbf{f}_1}{\partial \mathbf{x}_1} \leftrightarrow \frac{\partial f_{1i}}{\partial x_{1j}} = (x_{1i} - x_{2i})\frac{\partial \hat{t}}{\partial x_{1j}} + \delta_{ij}\hat{t} \tag{B.6}$$

where δ_{ij} is the Kronecker delta

$$\delta_{ij} \equiv \begin{cases} 0 \text{ for } i \neq j \\ 1 \text{ for } i = j \end{cases} . \tag{B.7}$$

This can be simplified by observing that

$$\frac{\partial \hat{t}}{\partial x_{1j}} = \frac{d\hat{t}}{dl}\frac{\partial l}{\partial x_{1j}} = \frac{d\hat{t}}{dl} n_j, \tag{B.8}$$

by rewriting $\frac{d\hat{t}}{dl}$ as

$$\frac{d\hat{t}}{dl} = \frac{d(t/l)}{dl} = \frac{1}{l}\left(\frac{dt}{dl} - \hat{t}\right), \tag{B.9}$$

and by considering that dt/dl is equal to the axial stiffness $g = \frac{EA_0}{l_0}$ (unless a cable is at its rest length), resulting in

$$\frac{d\hat{t}}{dl} = \frac{g - \hat{t}}{l} \tag{B.10}$$

which simplifies even further when the *modified axial stiffness* $\hat{g} = g - \hat{t}$ is introduced, giving

$$\frac{d\hat{t}}{dl} = \frac{\hat{g}}{l}. \tag{B.11}$$

Returning to equation B.6 and using the results in equations B.8 and B.11 we arrive at

$$\frac{\partial f_{1i}}{\partial x_{1j}} = n_i \hat{g} n_j + \delta_{ij}\hat{t} \tag{B.12}$$

or, in vector form

$$\frac{\partial \mathbf{f}_1}{\partial \mathbf{x}_1} = \mathbf{n}\hat{g}\mathbf{n}^T + \hat{t}\mathbf{I}. \tag{B.13}$$

When the above calculations are performed for the entire Jacobian, the tangent stiffness matrix of a single prestressed bar, relating small changes in nodal position to small changes in nodal forces can be written as

$$\mathbf{K}_s = \begin{bmatrix} \mathbf{n} \\ -\mathbf{n} \end{bmatrix} [\hat{g}] \begin{bmatrix} \mathbf{n}^T & -\mathbf{n}^T \end{bmatrix} + \hat{t}\begin{bmatrix} \mathbf{I} & -\mathbf{I} \\ -\mathbf{I} & \mathbf{I} \end{bmatrix}. \tag{B.14}$$

With

$$\mathbf{a}_s = \begin{bmatrix} \mathbf{n} \\ -\mathbf{n} \end{bmatrix} \quad ; \quad \mathbf{S}_s = \hat{t}\begin{bmatrix} \mathbf{I} & -\mathbf{I} \\ -\mathbf{I} & \mathbf{I} \end{bmatrix}$$

this becomes

$$\mathbf{K}_s = \mathbf{a}_s[\hat{g}]\mathbf{a}_s^T + \mathbf{S}_s \tag{B.15}$$

where the second part is referred to as the *stress matrix* in mathematical literature. It should be noted that in the case of zero-free-length springs the modified axial stiffness is equal to zero, because the tension coefficient $\hat{t}$ is identical to the *constant* spring stiffness of the zero-free-length spring, $\mathbf{K}_{zfl}$. This means that only the *stress matrix* is relevant in those situations; this implies that for zero-free-length springs merely topology and not geometry is relevant.

B.3 Geometrically non-linear FEA

The derivation of the tangent stiffness matrix in this section is largely based on calculations in Crisfield (1991), but with notations adapted to those in Guest (2006) for ease of comparison.

B.3.1 Strain of a bar element

The initial length l_0 and deformed length l_n of the bar are written as

$$l_0^2 = (\mathbf{x}_1 - \mathbf{x}_2)^T(\mathbf{x}_1 - \mathbf{x}_2) \tag{B.16}$$

$$l_n^2 = (\mathbf{x}_1' - \mathbf{x}_2')^T(\mathbf{x}_1' - \mathbf{x}_2') \tag{B.17}$$

where $\mathbf{x}_a'$ is the set of displaced coordinates for node a, related to the initial coordinates by the nodal displacements $\mathbf{p}_a$

$$\mathbf{x}_a' = \mathbf{x}_a + \mathbf{p}_a. \tag{B.18}$$

For computational ease, equation B.17 will henceforth be written as

$$l_n^2 = \mathbf{x}'^T\mathbf{A}\mathbf{x}' \tag{B.19}$$

with

$$\mathbf{A} = \begin{bmatrix} 1 & 0 & 0 & -1 & 0 & 0 \\ 0 & 1 & 0 & 0 & -1 & 0 \\ 0 & 0 & 1 & 0 & 0 & -1 \\ -1 & 0 & 0 & 1 & 0 & 0 \\ 0 & -1 & 0 & 0 & 1 & 0 \\ 0 & 0 & -1 & 0 & 0 & 1 \end{bmatrix} \quad \text{and} \quad \mathbf{x}' = \begin{bmatrix} x_{1i} \\ x_{1j} \\ x_{1k} \\ x_{2i} \\ x_{2j} \\ x_{2k} \end{bmatrix}'.$$

The engineering strain is defined as

$$\epsilon = \frac{l_n - l_0}{l_0}. \tag{B.20}$$

Now, when keeping equations B.20 and B.19 in mind, the following can be derived:

$$\frac{\partial \epsilon^T}{\partial \mathbf{p}} = \frac{1}{l_0}\frac{\partial l_n^T}{\partial \mathbf{p}} = \frac{1}{l_0}\frac{1}{l_n}\mathbf{A}\mathbf{x}' = \frac{1}{l_0 l_n}\mathbf{c}(\mathbf{x}') \tag{B.21}$$

with

$$\mathbf{c}(\mathbf{x}') = \begin{bmatrix} x_{12i}' \\ x_{12j}' \\ x_{12k}' \\ -x_{12i}' \\ -x_{12j}' \\ -x_{12k}' \end{bmatrix} \text{ and } x_{12i}' = x_{1i}' - x_{2i}'. \tag{B.22}$$

Note the similarity of $\mathbf{c}(\mathbf{x}')$ with the equilibrium vector $\mathbf{a}_s$ defined in section B.2. Their relation can be written as

$$\mathbf{c}(\mathbf{x}') = l_n \begin{bmatrix} \mathbf{n}_n \\ -\mathbf{n}_n \end{bmatrix} = l_n \mathbf{a}_s. \tag{B.23}$$

B.3.2 Equilibrium equations

The virtual work principle will be used to derive the equilibrium equations, by equating the external work δW_u as a result of nodal forces $\mathbf{q}$ and the internal work δW_i as a result of member elongations:

$$\delta W_u = \delta W_i$$

$$\delta \mathbf{p}^T \mathbf{q} = \delta \mathbf{p}^T \int \sigma \frac{\partial \epsilon}{\partial \mathbf{p}} dV$$

$$\mathbf{q} = \int \sigma \frac{\partial \epsilon}{\partial \mathbf{p}} dV = A_0 l_0 \sigma \mathbf{b} = \frac{\sigma A_0}{l_n} \mathbf{c}(\mathbf{x}') = \lambda \frac{\sigma A_0}{l_0} \mathbf{c}(\mathbf{x}') \tag{B.24}$$

with

$$\lambda = \frac{l_0}{l_n}. \tag{B.25}$$

B.3.3 Tangent stiffness matrix

Presently the tangent stiffness matrix can be derived,

$$\mathbf{K}_t = \frac{\partial \mathbf{q}}{\partial \mathbf{p}} = \frac{A_0}{l_n} \mathbf{c}(\mathbf{x}') \frac{\partial \sigma^T}{\partial \mathbf{p}} + \frac{\sigma A_0}{l_n} \frac{\partial \mathbf{c}(\mathbf{x}')}{\partial \mathbf{p}} - \frac{\sigma A_0}{l_n^2} \mathbf{c}(\mathbf{x}') \frac{\partial l_n}{\partial \mathbf{p}}. \tag{B.26}$$

It is clear that the tangent stiffness matrix consists of three individual matrices; the first is the *linear stiffness matrix*, the other two form the *geometric stiffness matrix*

$$\mathbf{K}_t = \mathbf{K}_{t1} + \mathbf{K}_{t\sigma 1} + \mathbf{K}_{t\sigma 2}. \tag{B.27}$$

Linear stiffness matrix

The first term in equation B.26 is the linear stiffness matrix, and when taking into account that

$$\frac{\partial \sigma}{\partial \mathbf{p}} = E \frac{\partial \epsilon}{\partial \mathbf{p}} = E \mathbf{b}^T = \frac{E}{l_0 l_n} \mathbf{c}(\mathbf{x}')^T \tag{B.28}$$

the linear stiffness matrix becomes

$$\mathbf{K}_{t1} = \frac{E A_0}{l_0 l_n^2} \mathbf{c}(\mathbf{x}') \mathbf{c}(\mathbf{x}')^T = \frac{E A_0}{l_0^3} \lambda^2 \mathbf{c}(\mathbf{x}') \mathbf{c}(\mathbf{x}')^T. \tag{B.29}$$

Geometric stiffness matrix

Keeping in mind that $\frac{\partial \mathbf{c}(\mathbf{x}')}{\partial \mathbf{p}} = \mathbf{A}$ the second term in equation B.26 can be rewritten as

$$\mathbf{K}_{t\sigma 1} = \frac{\sigma A_0}{l_0} \lambda \mathbf{A}. \tag{B.30}$$

The last term in equation B.26 can also be rewritten, because with equation B.21 it holds that

$$\frac{\partial l_n}{\partial \mathbf{p}} = \frac{1}{l_n} \mathbf{c}(\mathbf{x}')^T \tag{B.31}$$

which results in

$$\mathbf{K}_{t\sigma 2} = -\frac{\sigma A_0}{l_n^2} \mathbf{c}(\mathbf{x}') \frac{\partial l_n}{\partial \mathbf{p}} = -\frac{\sigma A_0}{l_0^3} \lambda^3 \mathbf{c}(\mathbf{x}') \mathbf{c}(\mathbf{x}')^T. \tag{B.32}$$

B.4 Comparison

Now it is time to compare the tangent stifness matrix found in Guest (2006) to the one derived in the previous section

$$\mathbf{K}_T = \mathbf{a}_s [\hat{g}] \mathbf{a}_s^T + \hat{t} \begin{bmatrix} \mathbf{I} & -\mathbf{I} \\ -\mathbf{I} & \mathbf{I} \end{bmatrix} \tag{B.33}$$

where

$$\mathbf{a}_s = \begin{bmatrix} \mathbf{n} \\ -\mathbf{n} \end{bmatrix} \quad ; \quad \hat{t} = \frac{t}{l} \quad ; \quad \mathbf{S}_s = \hat{t} \begin{bmatrix} \mathbf{I} & -\mathbf{I} \\ -\mathbf{I} & \mathbf{I} \end{bmatrix}$$

and importantly the *modified axial stiffness* is

$$\hat{g} = g - \hat{t} = \frac{E A_0}{l_0} - \hat{t}. \tag{B.34}$$

These results are now to be compared with equations B.29, B.30 and B.32:

$$\mathbf{K}_{t1} = \frac{E A_0}{l_0^3} \lambda^2 \mathbf{c}(\mathbf{x}') \mathbf{c}(\mathbf{x}')^T$$

$$\mathbf{K}_{t\sigma 1} = \frac{\sigma A_0}{l_0} \lambda \mathbf{A}$$

$$\mathbf{K}_{t\sigma 2} = -\frac{\sigma A_0}{l_0^3} \lambda^3 \mathbf{c}(\mathbf{x}') \mathbf{c}(\mathbf{x}')^T.$$

Bearing in mind equation B.25, $\lambda = \frac{l_0}{l_n}$, the equations become

$$\mathbf{K}_{t1} = \frac{EA_0}{l_0 l_n^2}\mathbf{c}(\mathbf{x}')\mathbf{c}(\mathbf{x}')^T \tag{B.35}$$

$$\mathbf{K}_{t\sigma1} = \frac{\sigma A_0}{l_n}\mathbf{A} \tag{B.36}$$

$$\mathbf{K}_{t\sigma2} = -\frac{\sigma A_0}{l_n^3}\mathbf{c}(\mathbf{x}')\mathbf{c}(\mathbf{x}')^T. \tag{B.37}$$

When using equation B.23, $\mathbf{c}(\mathbf{x}') = l_n\mathbf{a}_s$, these can be rewritten into

$$\mathbf{K}_{t1} = \frac{EA_0}{l_0}\mathbf{a}_s\mathbf{a}_s^T \tag{B.38}$$

$$\mathbf{K}_{t\sigma1} = \frac{\sigma A_0}{l_n}\mathbf{A} \tag{B.39}$$

$$\mathbf{K}_{t\sigma2} = -\frac{\sigma A_0}{l_n}\mathbf{a}_s\mathbf{a}_s^T. \tag{B.40}$$

Finally, when it is observed that $\frac{\sigma A_0}{l_n}$ is equal to $\hat{t}$ and using $g = \frac{EA_0}{l_0}$ the equations can be rewritten as:

$$\mathbf{K}_{t1} = \mathbf{a}_s[g]\mathbf{a}_s^T \tag{B.41}$$

$$\mathbf{K}_{t\sigma1} = \hat{t}\mathbf{A} \tag{B.42}$$

$$\mathbf{K}_{t\sigma2} = -\mathbf{a}_s[\hat{t}]\mathbf{a}_s^T. \tag{B.43}$$

Now it is obvious that $\mathbf{K}_{t\sigma1}$ is identical to the stress matrix $\mathbf{S}_s$ and when equations B.41 and B.43 are combined they produce the first term from equation B.33.

B.5 Conclusion

Concluding, the two approaches to the tangent stiffness matrix provide identical results, given the assumption that the length l in Guest (2006) is equal to the deformed length l_n. This is the case as the bar is assumed to be pretensioned and is thus already in a deformed state.

Unfortunately, most formulations of the tangent stiffness matrix used in tensegrity literature are not directly compatible with the formulation using the modified axial stiffness, as they ignore the contribution of equation B.43 due to a small strain assumption. In the case of zero-free-length springs, that assumption is no longer valid and the present formulation is required. By introducing the *modified axial stiffness*, the derivation used in Guest (2006) provides a valuable insight regarding the use of zero-free-length springs, which is harder to recognize when using the traditional FEA approach to the tangent stiffness matrix.

It must be added that the use of a global reference frame makes it easier to arrive at the tangent stiffness formulation mentioned above, compared to the use of local coordinates on the bars and performing coordinate transformations at a later stage (Crisfield, 1991, section 3.6).

Appendix C

MATLAB Code Description

C.1 Introduction

The main objective of the MATLAB program included on the CDROM is to calculate the tangent stiffness matrix of a tensegrity structure, and analyse its zero-stiffness modes. The code is commented throughout, and should be self-explanatory for future users reasonably well-versed in the topic. Nevertheless, a brief outline of the code will be given, some custom functions will be discussed in more detail, and finally, certain noteworthy parts of the code will be highlighted.

C.2 Code outline

The **geometry** of the tensegrity structure is specified in a separate file, and is defined by the two structure arrays `lmnt` and `node`. The `lmnt` array contains information about element type, node connectivity, stiffness and tension; the `node` array contains nodal coordinates.

With these properties of the structure known, the **tangent stiffness matrix** is calculated, and its eigenmodes and eigenvalues are investigated. The stiffness of each of the modes is decomposed into the contributions of the modified material stiffness matrix and the stress matrix to gain additional insight. As the structures are modelled free-standing, there are at least 6 **rigid-body motions** present in the zero-stiffness modes, which are subsequently removed by means of a **QR-decomposition**. The QR-decomposition is further utilized to check the linear dependence of the remaining zero-stiffness with the **affine transformations** of the structure. This numerically verified the developed theories concerning zero stiffness.

Additionally, the program includes the **symmetry analysis** (Kangwai and Guest, 1999) of a three bar rotationally symmetric tensegrity, which yields the zero-stiffness modes in a symmetry-adapted form. These symmetry-adapted modes are then used for performing a small step along the zero-stiffness path, which cannot be solved directly because the stiffness matrix is singular, and thus requires the use of the **pseudo-inverse** and several iterations until equilibrium is restored.

Limitations

Some remarks regarding the applicability of the code are in order. The code was written in tandem with the increasing understanding of zero-stiffness tensegrity structures, and was afterwards rewritten for more general applicability. As a result the code is not as versatile as one could hope, and it is for instance hard-coded to 3-dimensional structures. The symmetry analysis is written specifically for the three bar tensegrity structure and applying the routine to other structures will give nonsensical results. Finally, the path tracking routine (which aims to follow a zero-stiffness mode) is currently limited to only one step, because the newly calculated equilibrium position is no longer precisely symmetric and the symmetry analysis subsequently returns nonsensical values. This could be improved by correcting the intermediate iterations for symmetry, but it was considered beyond the scope of this program.

C.3 Custom functions

`[K,S,A,G] = Kt_extra(lmnt,node)` The `Kt_extra` function calculates the tangent stiffness matrix for a structure given by `lmnt`, `node`. The function returns the various components of the tangent stiffness matrix as used in Guest (2006): the modified material stiffness matrix **K**, the stress matrix **S**, the equilibrium matrix **A** and the modified material matrix **G**. This provides all the necessary information to fully analyse the stiffness of the structure. The tangent stiffness matrix is subsequently easily calculated as $\mathbf{K}_t = \mathbf{K} + \mathbf{S}$.

`drawtens(lmnt,node,‘off’,‘orig’)` This function creates a 3-dimensional image of the tensegrity given by `lmnt`, `node` in the current figure. It takes two additional arguments as strings. The first determines whether or not to plot the element and node numbers, and takes `‘on’` and `‘off’` as values. The second determines whether to plot the structure in its original or displaced position, respectively indicated by solid and dashed lines, and takes takes the values `‘orig’` and `‘disp’`.

`displacement_vectorplot(node,disp)` The nodal displacements of a stiffness mode can be plotted as a vectors, by using this function. The displacements `disp` are a column vector with xyz displacements for all nodes. The function uses the internal MATLAB function `quiver3` to actually plot the vectors.

`lengths(lmnt,node)` This function returns the lengths of the elements, which is of use for checking the length-preserving properties of the zero-stiffness modes.

`nodalforces(lmnt,node)` This function can be used to check the equilibrium of the tensegrity structure by calculating the resulting nodal forces at each of the nodes.

C.4 Various remarks

Symmetric tangent stiffness matrix By virtue of its construction, the tangent stiffness matrix should be symmetric. In practice this was not always precisely the case and the analysis would yield complex-valued eigenvalues, which are meaningless in a static analysis. To circumvent this problem, the tangent stiffness matrix is explicitly symmetrized by averaging the sum of $\mathbf{K}_t$ and its transpose $\mathbf{K}_t^T$.

QR-decomposition An important part in the zero stiffness analysis is played by the QR-decomposition; among other things it is used to remove the rigid-body motions from the zero-stiffness modes. The QR-decomposition is provided by MATLAB and splits up a matrix $\mathbf{A}$ in an upper triangular matrix $\mathbf{R}$ of original dimension, and a unitary matrix $\mathbf{Q}$ so that $\mathbf{A} = \mathbf{QR}$. In practice it makes it possible to identify the linear dependence of various vectors, by performing a QR-decomposition on the juxtaposed vectors: if the resulting $\mathbf{R}$-matrix is a strictly diagonal matrix, all vectors are independent. If there are off-diagonal elements, there is a linear relationship between the corresponding column vectors in $\mathbf{Q}$.

Tangent space The tangent stiffness matrix is only valid over infinitesimal displacements, i.e. the eigenmodes are in tangent space. When the rigid-body motions are removed from the zero-stiffness modes, these must therefore also be in tangent space. In practical terms this means that the conventional rotation matrix cannot be used, and that the rotational modes are given by the cross-product of the nodal positions and the unit direction vectors of the principal axes. It can quite easily be verified that the cross product is essentially the same as the derivative of the conventional rotation matrix, at zero rotation angle.

C.5 Conclusion

The MATLAB program was initially not written as a general purpose FEA analysis tool for tensegrity structures, but specifically crafted for the analysis of the three bar rotationally symmetric tensegrity structure. In that sense the program definitely served its purpose, as it not only provided insights into zero-stiffness structures prior to the development of the underlying theory, but also allowed for the verification of the theory by examining specific example structures. The code was later rewritten to accommodate more general functions and the rewrite resulted in the current form, of which the stiffness section of the code can be used for the analysis of any free-standing tensegrity structure.

Appendix D

Prototype Design

D.1 Introduction

Based on the theory described in Chapter 2, a demonstration prototype was constructed. It was built not only to verify the developed theory, and to demonstrate that it is actually possible to physically build these structures, but also to get a feel of the challenges that will be encountered when constructing these systems.

The design process turned out to be more complex than anticipated, and involved the balancing of various conflicting design considerations. A major issue was the fact that gravity is not taken into account in the theory, and the structure was therefore to be limited in size to minimize the effect of the mass of the structure. On the other hand, various other constraints provided a lower bound to the dimensions of the structure.

This appendix will describe the design process of the prototype, by first outlining the conceptual design in Section D.3, and subsequently detailing the final design in Section D.4. The latter chiefly involved establishing suitable dimensions to fit the components, and still obtain a sufficient range of motion. Section D.5 provides a brief evaluation of the final design, as well as some pictures of the prototype.

D.2 Design requirements

An important purpose of the prototype is to demonstrate the mechanism-like properties of this class of structure. Consequently the range of motion was (qualitatively) required to be ‘sufficiently large’ to clearly visualize those properties. Actually quantifying the desired range of motion proved to be so intertwined with the dimensions of the structure, that it was not considered until the specification of the dimensions in Section D.4.

A major requirement for the prototype is easy adjustment of the parameters, so that the balancing properties can be tuned. This translates into adjustable

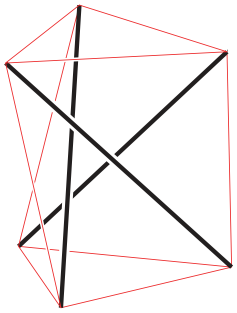

Figure D.1: Three bar rotationally symmetric tensegrity structure used for the prototype; when all cables are replaced by zero-free-length springs the structure is statically balanced.

attachment points for the springs and wires, as well as some control over the friction in the system. On one hand the aim was to reduce friction as far as possible, in order to get as close as possible to a true zero-stiffness structure. On the other hand, some control over friction would be needed to overcome the effects of gravity forces.

D.3 Prototype description

The structure chosen for the prototype was the three bar rotationally symmetric tensegrity structure shown in Figure D.1. Not only is this structure instantly recognizable to people working in the field of tensegrities and often used as a module for larger structures, it also has relatively few components, which simplified the design and construction process.

D.3.1 Conceptual design

For the static balancing of the tensegrity structure, the use of springs with a zero rest length is a condition *sine qua non.* However, the prototype does not actually feature pretensioned zero-free-length springs, and their properties are emulated by means of regular non-pretensioned springs. This choice is motivated by the manufacturing difficulties of zero-free-length springs, and the physical rest length of the springs which would unnecessarily limit the range of motion of the structure. The properties of the zero-free-length spring are emulated by running the wire over the endpoint of the bar, to a conventional spring (Herder, 2001). By correctly choosing the total wire length, the spring will be at its rest length when the endpoint of the wire coincides with the endpoint of the bar, and thus the tension will be proportional to the 'length' of the wire between the two bars it connects.

This translates into a design (schematically shown in Figure D.2) where wires run over a yarn guide on the endpoint of the bar, wrap around a pulley attached to the spring, and are fixed at a flange. This pulley construction halves the necessary elongation of the spring, so the springs would actually fit on the bar.

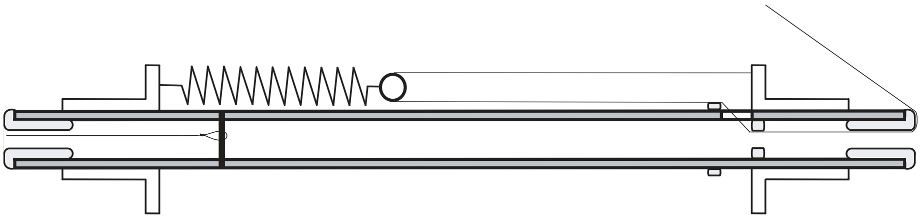

Figure D.2: Conceptual design of the bars of the tensegrity structure. Only one spring is shown, but two more are attached in similar manner, along the circumference of the flanges. Two springs (vertical and horizontal) are attached on one end, and one (horizontal) on the other. Note that this image is *not* to scale.

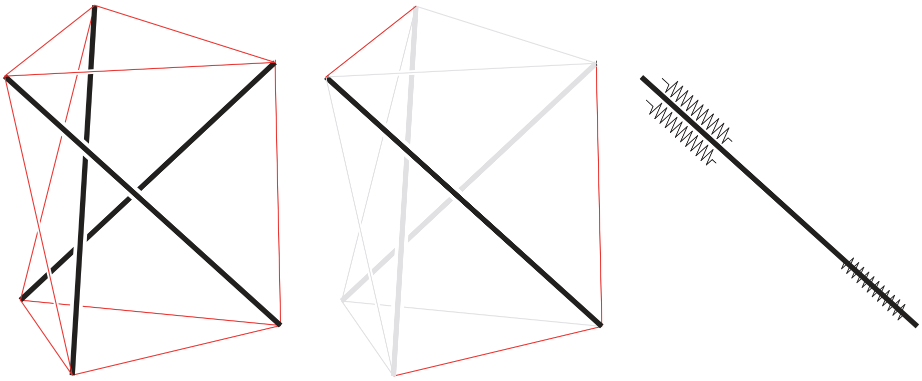

Figure D.3: The prototype with the springs corresponding to a single bar; this is identical for each of the three bars. The angles under which the springs are attached around the bar circumference are determined in Section D.4.

The other end of the wire is attached to a small pin inside the bar. As the total structure consists of three bars and nine springs (three horizontal and six vertical), each bar therefore has three springs attached: a 'horizontal' and 'vertical' spring on one end, and a 'horizontal' on the other (see Figure D.3).

Spring design

Unlike many spring applications, the precise spring stiffness was not relevant, as the springs balance eachother out. A crucial property of the springs, however, is the required spring stiffness ratio between the horizontal and vertical springs as calculated in section A.6: the vertical spring must be $\sqrt{3}$ times stiffer than the horizontal spring. What is more, most off-the-shelf springs are pretensioned to some degree. This would unnecessarily complicate the assembly of the structure, as the levels of pretension would have to be taken into account for the required wire length. The combination of these factors led to the decision to custom make the springs without pretension.

As the springs are custom made, further specific requirements could be made to the ends of the springs to facilitate the design of the total prototype (see

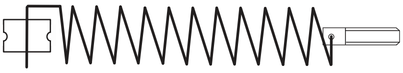

Figure D.4: Spring design: one end has a small teflon wheel attached, the other end a threaded rod for adjustability. The endpoint wires are twisted orthogonally to eachother.

Figure D.4). On one end a small threaded rod is attached to the spring, making adjustment of the spring position possible. The other end of the spring is twisted orthogonally to the spring body, so the pulley (a grooved teflon wheel) can directly be attached.

Adjustability

The structure can be tuned quite easily by adjusting the position of the spring, as well as the attachment of the wire, with respect to the flanges. This dual adjustability makes rough (spring attachment) and fine (wire attachment) adjustment possible. All adjustments are made by simply turning a nut.

D.4 Design detailing

This section describes the detailing of the final prototype design. First the bar dimensions are determined (with special attention to the range of motion of the structure), before the other components are described and finalized.

D.4.1 Range of motion

All calculations on the range of motion are performed using the equilibrium equations as found in Appendix A, based on the assumption that the structure is deformed in its fully symmetric zero-stiffness mode and *remains symmetric throughout its deformation.* The working range of the structure is then expressed in terms of a generalized parameter, the ratio between height h and radius r of the structure: h/r. It is very difficult to define a ‘sufficient’ h/r range of motion, but some idea will be given in the following section.

D.4.2 Bar dimensions

Bar length

Establishing the bar length involved balancing various factors. An upper bound was given by the increased weight of the structure, and although this was not quantified, it meant that the objective was to minimize the size of the structure, but at the same time maintain a sufficient range of motion. The range of motion is limited by a variety of factors. These factors will be discussed in detail, and by means of Figures D.11 to D.19 the constraints were translated into a suitable choice of bar length.

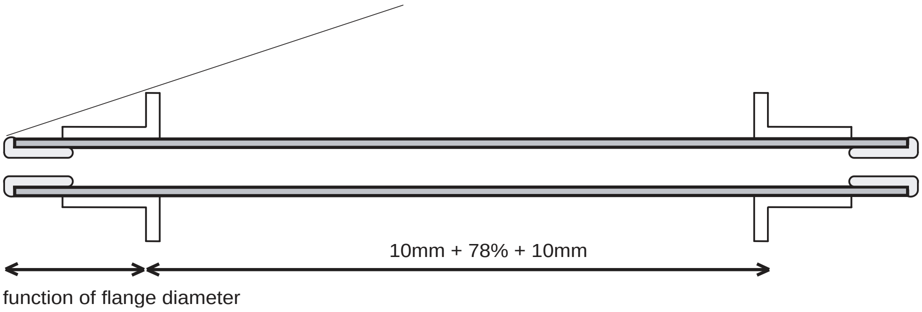

Figure D.5: Trade-off of design dimensions. The minimum required distance between the flanges conflicts with the desired distance of the flange to the endpoint to avoid contact between the flange and the wires.

spring length + elongation As can be seen in figure D.12, the maximum spring elongation is 47% of the bar length, and assuming that is at 150% elongation, the spring rest length is 31% and the total spring length at maximum elongation is 78% of the bar length. This determines the minimum distance between the flanges, along with some 'dead' length for the spring attachment and flange width. The latter was estimated at 10mm at each end. The above calculation implicitly uses another constraint, that of the maximum possible spring elongation of 150%. If that value cannot be reached, a larger distance is required between the flanges to reach a similar range of motion, which conflicts with the wire/flange clearance discussed further down.

wire length The wire length maximally reaches a value of 98% of the bar length (see Figure D.11) and when the spring is fully at rest length that length of wire should fit on the bar. As the wire is halved by the pulley, that requires 98/2=49% of the bar length, and with the spring rest length of 31% that totals to about 80%. The distance from the endpoint of the bar to the flange should be subtracted from that percentage, as some wire length is stored there as well. As a result, the 78% flange distance described above seems to be sufficient.

bar clearance During displacement, the bars with the springs might touch eachother. The likelihood can be reduced by choosing the total diameter of bar and springs as small as possible, but nevertheless a minimum clearance between the bars is required, in order to obtain a certain working range. The minimum required bar clearance is calculated at 30mm from heart to heart of the bars, working on the assumption that both the spring and bar diameter are 10mm, and that they lie side by side. That yields a certain working range, as can be found in Figure D.16, which is mostly limited in the lower end of the h/r ratio range.

flange and wire clearance During displacement the wires of the structure might collide with the flanges to which the spring and wires are attached; thus limiting the range of motion. The flanges couldn't be moved away from the endpoint indefinitely to avoid contact, as that would conflict with the minimum required distance between the two flanges. Another

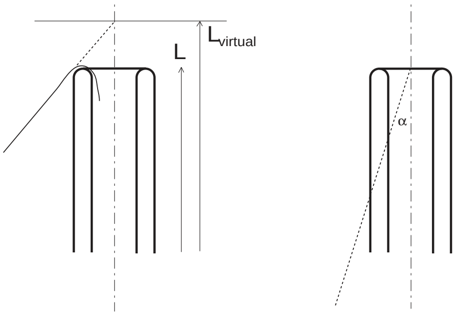

Figure D.6: Virtual length and angle assumption in calculations.

> approach would be to reduce the diameter of the flange, but that is determined by the diameter of the spring.
>
> The angle between bar and wire is plotted in Figure D.17, and this was used to create Figure D.19 which shows the required distance of the flange from the endpoint, for three different flange radii. The available endpoint length of three bar lengths was also plotted: that is 11% of bar length minus 10mm of 'dead' length required for spring attachment.
>
> **NB**: Some notes are in order with regard to this calculation, as it implies a false sense of accuracy. First of all, because the wires exit from an offset due to the bar diameter, there is a 'virtual' bar length, which should really be used for calculations of the angle. Secondly, the angle is taken from the heart line of the bar, and that is also how the required endpoint distance is calculated (see Figure D.6). These effects have conveniently been ignored.

Let us first summarize the above described constraints, before they are translated into a choice of bar length:

- minimum required flange distance of 78% plus a 'dead' length of 20mm;
- an estimated required clearance of 30mm;
- an estimated required flange radius of ∼15mm.

Using Figure D.16 and D.19, and with the consideration that a sufficient range of motion would be $h/r = [0.5 \ldots 4]$, we find a bar length of 450mm, provided the flange radius is maximally 15mm. This h/r ratio can be translated into a practical height and radius range by means of Figure D.14. When realizing that the width of the structure is roughly $\sqrt{3}R$, that translates into a height range of $110 \ldots 410$mm, and width range of $175 \ldots 390$mm for a bar length of 450mm. This range of motion was deemed sufficiently large to visualize the mechanism-like properties of the system.

Bar diameter

Based on the available diameter yarn guides in the ASCOTEX catalogue, the decision was made to use bars with an inner diameter of 6mm, which corresponds to an inner diameter of about 3.2mm for the yarn guide; this was deemed sufficient to guide three wires through. Next was the choice of material and wall thickness of the tube. Two options are compared in Table D.1.

Table D.1: Comparison of two bars; aluminium and steel with different wall thickness.

	Steel	**Aluminium**
Density (kg/m3)	7900	2700
Young's modulus	200E+09	70E+09
Bar properties		
Inner (m)	0,006	0,006
Outer (m)	0,007	0,008
Length (m)	0,450	0,450
Weight(kg)	0,036	0,027
Critical Load		
Inertia	5,42E-011	1,37E-010
P_{cr}(N)	528	468

With the inner diameter fixed at 6mm, the two options were steel and aluminium with respectively a wall thickness of 0.5 and 1mm. The weight and Euler buckling load were calculated for a bar length of 450mm with $P_{cr} = \frac{\pi^2 EI}{L^2}$. The aluminium bar has a slightly lower buckling load, but is about a third lighter, and was therefore chosen. Note that the axial stiffness of the bars is irrelevant as the lengths will remain constant throughout the displacement.

D.4.3 Springs

Some aspects of the spring design were already discussed in Section D.3, such as the spring stiffness ratio of $\sqrt{3}$, and the wish for the springs to be untensioned. Several more aspects had to be taken into consideration when designing the definitive springs: a maximum allowed spring stiffness is imposed by the buckling load of the bar, and the springs have to be able to extend at least 150% of their rest length.

Maximum stiffness

To calculate the maximum spring stiffness in order not to exceed the buckling load of the bar, a relatively large safety factor of 10 was taken to take into account excentric loading. This provides an upper bound for the forces that can be exerted by the spring on the bar. Using Figure D.15 and with the vertical spring stiffness $\sqrt{3}$ times higher than the horizontal spring stiffness, the maximum exerted (normalized) force on the bar (with two horizontal and one vertical spring) can be found at $h/r = 1.7$. At that point the elongation of all the springs is approximately 34% of the bar length (see Figure D.12). That means that the maximum spring stiffness may not exceed $\frac{47N}{0.34 \cdot 450 \cdot (2+\sqrt{3})} = K_{hor} = 0.082 N/mm$ for the horizontal spring.

Spring elongation

The allowed spring elongation is closely linked to the dimensions and material properties of the spring. The springs used in the structure were individually made to specification, by cutting the required length from a long strand of untensioned spring with an outer diameter of 10mm, and respectively a wire thickness of 1mm and 0.9mm for the vertical and horizontal spring. The spring material was stainless steel.

To see whether the springs could reach the desired elongation of $0.47 \cdot 450 = 212$mm, a back-of-the-napkin calculation was done, using the formulas and data tables from a spring manual (Verenfabriek Bakker, Hengelo). Input requirements were that the spring is untensioned, the coils are touching and the spring rest length *including* end attachments is maximally 31% of the bar length.

The relevant spring properties for calculating the spring stiffness, are:

- $d =$ wire diameter
- $D =$ spring diameter (centre to centre; $D_{outer} - d$)
- $n =$ number of coils
- $G =$ material shear modulus

The spring stiffness as a function of the spring properties is then given as

$$K = \frac{Gd^4}{8nD^3}. \tag{D.1}$$

The decisive question is whether the spring is capable of the desired elongation Δl, as established previously. This can be determined by calculating the spring force at maximum elongation, $F_{max} = K \cdot \Delta l$, and comparing the corresponding stress τ_{max} with the maximum allowed values from literature. The τ_{max} is given by

$$\tau_{max} = \frac{8F_{max}Dk}{\pi d^3} \tag{D.2}$$

where k is the Göhner correction factor given by

$$k = 1 + \frac{5}{4}\frac{1}{W} + \frac{7}{8}\frac{1}{W^2} + \frac{1}{W^3}$$

with W the spring index $W = D/d$. The allowed τ_{max} was further corrected for the load ratio and number of load cycles. The load ratio is given by the working range of the spring divided by the maximum force, in our case $(F_{max} - 0)/F_{max} = 1$, and with a maximum number of load cycles chosen to be 5000, the correction factor was 1.09.

With the above formulas and boundary conditions, the two springs in Table D.2 were calculated. At maximum elongation both springs remain within the maximum allowed stress. These theoretically calculated springs were used as guidelines when actually making the springs from a long strand.

Table D.2: Calculated values for the required springs.

	horizontal spring	vertical spring
body length (mm)	126	128
coils	140	128
stiffness (N/mm)	0.0556	0.0958

D.4.4 Yarn guides

The yarn guides were ordered at Ascotex Ltd., and the chosen material type was T27C, a very smooth titania ceramic. Two different parts were ordered: the flanged eyelet E120 (D1=6mm, d=3.2mm, H=8mm, D2=7.90mm, h=6.20mm), and the tube eyelet TE3 (A=6mm, B=3.5mm, h=6mm).

D.4.5 Wires

For visual effect, as well as reduced friction, the wires were chosen to be as thin as practically possible. Two requirements were placed on the material properties: a high stiffness (so that the length does not change significantly with the changing internal tension during displacement) and the absence of creep, so that the length actually remains fixed under a constant load. Eventually Kevlar fishing line was used, and because the applied load was much lower than the maximum possible load, the small amount of creep was deemed insignificant.

D.4.6 Pulleys

The pulleys were constructed as simple as possible, and consist of a small grooved PTFE (Teflon) wheel, which runs directly around the spring loop.

D.4.7 Flanges

The outer diameter of the flanges was established during the calculation of the required bar length, and was set at 30mm. A next question was under which angles to attach the springs around the circumference of the bar. The angles between the springs can be seen in Figure D.7, and their relation to h/r is plotted in Figure D.20. The initial configuration was, somewhat arbitrarily, chosen to be where the angles are approximately at their midpoint between the values at h/r=0.5 and 4. This is denoted by the vertical line in Figure D.20, and gave the following angles for spring attachment: 90°, 125° and 145°. As the angles will change during the displacement, it is very likely that the bars will rotate slightly along their axis.

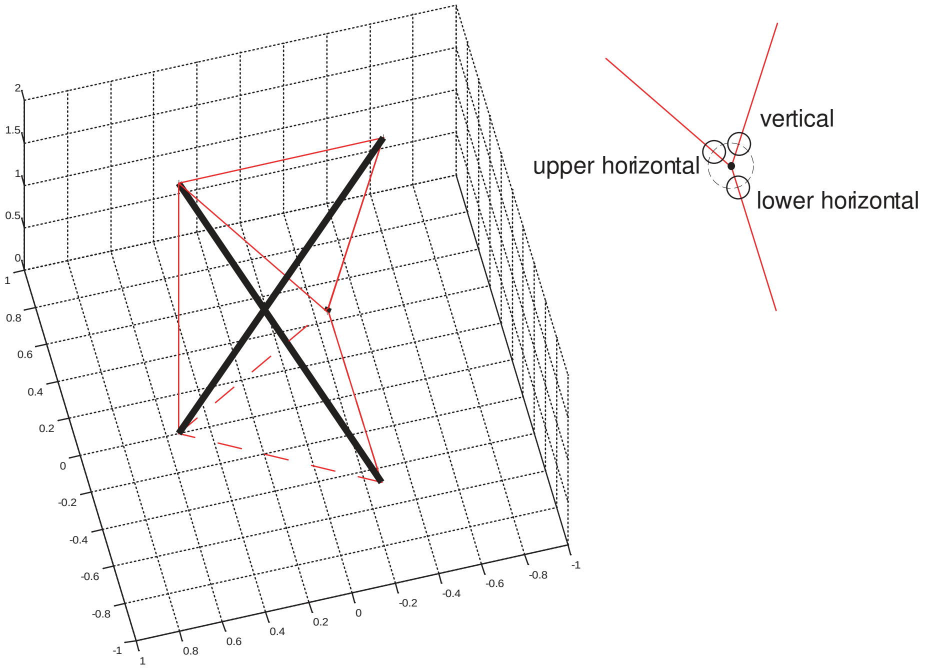
2
1.5
1
0.5
0
1
0.8
0.6
0.4
0.2
0
-0.2
-0.4
-0.6
-0.8
-1
1
0.8
0.6
0.4
0.2
0
-0.2
-0.4
-0.6
-0.8
-1
vertical
upper horizontal
lower horizontal

Figure D.7: View along the axis of a bar, showing the angles between the various wires connected to the bar. The detail shows the springs on the bar, and the corresponding wires.

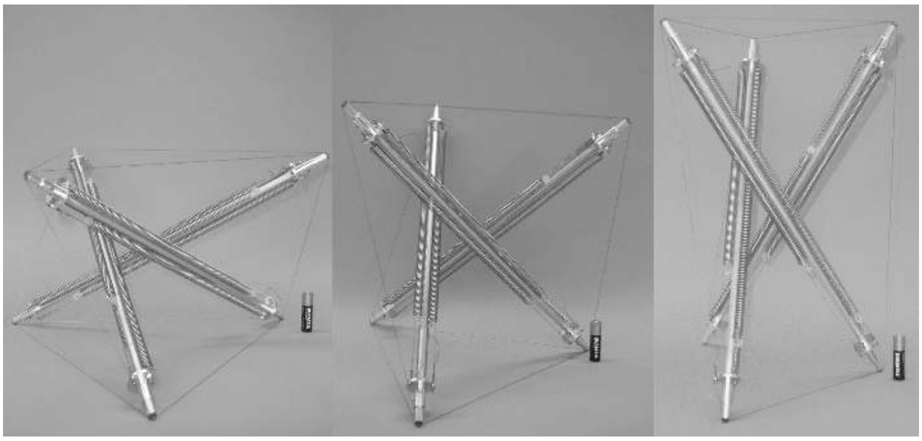

Figure D.8: Overview of range of motion of demonstration prototype, deformed in the symmetric zero-stiffness mode.

D.5 Design Evaluation

Several pictures of the prototype are given in Figure D.8 to D.10, showing several stages of the assembly process, and providing an indication of the working range of the final structure. A major issue in the model is the high level of friction, which is much greater than anticipated, and which reduces the feeling of 'zero' stiffness. It does serve a useful purpose by compensating for the gravity forces, which had not been taken into account for calculations.

D.5.1 Design process

In retrospect the numerical analysis of the range of motion was too detailed, and too optimistic. The various constraints discovered in the analysis proved to be much less significant than the practical problems posed by the actual components and complexity of assembly. Nevertheless, the analysis did provide a great deal of valuable insight in the structure, and it is definitely a necessary and worthwhile aspect of the design process.

D.5.2 Design and Components

The demonstration prototype has quite a lot of friction, which will have to be reduced in future designs. The use of roller bearings for the pulleys will be an improvement, but the main bottleneck is the tight curvature of the wires at the endpoint of the bars. The friction currently makes the spring and wire adjustment possibilities redundant, but it will become relevant when the friction has been reduced sufficiently.

The three (stiffer) vertical springs proved to be hard-pressed to reach the desired 150% elongation, and for a next prototype it would be worthwile to pay more attention to the design of the springs, and to consider more combinations of spring diameter and wire thickness to find a suitable spring. Also, a different attachment method for the springs would be advisable, which would allow some control over the stiffness of the spring, e.g. a threaded cylinder which can be screwed into the spring. Thirdly, the current method of attaching the pulleys does not scale up well for higher loads, as the spring loop deforms under increasing load and consequently the wires often slip out of the grooves. This limits the range of motion slightly.

Finally, in the prototype springs without pretension were used in order to facilitate assembly. It would also be possible to use pretensioned springs, and they would reduce the required distance between the flanges as less extension would be needed to reach the same tension. On the other hand, the pretension will reduce the range of motion, as the force/displacement curve is cut off sharply when the spring reaches its rest length. It is nevertheless worthwile to consider the use of standard pretensioned springs in future designs.

D.5.3 Assembly

The assembly of the structure is a fairly complex and tedious job. The tediousness largely results from having to individually measure the spring properties and the required wire lengths. Also, attaching the wires inside the bars, and ‘threading’ the wires through the yarn guides, is a fiddly job. The complexity lies in the fact that all bars need to be firmly fixed when tensioning the springs, as the structure is out of balance until all springs are attached. If there is less friction in the system, the structure will have to be finetuned to be precisely in balance, and it will be a difficult task to determine which of the springs has to be adjusted.

D.5.4 Conclusion

Although the prototype serves its purpose as a proof of concept, it clearly shows that a lot of work lies ahead, before these types of structures can be put to practical use. Especially the friction has to be reduced drastically to obtain a feeling of zero stiffness. The design process further showed that a thorough analysis of the desired range of motion is advisable, not only to determine the required spring elongations, but also to determine the dimensions of the components of the structure.

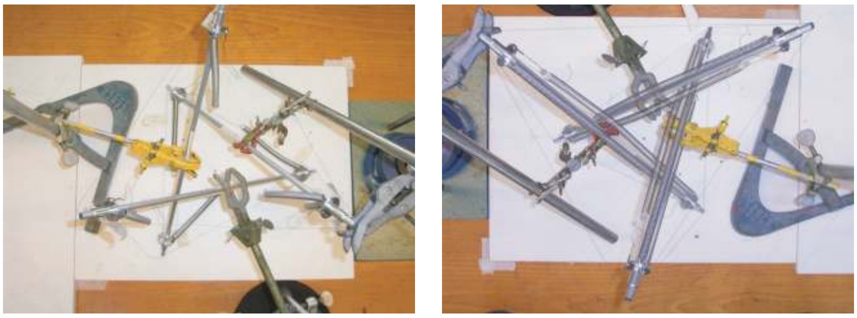

(a) When all springs are attached and all wirelengths are measured out, the bars are firmly fixed with clamps . . .

(b) . . . so that the springs can be tensioned one by one.

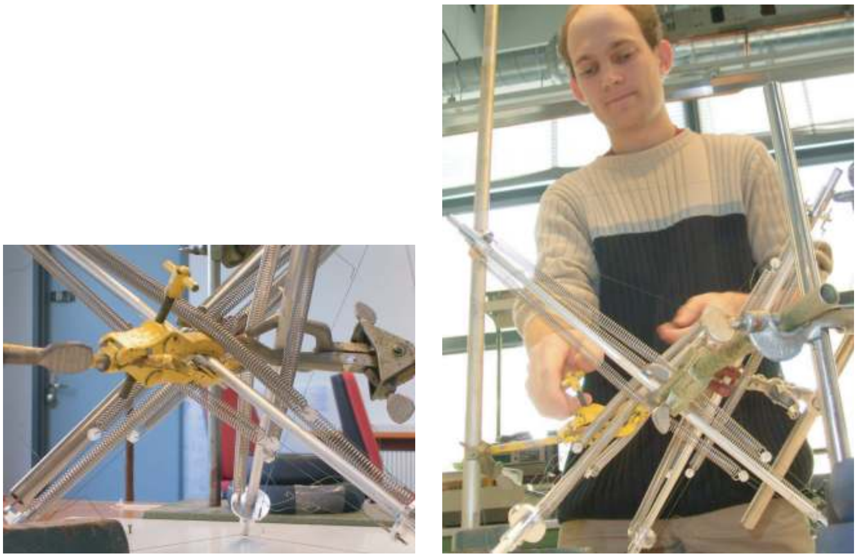

(c) Close-up of springs during assembly.

(d) Removing the clamps that fix the bars.

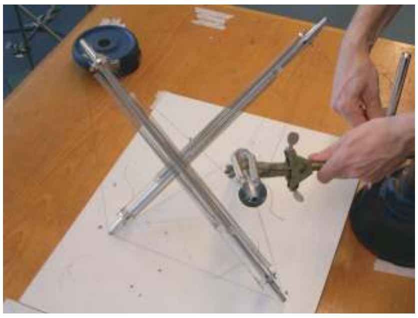

(e) Removing last clamp.

Figure D.9: The assembly process involved fixing the bars tightly at a given initial position, in order to tension the springs one by one. Once all springs are tensioned, the structure is in equilibrium and the clamps can be removed.

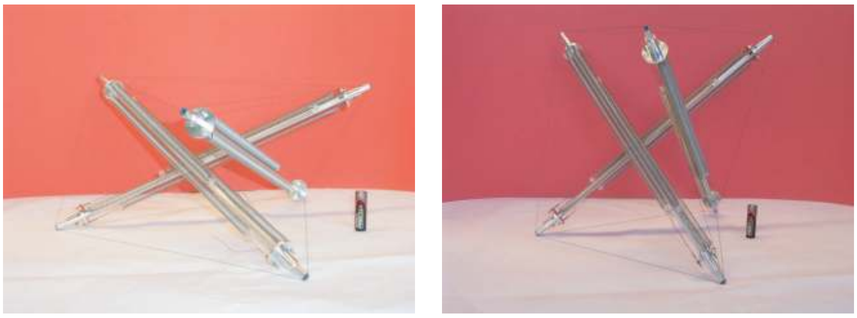

(a) Low position (b) Medium position

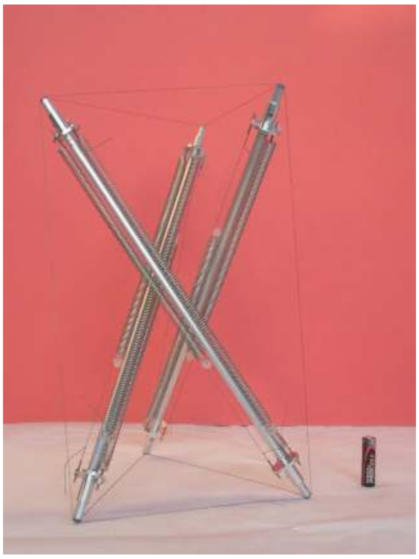

(c) High position

Figure D.10: Prototype deformed in symmetric zero-stiffness mode. It can be deformed into a wide range of other shapes as well, as there are two additional anti-symmetric zero-stiffness modes.

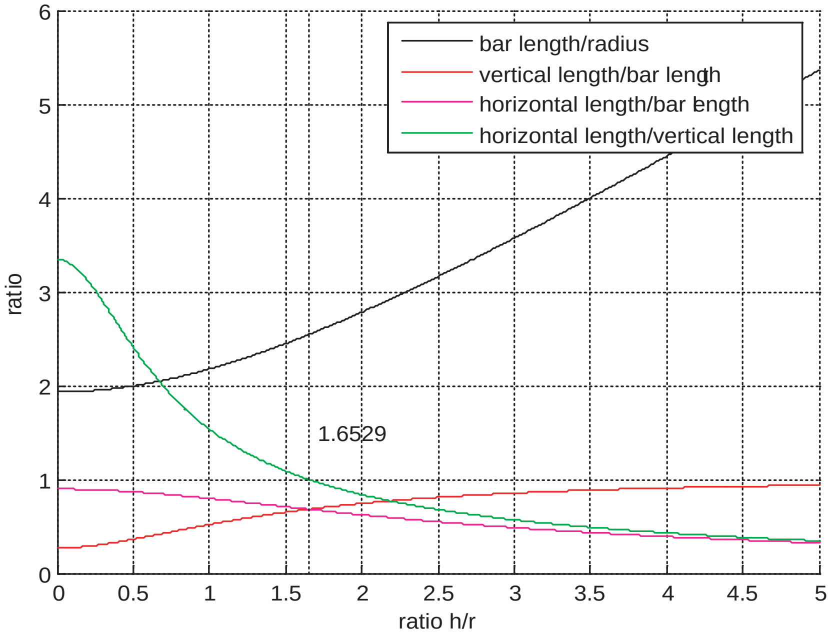

Figure D.11: Lengths of members, versus the h/r ratio. The vertical line indicates where the horizontal and vertical wires are of equal length.

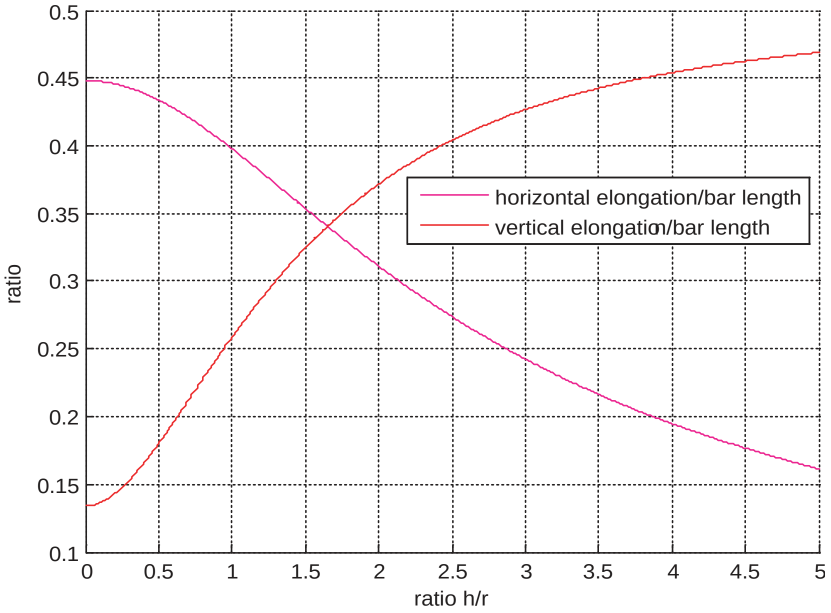

Figure D.12: Spring elongation as ratio of bar length, versus the h/r ratio. This is essentially just half of the length of the corresponding wires, plotted in Figure D.11, but zoomed in for better judgement of the values.

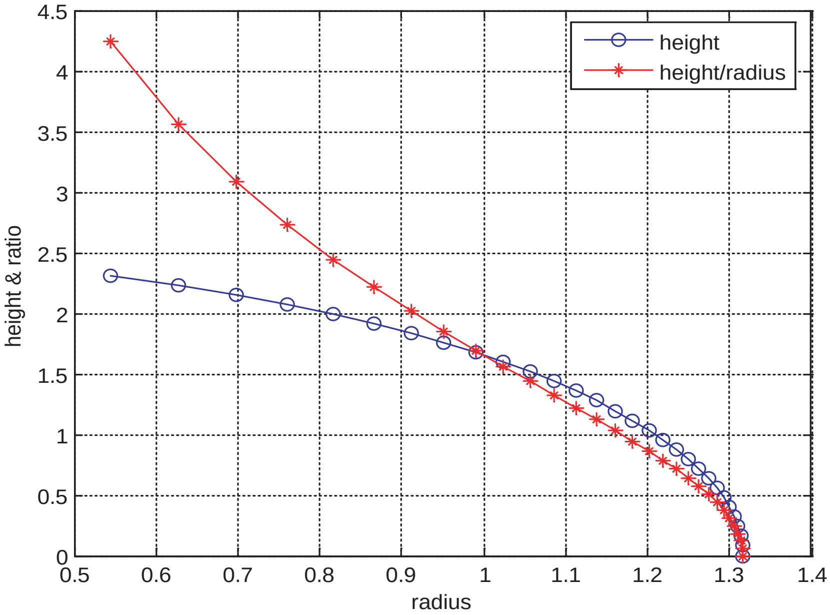

Figure D.13: Height and radius (ratio) during displacement with constant bar length. This graph makes it possible to read the physical working range of the structure, once the h/r working range is known.

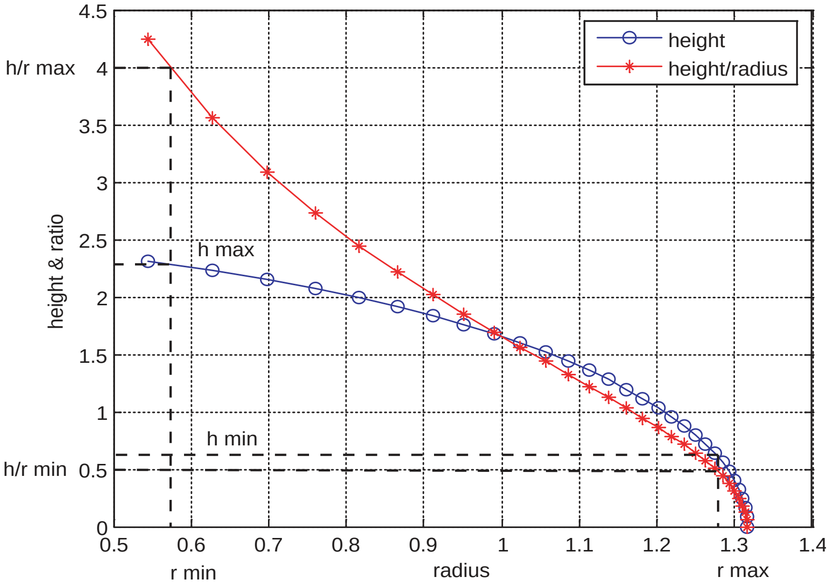

Figure D.14: Height and radius (ratio) during displacement with constant bar length. This example shows how the working range of h/r can be translated into height and radius; the h/r working range of $0.5 \ldots 4$ translates into $h = 0.6 \ldots 2.3$ and $r = 0.57 \ldots 1.28$. These values have to be multiplied with a scaling factor to obtain the actual displacement of the prototype.

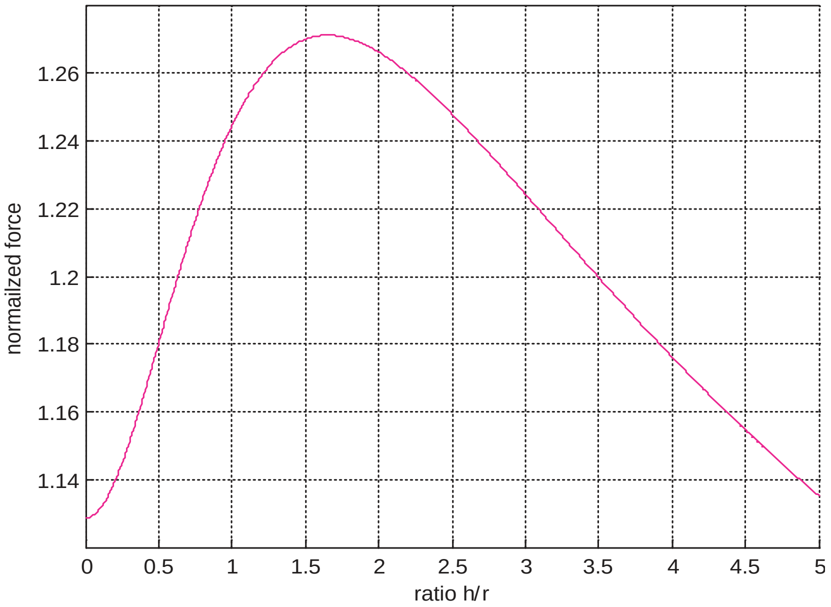

Figure D.15: Normalized bar forces due to spring elongations. The maximum force is compared with the buckling load of the bar.

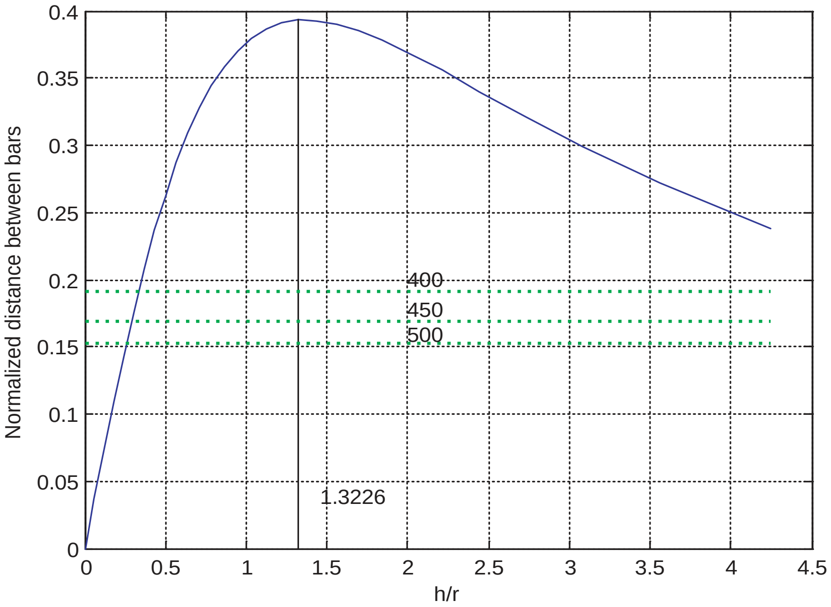

Figure D.16: The normalized clearance between the bars, versus the h/r ratio. The horizontal lines show the 30mm clearance line for various bar lengths, and allows the judgement of working range.

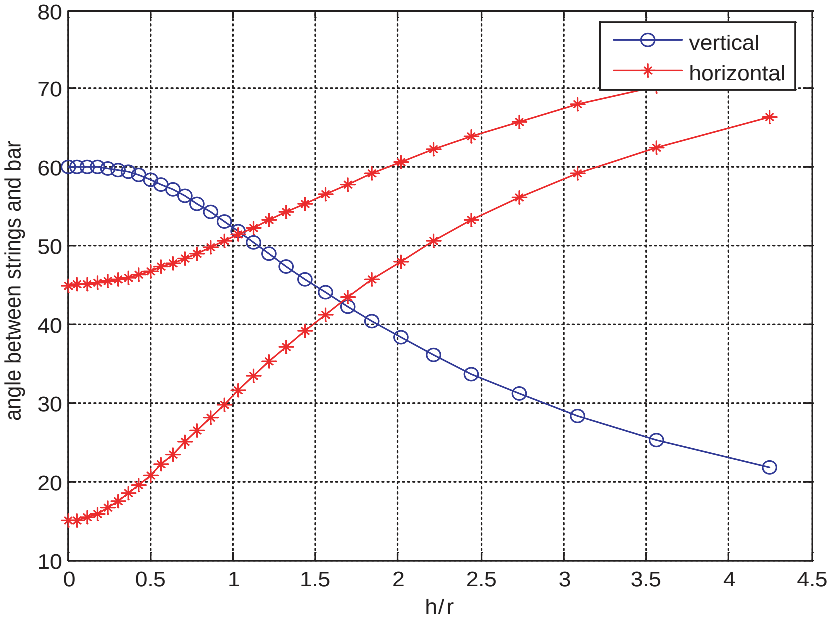

Figure D.17: Angle between the bar and the horizontal and vertical wires, versus the h/r ratio.

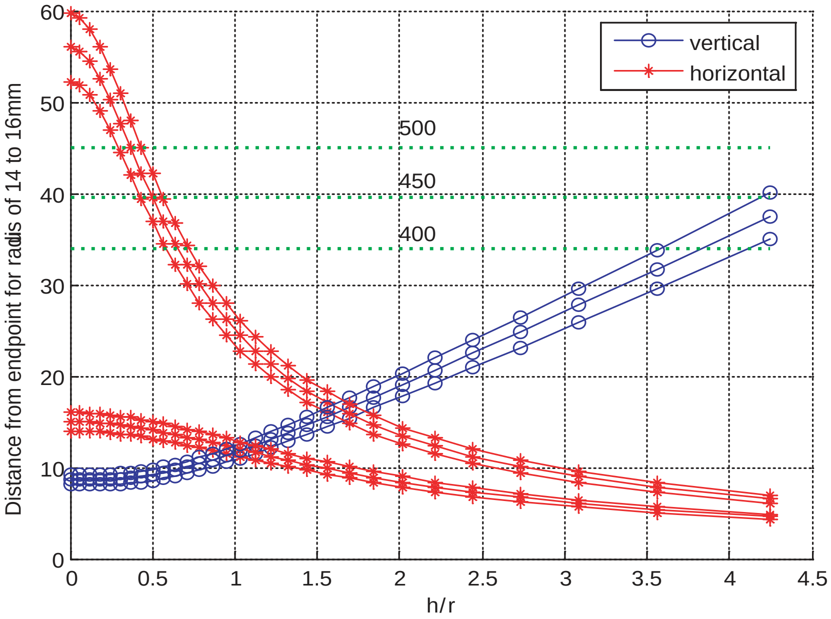

Figure D.18: Required distance from endpoint for various flange diameters. The horizontal lines show the available endpoint length, as in 11% of bar length - 10mm.

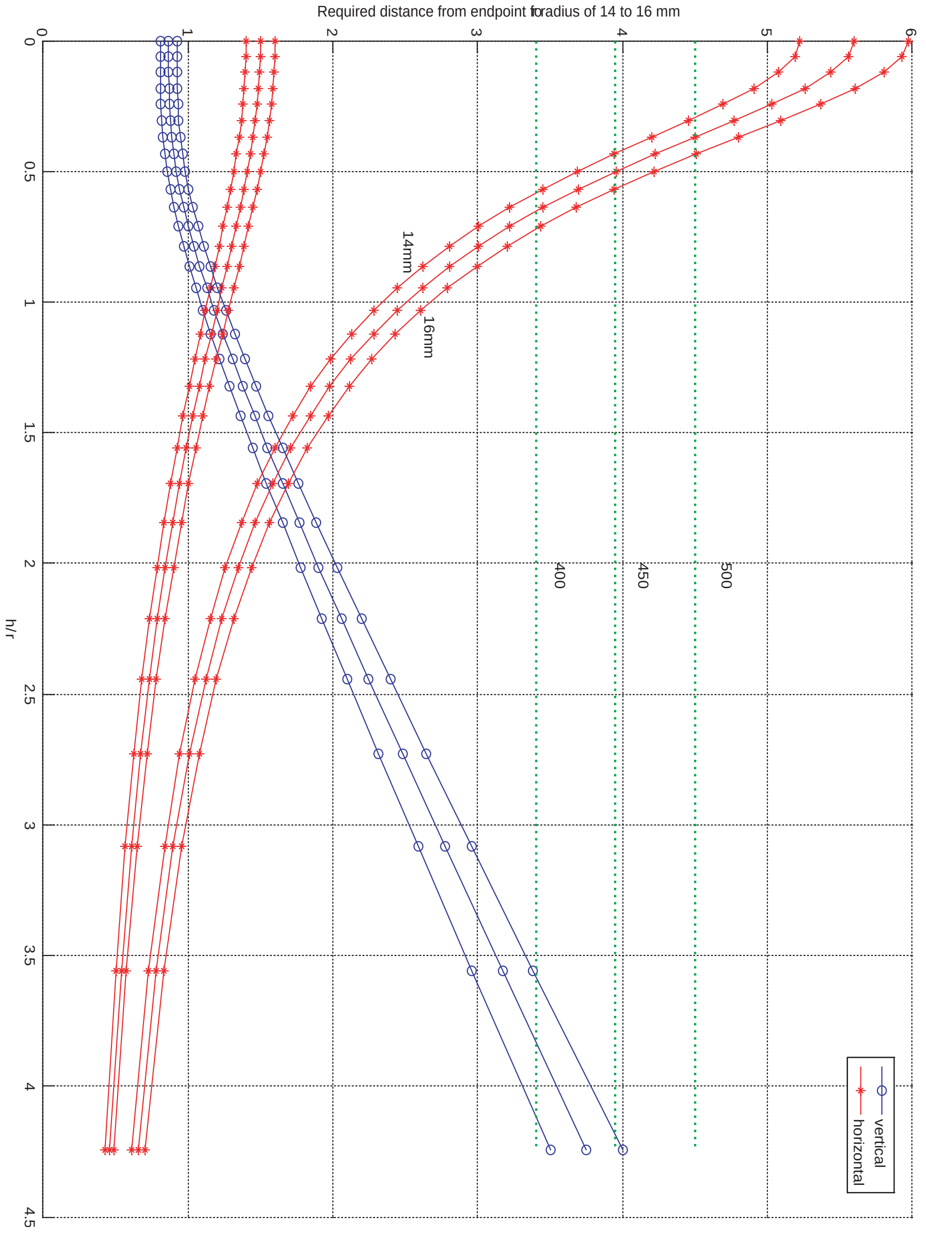

Figure D.19: Enlarged version of Figure D.18.

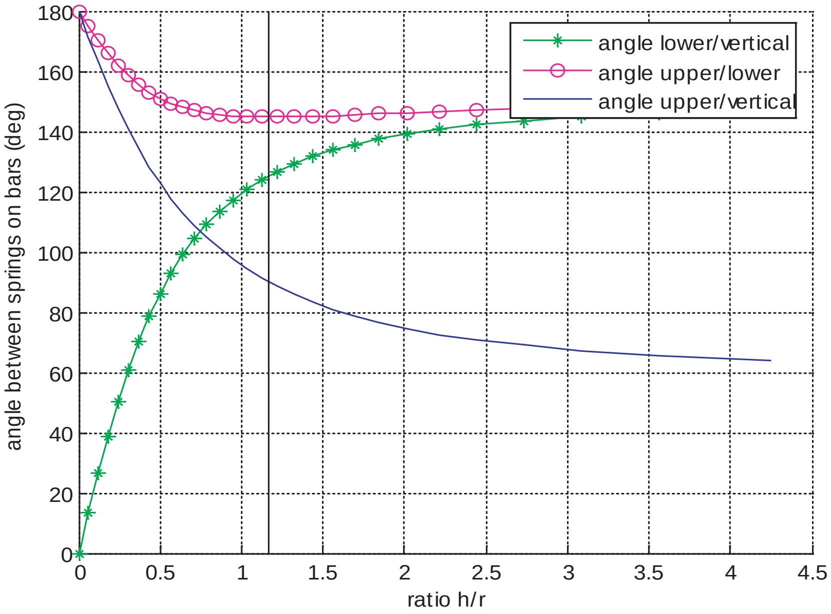

Figure D.20: The angles between the wires on the bar during displacement. This is used to find an initial configuration for the spring attachment on the bars.

Appendix E

Zero Stiffness Examples

E.1 Introduction

Several tensegrity geometries with zero-free-length springs as tension members have been numerically analysed for zero stiffness, using the MATLAB program described in Appendix C. These include the famous 'babytoy' tensegrity, as well as several rotationally symmetric tensegrities.

For the first, the equilibrium configuration is derived in Section E.2, and for the latter the equilibrium equations from Appendix A are used; the naming scheme is that of Hinrichs (1984). The structures are plotted in Figures E.2 to E.4, and an overview of the number of zero-stiffness modes in each of the structures is given in Table E.1.

Structure	No. of bars on conic	No. of zero-stiffness modes
'Babytoy'	3	3
$P_3(1,1)$	3	3
$P_4(1,1)$	4	2
$P_5(1,1)$	5	1

Table E.1: Structures analysed for zero-stiffness in this section. The number of zero-stiffness modes and the number of bar directions lying on a conic are listed, and they correspond to the theory described in Chapter 2.

E.2 'Babytoy' equilibrium

The 'babytoy' tensegrity consists of 6 identical bars, divided into three orthogonal parallel pairs, connected by 24 cables of equal length. The equilibrium position is calculated by means of the kinematic form-finding method, which utilizes the fact that cable lengths reach a minimum at the tensegrity equilibrium configuration.

With x the distance between two parallel bars of length L, the cable length

L_{cable} is written as

$$\begin{aligned} L_{cable} &= \sqrt{\left(\frac{L-x}{2}\right)^2 + \left(\frac{x}{2}\right)^2 + \left(\frac{L}{2}\right)^2} \\ &= \frac{1}{\sqrt{2}}\sqrt{L^2 - xL + x^2} \end{aligned} \tag{E.1}$$

and the derivate to bar distance x yields

$$\begin{aligned} \frac{\partial L_{cable}}{\partial x} &= \frac{(2x-L)}{\sqrt{L^2 - xL + x^2}}\frac{1}{2\sqrt{2}} = 0 \\ &= 2x - L = 0 \end{aligned}$$

which gives the solution $x = \frac{L}{2}$. Subsequent analysis of nodal equilibrium yields that the tensions coefficients are related as follows:

$$\hat{t}_{bar} = \frac{3}{2}\hat{t}_{cable} \tag{E.2}$$

These values were used for calculating the three zero-stiffness modes of the structure, which are plotted in Figure E.1.

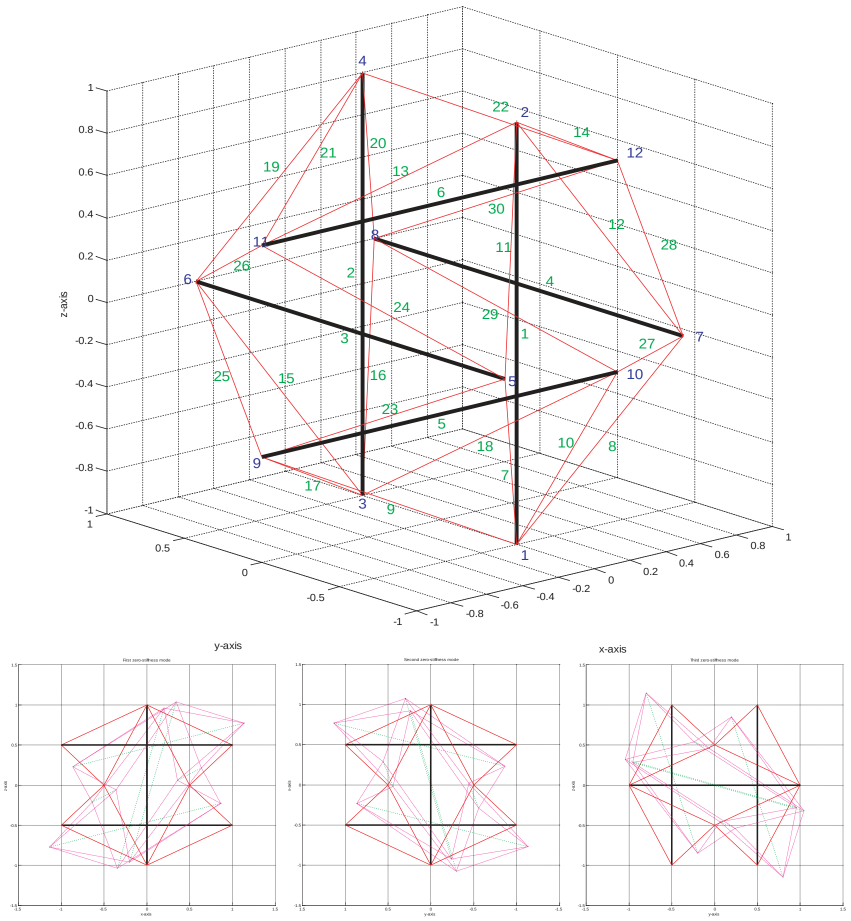
4
2
12
11
8
6
7
5
10
9
3
1
22
14
20
21
19
13
6
30
12
28
11
26
2
4
24
29
3
1
27
25
15
16
23
5
18
10
8
7
17
9
z-axis
y-axis
x-axis
First zero-stiffness mode
Second zero-stiffness mode
Third zero-stiffness mode

Figure E.1: The ‘babytoy’ tensegrity structure. Its three zero-stiffness modes roughly correspond to shear on three orthogonal planes. No symmetrization has been performed on the modes, and it is expected that such an analysis would yield perfectly orthogonal shears.

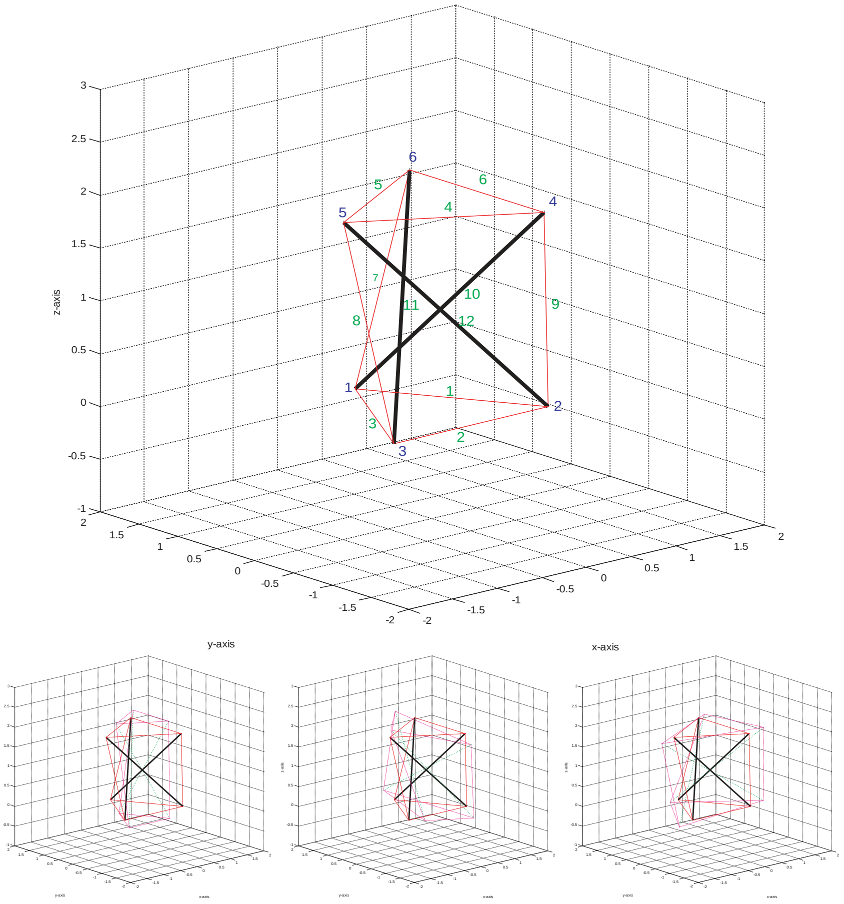
z-axis
3
2.5
2
1.5
1
0.5
0
-0.5
-1
y-axis
2
1.5
1
0.5
0
-0.5
-1
-1.5
-2
x-axis
-2
-1.5
-1
-0.5
0
0.5
1
1.5
2
1
2
3
4
5
6
1
2
3
4
5
6
7
8
9
10
11
12

Figure E.2: A $P_3(1, 1)$ structure with its three *symmetrized* zero-stiffness modes. The first corresponds to a scaling transformation, the latter two are combinations of shear and scaling.

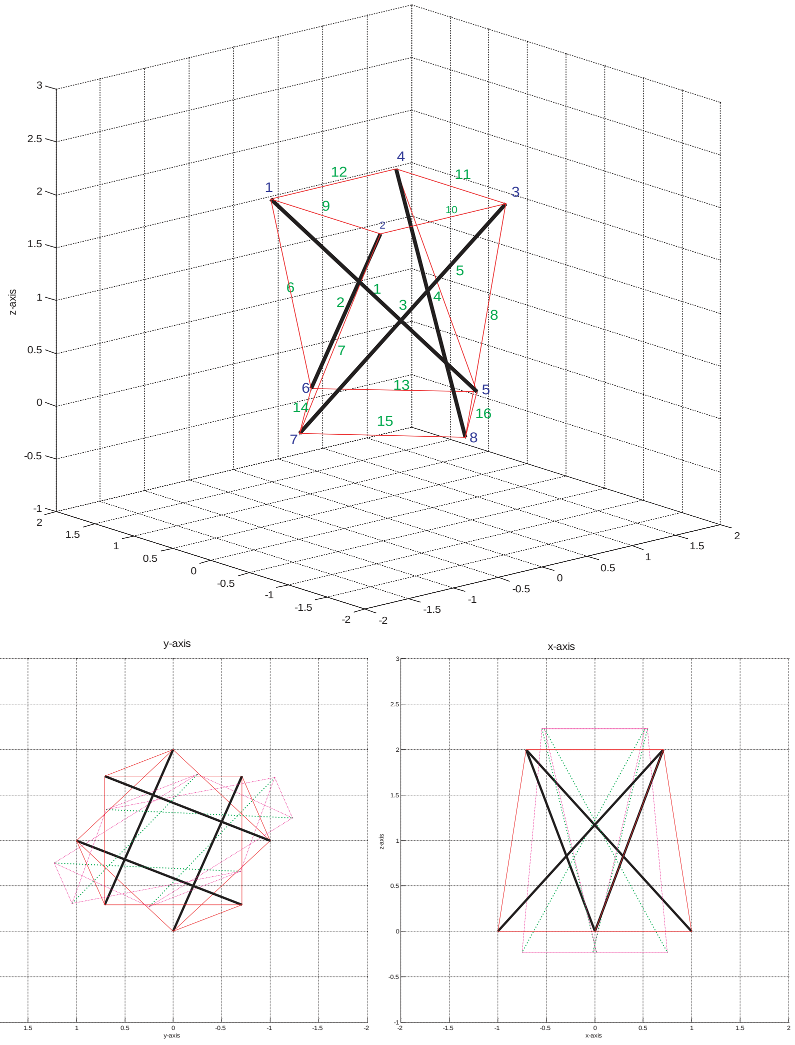
1
2
3
4
5
6
7
8
1
2
3
4
5
6
7
8
9
10
11
12
13
14
15
16
z-axis
3
2.5
2
1.5
1
0.5
0
-0.5
-1
2
1.5
1
0.5
0
-0.5
-1
-1.5
-2
y-axis
x-axis
z-axis
x-axis
y-axis
x-axis

Figure E.3: A $P_4(1,1)$ structure with its zero-stiffness modes. The first mostly consists of a skewing transformation, the second mostly of a scaling transformation.

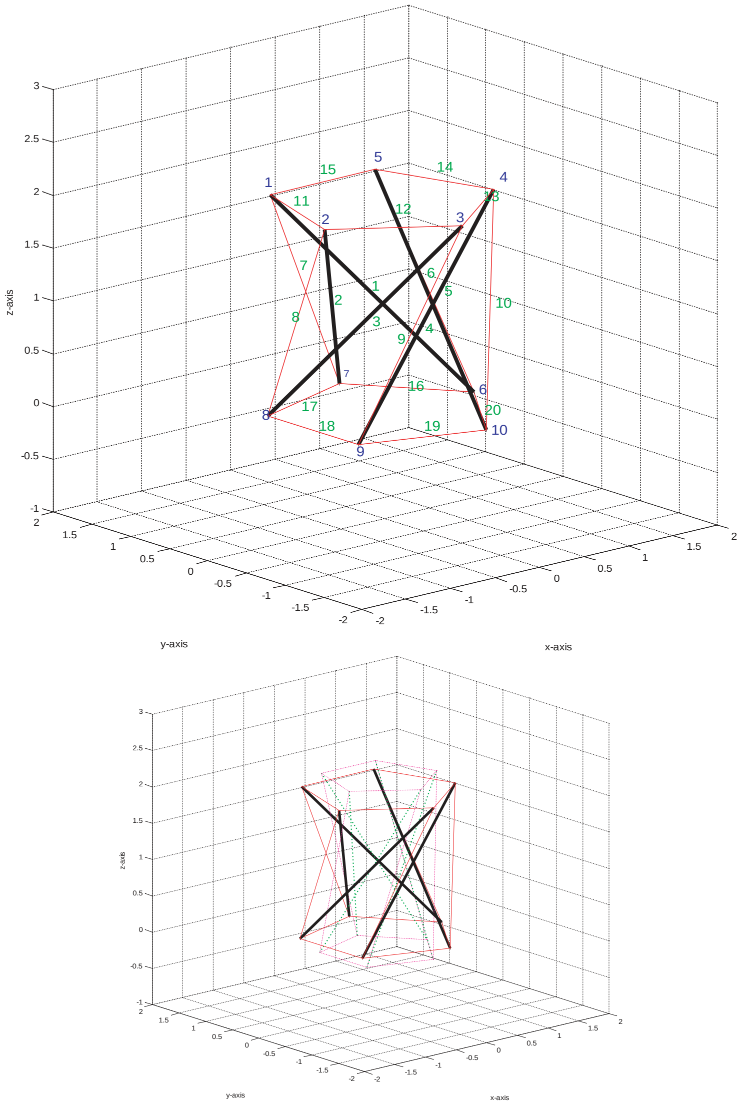
z-axis
y-axis
x-axis
3
2.5
2
1.5
1
0.5
0
-0.5
-1
2
1.5
1
0.5
0
-0.5
-1
-1.5
-2
1
2
3
4
5
6
7
8
9
10
11
12
13
14
15
16
17
18
19
20

Figure E.4: A $P_5(1,1)$ structure with its zero-stiffness mode, which corresponds to a scaling transformation.

Appendix F

Future Work

F.1 Introduction

The work described in this MSc. thesis has been a first step in the direction of a fundamental understanding of zero-stiffness structures. This section briefly discusses some possible directions for future research, and where possible, provides some pointers. The limitations imposed by only considering tensegrity structures, namely absence of external forces and constraints, are first to be considered, before other issues such as range of motion and practical applications are looked into.

F.2 Future work

external forces The current theory cannot take into account exernal loads, as it makes use of the fact that in *unloaded* state, affine transformations of the nodal coordinates are in the nullspace of the stress matrix. This no longer holds when there are external loads present.

A priority is to include *constant* gravity forces in the calculations, and some possible approaches were considered, but none were carried through to fruition. The first would be to qualitatively include gravity forces as a special type of 'gravity element' with a specific direction and of infinite length, which might or might not lie on the conic. The next step would then be to say that the affine transformation $\mathbf{U}$ should maintain the *direction* $\mathbf{v}$ of that element, and therefore

$$\mathbf{U}(\mathbf{p}_i - \mathbf{p}_j) = \mathbf{U}\mathbf{v}_{ij} = \lambda\mathbf{v}_{ij}$$

and the element direction is thus an eigenvector with eigenvalue λ. The eigenvalue would be 1 if the 'gravity element' lies on the conic, and its length is therefore preserved.

Another (quantitative) approach would be to reconsider the structural equilibrium as

$$\tilde{\mathbf{\Omega}}\mathbf{p} = \mathbf{f}_{ext}$$

where the effect of the affine transformation $\mathbf{U}$ on each of the n nodes, can be written as

$$\begin{aligned} \tilde{\mathbf{\Omega}}\mathbf{U}'\mathbf{p} &= \mathbf{U}'\mathbf{f}_{ext} \\ &= 1 \cdot \mathbf{f}_{ext} \end{aligned}$$

with $\mathbf{U}' = \mathbf{I}^n \otimes \mathbf{U}$ a blockdiagonal matrix with $\mathbf{U}$ working on each of the nodal coordinates/forces. As a result, one can see that a constant $\mathbf{f}_{ext}$ is an eigenvector of the blockdiagonal $\mathbf{U}'$ with eigenvalue 1.

constraints Although traditionally tensegrity structures are analysed as free standing, in practice some degrees of freedom are fixed in order to remove rigid-body motions. The choice of constraints strongly influences the possible deformations of the structure, and therefore the structure needs to be fixed without prohibiting the length-preserving affine transformations that have zero stiffness. It is as of yet unclear how to do this in a general manner.

An interesting approach is to first only consider the subset of displacements that are length-preserving for the conventional elements. This is done numerically by means of a QR-decomposition, where the rows of the compatibility matrix $\mathbf{C}$ are orthogonalized in two parts: one that involves elongations of conventional members, and a set $\mathbf{C}_{zfl}$ that does not. With the latter set, a reduced stiffness matrix can be obtained, which is limited to only those displacements that are length-preserving for conventional elements.

$$\mathbf{K}_{t,reduced} = \mathbf{C}_{zfl}^T \mathbf{K}_t \mathbf{C}_{zfl}$$

This technique might facilitate finding affine transformations that are not prohibited by the nodal constraints.

non-pin-jointed structures Once the issues of external loads and constraints have been solved, the question arises whether (some of) the above developed theory can be extended to also include non-pin-jointed structures such as the ‘Anglepoise’ lamp, and to confirm and extend the modification rules developed by Herder (2001).

range of motion Numerical calculation of the zero-stiffness modes produces displacements in *tangent space*. Therefore, for large displacements iterative techniques need to be employed to find a next equilibrium configuration, even more so because the tangent stiffness matrix is per definition singular.

It is therefore very difficult to intuitively extrapolate from the calculated zero-stiffness modes, to see how it is best interpreted over large displacements and what the range of motion would be. For instance consider

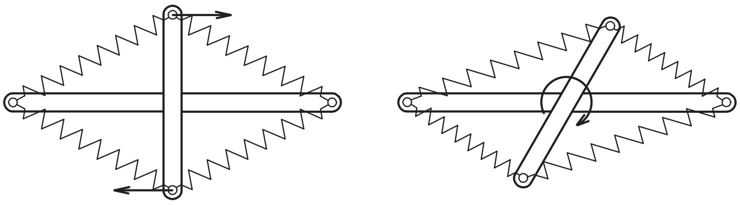

Figure F.1: In tangent space, the zero-stiffness mode of this statically balanced structure corresponds to shear and scaling, but on macro scale, it corresponds to the rotation of the two bar with respect to each other.

the simple statically balanced structure in Figure F.1; the structure has a zero-stiffness mode that can numerically be described as consisting of shear and scaling. However, on a macro level, one can see that the two bars rotate with respect to eachother. The question is, how this can be done more generally and for more complex (three-dimensional) structures.

An approach to this would be either to analytically analyse the structures, or look at mechanism theory and try to find techniques from that field; mechanisms concepts such as the number of Degrees of Freedom of a mechanism should also be investigated.

practical application The demonstration prototype described in Appendix D was constructed not only to demonstrate that these types of structure actually exist, but also to get a feel for the practical issues that arise when trying to construct zero stiffness tensegrities.

There is a lot more (practical) work to be done here, not only to reduce friction and to device more efficient methods of construction, but also to make the structures simpler and more robust, and thus suitable for practical applications.

overview of zero-stiffness modes As indicated in Chapter 3 there exist types of zero stiffness which are not yet fully understood, and several example structures were given. In order to understand these structures, further research is needed, with special attention to the presence of unstressed nodes.

other forms of zero stiffness Other forms of zero stiffness are described in literature, such as by Tarnai (2003) where the equilibrium paths at a bifurcation point remain neutrally stable over a finite range of motion. It is currently unclear how these forms of zero stiffness are related to the ones described in this research.

sensitivity analysis It would be interesting to analyse the sensitivity of the zero-stiffness modes to perturbations and/or imperfections of initial conditions. Will the calculated modes zero-stiffness modes also be present in configurations close to the analysed ones; for example if the conventional members do not precisely lie on a conic?

F.3 Conclusion

The above suggestions for future work illustrate that only the first steps have been taken in fully understanding zero-stiffness tensegrity structures. A lot of work is left in the theoretical field, and also (and in common with tensegrities in general) in practical design and applications. As the applications will most likely be based on the mechanism-like properties of the structures, the links to mechanism theory should definitely be explored.

Bibliography

Calladine, C. R., 1978. Buckminster Fuller's 'tensegrity' structures and Clerk Maxwell's rules for the construction of stiff frames. International Journal of Solids and Structures 14, 161–172.

Calladine, C. R., Pellegrino, S., 1991. First-order infinitesimal mechanisms. International Journal of Solids and Structures 27 (4), 505–515.

Calladine, C. R., Pellegrino, S., 1992. Further remarks on first-order infinitesimal mechanisms. International Journal of Solids and Structures 29 (17), 2119–2122.

Connelly, R., 1999. Tensegrity structures: Why are they stable? In: Thorpe, M. F., Duxbury, P. M. (Eds.), Rigidity Theory and Applications. Kluwer Academic/Plenum Publishers, pp. 47–54.

Connelly, R., Back, W., 1998. Mathematics and Tensegrity. American Scientist 86, 142–151.

Connelly, R., Terrell, M., 1995. Globally Rigid Symmetric Tensegrities. Structural Topology 21, 59–77.

Connelly, R., Whiteley, W., 1992. The Stability of Tensegrity Frameworks. International Journal of Space Structures 7 (2), 153–163.

Connelly, R., Whiteley, W., 1996. Second-order rigidity and prestress stability for tensegrity frameworks. SIAM Journal of Discrete Mathematics 7 (3), 453–491.

Coxeter, H. S. M., 1989. Introduction to geometry, 2nd Edition. John Wiley & sons, inc.

Crisfield, M. A., 1991. Non-linear Finite Element Analysis of Solids and Structures. Volume 1: Essentials. John Wiley & Sons.

Deng, H., Kwan, A. S. K., 2005. Unified classification of stability of pin-jointed bar assemblies. International Journal of Solids and Structures 42 (15), 4393–4413.

French, M. J., Widden, M. B., 2000. The spring-and-lever balancing mechanism, George Carwardine and the Anglepoise lamp. Proceedings of the Institution of Mechanical Engineers part C – Journal of Mechanical Engineering Science 214 (3), 501–508.

Guest, S. D., 2006. The stiffness of prestressed frameworks: A unifying approach. International Journal of Solids and Structures 43 (3–4), 842–854.

Herder, J. L., 2001. Energy-Free Systems. Theory, conception and design of statically balanced spring mechanisms. Ph.D. thesis, Delft University of Technology.

Hinrichs, L. A., 1984. Prismic Tensigrids. Structural Topology 9, 3–14.

Kangwai, R. D., Guest, S. D., 1999. Detection of finite mechanisms in symmetric structures. International Journal of Solids and Structures 36 (36), 5507–5527.

Love, A. E. H., 1927. A treatise on the mathematical theory of elasticity, 4th Edition. Dover publications.

Masic, M., Skelton, R. E., Gill, P. E., 2005. Algebraic tensegrity form-finding. International Journal of Solids and Structures 42 (16–17), 4833–4858.

Motro, R., 1992. Tensegrity Systems: The State of the Art. International Journal of Space Structures 7 (2), 75–83.

Murakami, H., 2001. Static and dynamic analyses of tensegrity structures. Part II. Quasi-static analysis. International Journal of Solids and Structures 38, 3615–3629.

Pellegrino, S., 1990. Analysis of Prestressed Mechanisms. International Journal of Solids and Structures 26 (12), 1329–1350.

Pellegrino, S., Calladine, C. R., 1986. Matrix analysis of statically and kinematically indeterminate frameworks. International Journal of Solids and Structures 22 (4), 409–428.

Schenk, M., Guest, S. D., Herder, J. L., 2006. Zero Stiffness Tensegrity Structures, to be submitted.

Tarnai, T., 2003. Zero stiffness elastic structures. International Journal of Mechanical Sciences 45 (3), 425–431.

Tibert, A. G., Pellegrino, S., 2003. Review of Form-Finding Methods for Tensegrity Structures. International Journal of Space Structures 18 (4), 209–223.

Weisstein, E. W., 1999. Conic Section. From Mathworld – a Wolfram Web Resource. http://mathworld.wolfram.com/ConicSection.html.